



Vectorized peptidic inhibitors to rescue  
F508del-CFTR in Cystic Fibrosis.

Inaugural Dissertation

to obtain the academic degree

doctor rerum naturalium (Dr. rer. nat.)

submitted to the Department of

Biology, Chemistry, and Pharmacy of Freie Universität Berlin

by

Dipl. Biol. Anja Heiduk from Halle/Saale

2016

Dieser Arbeit wurde in der Gruppe "Molekulare Bibliotheken" des Institutes für Medizinische Immunologie der Charité-Berlin unter der Leitung und Betreuung von Dr. Rudolf Volkmer angefertigt.

This work was realized from May 2012 till February 2016 in the "Molecular Libraries and Recognition" group of Dr. Rudolf Volkmer at the Institute of Medical Immunology of Charité-Berlin.

1. Gutachter: Dr. Rudolf Volkmer

2. Gutachter: Prof. Dr. Christian Freund

**Disputation am: 20.10.2016**

# I Contents

<b>I</b>	<b>CONTENTS .....</b>	<b>1</b>
<b>II</b>	<b>LIST OF FIGURES.....</b>	<b>4</b>
<b>III</b>	<b>LIST OF TABLES .....</b>	<b>6</b>
<b>1</b>	<b>SUMMARY .....</b>	<b>7</b>
<b>2</b>	<b>ZUSAMMENFASSUNG .....</b>	<b>10</b>
<b>3</b>	<b>INTRODUCTION .....</b>	<b>13</b>
<b>3.1</b>	<b>THE PATHOLOGY OF CYSTIC FIBROSIS(CF)</b>	<b>13</b>
<b>3.2</b>	<b>CHARACTERISTICS OF CFTR ION CHANNEL</b>	<b>13</b>
<b>3.3</b>	<b>TARGETING POST-ENDOCYTIC DEGRADATION MATURE CFTR</b>	<b>14</b>
<b>3.4</b>	<b>CFTR MUTATIONS AND THEIR CLASSIFICATIONS</b>	<b>18</b>
<b>3.5</b>	<b>RESEARCH AND TREATMENT OF CYSTIC FIBROSIS</b>	<b>20</b>
<b>3.6</b>	<b>TARGETING THE CFTR CAL INTERACTION TO DEVELOP NEW THERAPEUTICS</b>	<b>23</b>
<b>3.7</b>	<b>CROSSING BIOLOGICAL MEMBRANES</b>	<b>25</b>
<b>3.7.1</b>	<b>CELL PENETRATING PEPTIDES (CPP)</b>	<b>26</b>
<b>3.7.1.1</b>	<b>MECHANISM OF CPP CELLULAR INTERNALISATION</b>	<b>27</b>
<b>3.7.1.2</b>	<b>MPG AND PENETRATIN</b>	<b>29</b>
<b>3.7.1.3</b>	<b>CELLULAR INTERNALIZATION VIA N-MYRISTOYLATION</b>	<b>30</b>
<b>4</b>	<b>OBJECTIVE OF THE WORK.....</b>	<b>32</b>
<b>5</b>	<b>MATERIALS AND METHODS .....</b>	<b>34</b>
<b>5.1</b>	<b>FLUORESCENCE ANISOTROPY BINDING EXPERIMENTS</b>	<b>34</b>
<b>5.2</b>	<b>CELL CULTURE</b>	<b>35</b>
<b>5.3</b>	<b>MYCOPLASMAE TEST</b>	<b>35</b>
<b>5.4</b>	<b>SOLUBILIZATION OF PEPTIDES</b>	<b>36</b>
<b>5.5</b>	<b>FLUORESCENCE MEASUREMENT</b>	<b>36</b>
<b>5.5.1</b>	<b>SELECTION OF FLUORESCENCE DYE</b>	<b>37</b>
<b>5.5.2</b>	<b>FLUORESCENCE INTENSITIES OF TAMRA LABELED PEPTIDES</b>	<b>37</b>
<b>5.6</b>	<b>CELLULAR UPTAKE</b>	<b>38</b>
<b>5.7</b>	<b>THE DELIVERY OF TAMRA LABELED PEPTIDES</b>	<b>39</b>
<b>5.8</b>	<b>CONFOCAL LASER SCANNING MICROSCOPY</b>	<b>41</b>
<b>5.9</b>	<b>CELL VIABILITY ASSAY</b>	<b>42</b>
<b>5.10</b>	<b>EVALUATION OF INTERNALIZATION PATHWAY</b>	<b>43</b>

<b>5.11</b>	<b>PEPTIDE STABILITY IN HUMAN SERUM</b>	<b>44</b>
<b>5.12</b>	<b>CO-LOCALIZATION OF CAL PDZ AND ICAL</b>	<b>45</b>
5.12.1	PRODUCTION OF COMPETENT CELLS	45
5.12.2	TRANSFORMATION OF DH5ALPHA BACTERIA	45
5.12.3	TRANSFECTION OF CACO-2 CELLS FOR MICROSCOPY EXPERIMENTS	46
<b>5.13</b>	<b>USSING CHAMBER MEASUREMENT</b>	<b>47</b>
<b>6</b>	<b>RESULTS.....</b>	<b>53</b>
<b>6.1</b>	<b>CHARACTERIZATION OF DIFFERENT ICAL VEHICLES</b>	<b>53</b>
6.1.1	AFFINITY MEASUREMENTS OF THE ICAL CONSTRUCTS AND CAL PDZ	53
6.1.2	VIABILITY ASSAY WITH CACO-2 CELLS	54
<b>6.2</b>	<b>VARIABILITY OF THE FLUORESCENCE INTENSITY OF THE ICAL PEPTIDES</b>	<b>56</b>
<b>6.3</b>	<b>INTERNALIZATION OF *CPP/*MYR-ICAL IN CACO-2 CELLS</b>	<b>58</b>
6.3.1	TIME DEPENDENT INTERNALIZATION OF *CPP/MYR-ICAL	59
6.3.2	INTERNALIZATION OF *ICAL AND CPP/MYR-ICAL IN COMPARISON	60
6.3.3	PEPTIDE RELEASE AFTER CELLULAR INTERNALIZATION	61
6.3.4	CELLULAR ICAL LOCALIZATION DEPENDING ON THE USED CARRIER	63
6.3.4.1	*MYR-ICAL INTERNALIZATION AND CELLULAR LOCALIZATION	67
6.3.5	TEMPERATURE AND ATP DEPENDENCY OF INTERNALIZATION	69
<b>6.4</b>	<b>EVALUATION OF THE STABILITY OF ICAL; CPP-ICAL AND MYR-ICAL</b>	<b>71</b>
6.4.1	IMPROVEMENT OF PRECIPITATION CONDITIONS.	73
6.4.2	COMPARISON OF THE PROTEASE STABILITY OF ICAL COMPOUNDS	74
<b>6.5</b>	<b>CO-LOCALIZATION OF *MPG-ICAL36 AND CAL PDZ IN CELLULO</b>	<b>77</b>
<b>6.6</b>	<b>MEASURING THE BIOLOGICAL EFFECT OF ICAL36 ON CFTR ACTIVITY</b>	<b>79</b>
6.6.1	THE SUITABLE CELL LINE AND MPG-ICAL36 CONCENTRATION	81
6.6.2	FUNCTIONALITY WITH HT29/B6 CELLS AND MPG-ICAL36	83
<b>6.7</b>	<b>HUMAN RECTAL EPITHELIAL SUCTION BIOPSIES</b>	<b>85</b>
6.7.1	INFLUENCE OF MPG-ICAL36 ON VIABILITY	85
6.7.2	INTERNALIZATION OF MPG-ICAL36	86
6.7.3	EFFECT OF MPG-ICAL36 AND VX-809 ON CFTR FUNCTION	86
<b>7</b>	<b>DISCUSSION.....</b>	<b>90</b>
<b>7.1</b>	<b>CELLULAR INTERNALIZATION OF CPP-ICAL AND MYR-ICAL IN CACO-2 CELLS AND BIOPSY SAMPLES</b>	<b>91</b>
<b>7.2</b>	<b>FIRST INSIGHT IN THE INTERNALIZATION MECHANISM OF *CPP-ICAL AND *MYR-ICAL IN CACO-2 CELLS</b>	<b>93</b>
<b>7.3</b>	<b>DETAILED EVALUATION OF CPP/MYR-ICAL INTERACTION WITH THE CAL PDZ DOMAIN IN VITRO AND IN CELLULO</b>	<b>95</b>
<b>7.4</b>	<b>USSING CHAMBER EXPERIMENTS: THE CHALLENGE TO MEASURE THE BIOLOGICAL ACTIVITY OF MPG-ICAL AS A "STABILIZER"</b>	<b>97</b>
<b>7.5</b>	<b>PROTEASE STABILITY OF THE CPP/MYR-ICAL CONJUGATES AS PREREQUISITE FOR A LONG TERM STABILIZER EFFECTIVITY</b>	<b>100</b>

---

<b><u>8</u></b>	<b><u>CONCLUSION .....</u></b>	<b><u>102</u></b>
<b><u>9</u></b>	<b><u>DANKSAGUNG.....</u></b>	<b><u>104</u></b>
<b><u>10</u></b>	<b><u>REFERENCES .....</u></b>	<b><u>106</u></b>
<b><u>11</u></b>	<b><u>EIDESSTÄTTLICHE ERKLÄRUNG .....</u></b>	<b><u>111</u></b>
<b><u>12</u></b>	<b><u>CURRICULUM VITAE.....</u></b>	<b><u>112</u></b>

## II List of figures

<i>Figure 1: Structure of the CFTR</i>	14
<i>Figure 2: PDZ structure and the interaction with its binding partner</i>	16
<i>Figure 3: Regulation of CFTR trafficking</i>	18
<i>Figure 4: Categories of CFTR mutations</i>	20
<i>Figure 5: The underlying principle of “potentiators” and “correctors”</i>	22
<i>Figure 6: “Stabilizers” address the half-life deficiency</i>	24
<i>Figure 7: Endocytosis</i>	28
<i>Figure 8: Bleaching effect</i>	38
<i>Figure 9: Cellular internalization</i>	39
<i>Figure 10: Test of internalization pathway</i>	44
<i>Figure 11: Measurement of the protease stability</i>	45
<i>Figure 12: Transformation of E.coli Dh5<math>\alpha</math> cells and transfection of eukaryotic Caco-2 cells</i>	47
<i>Figure 13: Schematic representation of an Ussing chamber</i>	49
<i>Figure 14: Current values of Caco-2 cells after treatment with different ion channel stimulators</i>	50
<i>Figure 15: Current values of HT29/B6 cells after treatment with different ion channel stimulators</i>	51
<i>Figure 16: Influence of CPP/Myr-iCAL36/42 to the viability of Caco-2 cells</i>	56
<i>Figure 17: The fluorescence intensities of TAMRA are dependent on coupled peptides</i>	57
<i>Figure 18: Experimental setup for internalization tests</i>	59
<i>Figure 19: Internalization rates of *MPG/*Pen-iCal42 and *Myr-iCal42</i>	60
<i>Figure 20: Internalization with *CPP/Myr-iCAL and *iCAL treated Caco-2 cells</i>	61
<i>Figure 21: The release of *Pen/*MPG-iCal42 and *Myr-iCal42</i>	62
<i>Figure 22: Dose-dependent intracellular distribution of *CPP-iCAL36 in Caco-2 cells</i>	64

---

<i>Figure 23: Representative images of the internalization of *CPP-iCAL in Caco-2 cells</i>	66
<i>Figure 24: The internalization efficiency of *Myr-iCAL42 depending on the incubation time</i>	68
<i>Figure 25: Experimental setup for analyzing ATP dependency</i>	70
<i>Figure 26: Evaluation of the internalization mechanism of *CPP/Myr-iCAL</i>	71
<i>Figure 27: General procedure of stability tests and comparison of two different spectra</i>	72
<i>Figure 28: Different precipitations to find the suitable procedure</i>	74
<i>Figure 29: Degradation of CPP-iCAL36/42 and iCAL36/42 in human serum</i>	75
<i>Figure 30: Protease stability of Myr-iCAL36 and Myr-iCAL42 in human serum</i>	76
<i>Figure 31: Co-localization experiments of *MPG-iCAL36 and *MPG-SC with GFP-CAL</i>	79
<i>Figure 32: Schematic representation of an Ussing chamber</i>	81
<i>Figure 33: The dependency of resistance of the concentration of MPG-iCAL36</i>	83
<i>Figure 34: Influence of MPG-iCAL36 to the Cl<sup>-</sup> secretion of CFTR</i>	84
<i>Figure 35: Cytotoxic effect of MPG-iCAL36 to rectal epithelial biopsies</i>	85
<i>Figure 36: Internalization of *MPG-iCAL36 in cells of human rectal epithelial biopsies</i>	86
<i>Figure 37: Effect of MPG-iCAL36 and VX-809 on Cl<sup>-</sup> secretion of human rectal biopsies</i>	88

**III List of tables**

<i>Table 1: Evaluation of <math>K_i / K_d</math> values (in <math>\mu\text{M}</math>)</i>	54
<i>Table 2: Multiplication factors of different fluorescence intensities of TAMRA</i>	58



## 1 Summary

Cystic fibrosis (CF) is a life-shortening multisystem disease with an incidence of around 1:3,000 individuals. CF is an autosomal recessive genetic disorder which affects the cystic fibrosis transmembrane conductance regulator (CFTR) chloride ion channel expressed in epithelial cells. More than 1,900 different mutations are known in the CFTR gene, whereby the most common is a deletion of a phenylalanine residue at position 508 of the protein (F508del). These primary defects in epithelial ion transport affect many tissues such as the lungs and the pancreas. Symptomatic treatments are beneficial but impose a large compliance burden, and life expectancy remains under 40 years. Thus, there is a critical unmet need to correct the underlying molecular defect: loss of function in the CFTR. A breakthrough in the molecular treatment of CF was recently shown in a phase 2 trial. Combined administration of VX-809 as “corrector” that acts as a chemical chaperone to assist F508del-CFTR folding and Kalydeco (VX-770) as “potentiator” that enhances CFTR activity showed an improvement of lung function (FEV1) by >10 % for 25 % of patients homozygous for F508del. Success was all the more impressive, because the drugs were designed to address only two of the three molecular defects of F508del-CFTR (inefficient folding and impaired channel gating). In fact, no agent specifically addresses the third defect: rapid degradation of rescued F508del-CFTR. Thus, our hypothesis is that therapeutic targeting of the degradation of mature protein will significantly enhance current combination therapies to rescue F508del-CFTR.

In this context, we have validated the CFTR-associated ligand (CAL) as key mediator of CFTR degradation and thus have developed specific peptide inhibitors of CAL (iCAL), as first “stabilizer” compounds that extend CFTR apical half-life and increase chloride channel activity in CF bronchial epithelial cells, both alone and additively in combination with a “corrector”.

In the present work, we will characterize different carriers such as cell penetrating peptides (CPPs) or a fatty acid (myristic acid, Myr) covalently coupled to iCAL36/42 and we will evaluate their potential activity as “stabilizer”. First of

all, we clearly demonstrated that the coupling of a carrier (CPP or Myr) increase significantly the uptake of iCAL peptides in Caco-2 cells as revealed by spectroscopic fluorescence measurements from cell lysis or by confocal microscopy. However, Myr-iCAL conjugates enter the cells in delayed manner compared to the CPP-iCAL because they stayed trapped in the cell membrane during the first hour of incubation. After a longer period ( $\approx 3$  hours), all used molecules are internalized in the cytosol of Caco-2 cells. Viability experiments on polarized Caco-2 cells revealed no significant cytotoxic effect of all compounds even at 100  $\mu\text{M}$ . Internalization experiments at 4°C or under ATP-depletion revealed that the CPP-iCAL conjugates enter the cells by direct translocation (energy-independent) whereas the uptake of Myr-iCAL compounds at 4°C is reduced (temperature-dependent) probably due to the composition of the membrane. Affinity measurements by fluorescence polarization (FP) indicated that the N-terminal prolongation (by the CPP or Myr) showed a 10 – 20-fold increase in affinity, which could of great interest for the pharmacological development of our compounds. More importantly and for the first time, we can clearly show a specific co-localization of MPG-iCAL36 with overexpressed full-length CAL protein *in cellulo*, a phenomenon which is not seen with the scrambled sequence (MPG-SC).

To assess the potential of our vectorized iCAL peptides to act as “stabilizer”, we measured the change in chloride secretion through the CFTR using Ussing chamber experiments. First attempts done on polarized cells (Caco-2 and HT29/B6 cells) with MPG-iCAL36 pointed incomprehensible problems concerning a drastic decrease of epithelial resistance without a direct effect on cell viability. To obtain suitable epithelial resistance values the Ussing experiments were performed at low MPG-iCAL36 concentration (5  $\mu\text{M}$ ), however, at this concentration no increase in chloride secretion could be determined.

In a more physiological context, we have also analyzed the internalization, the cytotoxic effect and the ‘stabilizing’ activity of MPG-iCAL36 in human rectal epithelial biopsies from CF-patients. For the first time, we were able to show an increase in  $\text{Cl}^-$  efflux from the biopsy samples after the MPG-iCAL36 incubation (Ussing chamber experiments). More importantly, co-incubation of MPG-iCAL36

and VX-809 revealed an additional increase in Cl<sup>-</sup> efflux showing a synergistic effect of both molecules.

Finally, we looked on protease stability of all our used compounds which is an important requirement in the development of therapeutics. CPP-iCAL compounds are degraded within the first two hours, whereas Myr-iCAL compounds are more stable (>24 hours).

Altogether, the presented results are very encouraging concerning the development of CPP- or Myr-based iCAL inhibitors. Tri-therapeutic approach combining a “corrector”, a “potentiator”, and a “stabilizer” should open up promising future treatments to attenuate CF symptoms and to increase life expectancy of CF-patients.

## 2 Zusammenfassung

Cystische Fibrose ist eine lebensverkürzende Multisystemerkrankung mit einer Häufigkeit von 1:3.000 Individuen. CF ist eine autosomal rezessiv vererbte Erkrankung, welche den Cystic Fibrosis Transmembrane Conductance Regulator (CFTR) betrifft, der von Epithelzellen exprimiert wird. Es sind mehr als 1.900 unterschiedliche Mutationen im CFTR Gen bekannt, wobei die häufigste eine Deletion des Phenylalaninrestes in Position 508 des Proteins (F508del) darstellt. Diese primären Defekte des epithelialen Ionentransportes betreffen viele Gewebe, wie z.B. die Lunge und das Pankreas. Symptomatische Behandlungen sind erfolgreich, aber erschweren die Compliance und die Lebenserwartung bleibt unter 40 Jahren. Daher gibt es einen dringenden bisher nicht umgesetzten Bedarf, den zugrundeliegenden molekularen Defekt zu beheben: nämlich den Funktionsverlust des CFTR selbst. Einen Durchbruch in der molekularen Behandlung von CF wurde kürzlich in einem Phase 2 Zulassungsverfahren gezeigt. Die kombinierte Verabreichung von VX-809, einem „Corrector“ der als ein chemisches Chaperon zur Unterstützung der Faltung des F508del-CFTRs fungiert und Kalydeco (VX-770) als „Potentiator“ der die CFTR Aktivität erhöht, zeigte eine Verbesserung der Lungenfunktion (FEV1) um 10 % von 25 % der Patienten, die homozygot für die F508del Mutation sind. Der Erfolg war umso beachtlicher, weil diese Medikamente nur auf zwei der drei molekularen Defekte abzielten (ineffiziente Faltung und eine gestörte Leitung des Ionenkanals). Tatsächlich ist es so, dass kein Wirkstoff den dritten Defekt adressiert: den schnellen Abbau von verbliebenem F508del-CFTR. Darauf beziehend ist unserer Hypothese, dass ein Therapeutikum, das den Abbau von ausgereiftem Protein beeinflusst, aktuelle Kombinationstherapien zum Erhalt von F508del-CFTR signifikant verbessern könnte.

In diesem Zusammenhang haben wir den CFTR assoziierten Liganden (CAL) als Schlüsselmediator des CFTR Abbaus ermittelt und daraus folgend einen spezifischen Peptidinhibitor von CAL (iCAL) entwickelt, der als erster „Stabilisator“ die apikale CFTR Halbwertszeit verlängert und die

Chloridionenkanal-Aktivität in bronchialen CF Epithelzellen erhöht, beides allein und additiv in Kombination mit einem „Corrector“.

In der hier vorliegenden Arbeit, werden wir unterschiedliche Transporter wie zellpenetrierende Peptide (CPP) oder eine Fettsäure (Myristinsäure) kovalent an iCAL36/42 koppeln und ihre mögliche Aktivität als „Stabilizer“ evaluieren. Nach einer längeren Zeiteinheit ( $\approx 3$  hours) sind alle Moleküle in das Zytosol von Caco-2 Zellen internalisiert. Viabilitätsexperimente zeigten keinen signifikanten zytotoxischen Effekt bei polarisierten Caco-2 Zellen nach Inkubation mit allen Komponenten sogar bei einer Konzentration von  $100 \mu\text{M}$ . Internalisierungsexperimente bei  $4^\circ\text{C}$  oder unter ATP-Depletion machten deutlich, dass die CPP-iCAL Konjugate in die Zellen durch direkte Translokation eindringen (energieunabhängig), während die Aufnahme der Myr-iCAL Komponenten unter  $4^\circ\text{C}$  (temperaturabhängig) wahrscheinlich durch die Beschaffenheit der Membranen reduziert ist. Affinitätsmessungen durch Fluoreszenzpolarisation zeigen, dass eine N-terminale Verlängerung (durch ein CPP oder Myristinsäure) eine 10-20 fache Erhöhung der Affinität zur Folge hat, was von größtem Interesse für die pharmakologische Entwicklung unserer Komponenten sein könnte. Zum ersten Mal, konnten wir eine klare Kollokalisierung von MPG-iCAL36 mit einem überexprimierten CAL protein *in cellulo* zeigen, ein Phänomen das mit der veränderten iCAL Sequenz (MPG-SC) nicht zu sehen war.

Um das Potential als „Stabilisator“ unseres vektorisierten iCAL Peptides zu beurteilen, bestimmten wir mit Ussing Kammer Experimenten die Änderung der  $\text{Cl}^-$  Sekretion durch den CFTR. Erste Versuche mit polarisierten Zellen (Caco-2 und HT29/B6 Zellen) und MPG-iCAL36 zeigten jedoch unklare Probleme, die den drastischen Abfall des epithelialen Widerstandes ohne direkten Einfluss auf die Zellviabilität betrafen. Um verwendbare epitheliale Widerstandswerte zu erhalten, mussten wir die Ussing Experimente mit einer niedrigen MPG-iCAL36 Konzentration ( $5 \mu\text{M}$ ) durchführen und konnten letztlich keinen Anstieg der  $\text{Cl}^-$  Sekretion verzeichnen.

Für einen physiologischeren Kontext haben wir mit humanen epithelialen Rektumsbiopsien ebenfalls die Internalisierung, die Zytotoxizität und die

Stabilisierungsaktivität von MPG-iCAL36 analysiert. Zum ersten Mal waren wir in der Lage einen Anstieg des Cl<sup>-</sup> Ausstromes bei Biopsieproben nach MPG-iCAL36 Inkubation (Ussing Kammer Experimente) zu zeigen. Noch wichtiger dabei war, dass die Inkubation von MPG-iCAL36 und VX-809 zusammen einen zusätzlichen Anstieg des Cl<sup>-</sup> Transportes zur Folge hatte, was einen synergistischen Effekt zeigt.

Zum Schluss untersuchten wir die Proteasestabilität aller unserer benutzten Komponenten, was eine wichtige Voraussetzung in der Entwicklung von Medikamenten ist. Die CPP-iCALs wurden während der ersten 24 hours komplett abgebaut, wohingegen die Myr-iCALs stabiler waren (>24 hours).

Insgesamt sind die hier präsentierten Ergebnisse sehr ermunternd bezüglich der Entwicklung von CPP- oder Myr- basierten iCAL Inhibitoren. Ein dreitherapeutischer Ansatz der einen „Corrector“, einen „Potentiator“ und einen ‘Stabilisator’ verbindet, könnte eine vielversprechende Zukunft der Behandlung eröffnen, die dann die CF Symptome abmildert und die Lebenserwartung von CF Patienten erhöht.

## 3 Introduction

### 3.1 The pathology of cystic fibrosis

Cystic fibrosis (CF), also known as mucoviscidosis, is an autosomal recessive genetic disorder affecting the gene of the cystic fibrosis transmembrane conductance regulator (CFTR) chloride ion channel [1; 2]. The CFTR gene is located on the long arm of chromosome 7 and its structure comprises 27 exons spanning over 190 kb [1]. CF is one of the most common single-gene disorders in the Caucasian population, with an incidence between 1 in 3000 to 1 in 3300 individuals [1; 3]. More than 1900 different mutations are known in the CFTR gene [4]. The most common mutation is a deletion of a phenylalanine residue at amino acid position 508 of the protein (F508del). It is found in 70 % of the CF chromosomes and therefore 90 % of the CF patients have at least one F508del allele. While 10 – 20 less common mutations represent a further 10 – 15 % of all mutant alleles, the frequency depends on the ethnic background of the patient [5; 6]. Cystic fibrosis is a multisystem disease that is characterized by salty sweat with elevated sweat chloride, chronic cough, sinopulmonary disease, pancreatic insufficiency and poor growth due to the poor absorption of nutrients through the affected gastrointestinal tract [2; 3]. The most affected organ is the lung. In airway epithelia, loss of CFTR impairs mucociliary clearance and facilitates chronic bacterial infections. Chronic lung infections are the primary cause of morbidity and mortality in cystic fibrosis [7].

### 3.2 Characteristics of the CFTR ion channel

The CFTR is a cAMP-regulated chloride channel located primarily at the apical or luminal surfaces of epithelial cells of mucus producing organs such as the lung, intestine, pancreas, kidney as well as male reproductive tract [8]. CFTR is a member of the ATP-binding cassette (ABC) transporter family of membrane proteins which use ATP hydrolysis to pump substrates across cellular

membranes, against a concentration gradient. It is the only known ABC family member that acts as an ion channel. CFTR also operates as a modulator over a wide variety of other ion channels, transporters, and processes, such as the epithelial Na<sup>+</sup> channel (ENaC). CFTR is a 1480-residue long membrane protein, with the typical ABC transporter architecture of two membrane spanning domains (MSD) and two nucleotide binding domains (NBD). Unique to CFTR is an additional regulatory (R) region, as well as long N- and C-terminal extensions about 80 and 30 residues in length, respectively. All these domains are arranged from N- to C-terminus: MSD1-NBD1-R-NBD2-MSD2 (Figure 1). The membrane spanning domains contain six helices and the cytosolic nucleotide binding domains can bind and hydrolyze ATP. The position of the most frequent mutation F508del is in NBD1 [9]. The regulatory domain contains a number of charged residues and a multiple phosphorylation sites as substrates for protein kinases A and C, cGMP-dependent protein kinase II, etc. The N- and C-terminal tails of the chloride channel are in the cytoplasm and mediate the interaction between CFTR and a wide variety of binding proteins [10; 8; 11].

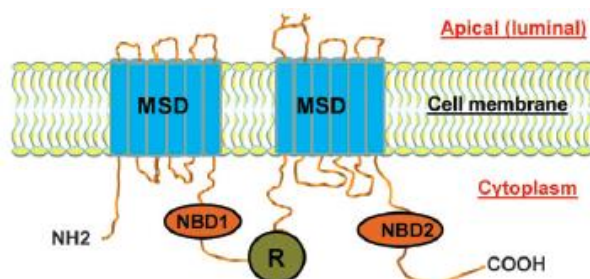


**Figure 2: Structure of the CFTR**

The CFTR is composed of two repeated motifs, each consisting of a membrane spanning domain (MSD) and a nucleotide binding domain (NBD). These two identical motifs are linked by a cytoplasmic regulatory (R) domain. The amino and carboxyl tails of the CFTR mediate the interaction of CFTR and other proteins [8].

### 3.3 Targeting post-endocytic degradation of mature CFTR

Because only 10 – 35 % of wild-type (WT) activity may be required for therapeutic benefit [6], many efforts have been made to identify “corrector” and “potentiator” compounds that address the primary folding and gating defects of



F508del-CFTR, respectively [12; 13]. There is now a growing prospect that the maturation and specific activity of F508del-CFTR can be pharmacologically enhanced. However, the rescued protein remains unstable [11; 14; 15]. Optimal therapy is thus likely to require repair of all three defects: folding, open probability, and stability.

To identify “stabilizers” – a new class of drugs that extend the half-life of F508del-CFTR we targeted a key regulator of its post-endocytic trafficking. The CFTR-associated ligand (CAL) negatively regulates F508del-CFTR cell surface abundance [16]. However, CFTR interacts not only with CAL, but also with the Na<sup>+</sup>/H<sup>+</sup> exchanger regulatory factors NHERF1 and NHERF2, which counteract CAL’s effect, enhancing the activity and the abundance of F508del-CFTR at the apical membrane [9; 17; 18].

All these protein complexes that are necessary to regulate the CFTR level in the plasma membrane of mucus producing epithelial cells, are regulated via the outstanding role of PDZ domains – a domain family which are widespread in nature and range from *Drosophila* to humans. The name PDZ domain is an abbreviation for postsynaptic density protein-95 (PSD-95), discs large tumor suppressor (DLG1) and zonula occludens-1 (ZO-1) [19; 20]. PDZ domains contain five to six  $\beta$ -strands ( $\beta$ A- $\beta$ F) and two  $\alpha$ -helices ( $\alpha$ A and  $\alpha$ B). In general the PDZ domains interact with the C terminus of their binding partners as an antiparallel  $\beta$ -strand in a groove between  $\beta$ B-strand and  $\alpha$ B-helix [21]. One example for the structure of a PDZ domain and the interaction between a PDZ domain and its partner is shown in figure 2.

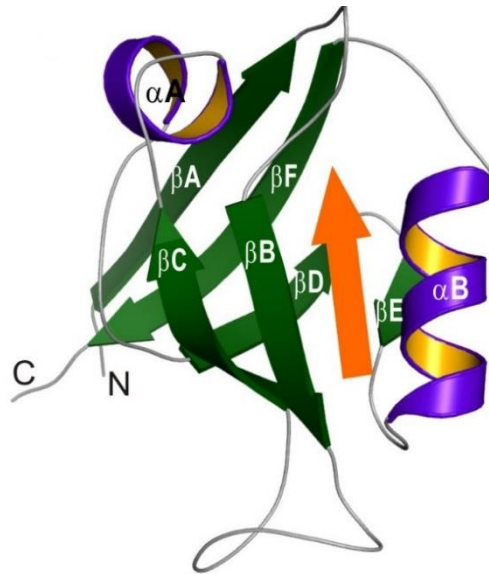


**Figure 2: PDZ structure and the interaction with its binding partner**

The PDZ domain (PSD-95 PDZ2) contains six  $\beta$ -sheets and two  $\alpha$ -helices. A peptide ligand (orange) is shown bound to the PDZ. [<http://bcz102.ust.hk/pdzex/>]

In an earlier publications PDZ domains were divided into three specificity classes which are defined by their target motif structures.  $X[T/S]X\phi\text{-COOH}$  is the class I motif,  $X\phi X\phi\text{-COOH}$  the class II motif, and  $X[D/E]X\phi\text{-COOH}$  the class III motif ( $X$  is any natural amino acid and  $\phi$  is a hydrophobic amino acid). But recent publications reveal that these conventional motifs are not adequate to explain the PDZ domain interaction. Especially since it is known that each residue of the interaction partner contributes to the binding specificity. Different groups use computational approaches to differentiate binding partners of PDZ domains and built a PDZ interaction network [20; 21]. Kousik Kundu and Rolf Backofen for example published a phylogenetic tree of all available PDZ domains from human, mouse, fly and worm in 2014. They identified 138 PDZ families comprising of 548 PDZ domains of the before mentioned organisms [22].

A detailed model describing the regulation of molecular switches of CFTR trafficking is shown in figure 3. As mentioned before, the CFTR-associated ligand (CAL) plays an important role in this post-endocytic CFTR degradation. The CAL protein contains two coiled-coiled domains for association with membranes and one PDZ domain for binding the C terminus of CFTR [8]. The SNARE (Soluble *N*-ethylmaleimide sensitive factor attachment protein receptors) protein SYN-6

(syntaxin-6) tethers CAL to the trans-Golgi network (TGN) and facilitates the trafficking of CAL-CFTR from TGN to lysosomes which provokes the depletion of CFTR. Another important protein is the Rho GTPase TC10. If TC10 is activated by GTP it also binds to the coiled-coiled domain of CAL and this facilitates the transport of CFTR-containing vesicles to the membranes of mucus producing cells [18].

NHERF1 and NHERF2 contain two PDZ domains and are also involved in the regulation of CFTR in cell membranes. Interaction with NHERF is necessary for the insertion of CFTR in the apical membrane. If the first PDZ domain of NHERF interacts with the cytoplasmic tail of CFTR then the second PDZ domain is blocked due to the CFTR binding. This process is only interrupted in the presence of active ezrin [23; 24].

In the recycling pathway (Figure 3) with recycling endosomes the NHERF1-ezrin complex is able to block CAL from interacting with CFTR. Finally the CFTR is transported to and inserted into the cell membrane. This process is promoted by myosin-Vb that drives the recycling endosomes toward actin and the GTPase RAB11. The NHERF1-ezrin complex is able to stabilize CFTR in the plasma membrane which is supported by the binding of the complex to the sub-membrane actin network. When NHERF1-ezrin dissociates from the CFTR the CFTR is released in the endocytic pathway resulting either in CAL binding to it and the CFTR being endocytosed subsequently or in NHERF-ezrin interacting with it which leads to CFTR entering the recycling pathway and being delivered to the apical membrane again [18].

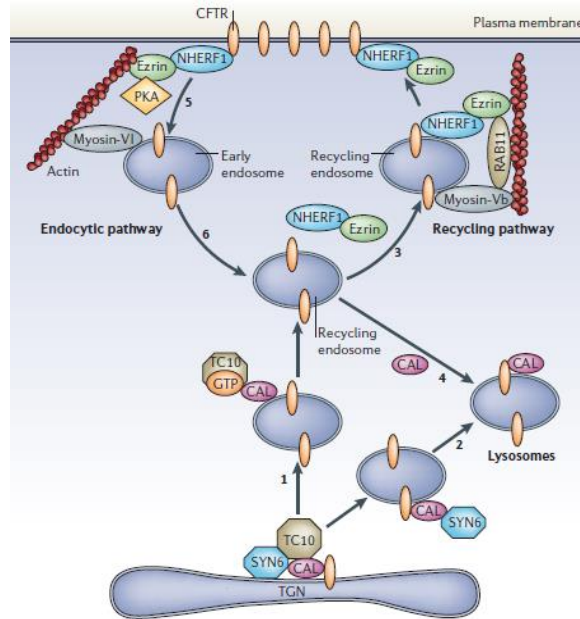


**Figure 3: Regulation of CFTR trafficking**

**1 and 2:** SYN-6 (syntaxin-6) tethers CAL to the trans-Golgi network (TGN) and facilitates the trafficking of CAL-CFTR from TGN to lysosomes which finally leads to the degradation of CFTR proteins. Or TC10 facilitates through step 3 the transport of CFTR to the apical membrane. **3:** NHERF1 (Na<sup>+</sup>/H<sup>+</sup> exchanger regulatory factor isoform-1)-ezrin complex is able to displace CAL from interacting with CFTR. Finally the CFTR is transported and inserted into the cell membrane which is promoted by myosin-Vbn and the GTPase RAB11. **4:** If CAL binds the CFTR the endosome is changing to lysosome **5:** The NHERF1-ezrin complex stabilizes CFTR in the plasma membrane. **6:** When NHERF1-ezrin detached CFTR the Cl<sup>-</sup> channel is released in the endocytic pathway which offers two opportunities. Either CAL binds and the CFTR is endocytosed (step 4) or NHERF-ezrin interacts and the CFTR enters the recycling pathway and is again delivered to the apical membrane (step 3).

### 3.4 CFTR mutations and their classification

The CFTR mutation is quite common in the general population, with millions of asymptomatic carriers estimated in Europe and the United States. An individual with CF can carry an identical CFTR mutation on either allele, or two different CFTR mutations — one on each allele. Depending on the type of mutation, the effect on disease severity and prognosis can be quite different. More than 1900 different mutations are known in the CFTR gene. This high number of mutations results in diverse effects to the CFTR protein such as an affected production of full length protein, a defective protein processing or a decreased quantity of channels that reach the cell membrane [2]. Different databases were created in the last years in various countries to summarize the CFTR mutations such as “the

CFTR mutations database” (<http://www.umd.be/CFTR/>) in Belgium or the “Cystic Fibrosis Mutation Database” (<http://www.genet.sickkids.on.ca/app>) in the United-States only to cite some few examples.

All the defects can be categorized into six different classes on the basis of the mechanisms by which they disrupt the synthesis, traffic and function of CFTR [25]:

- Class I mutations are characterized by an impaired synthesis of CFTR proteins due to premature truncation or nonsense alleles (designated by “X”, such as G542X). Nonsense mutations result in mRNA degradation by a process called nonsense mediated decay. One example for a class I mutation is 394delTT which is an alteration in exon 3 [26].

- Class II mutations lead to an inadequately processed protein which is recognized and targeted by the endoplasmatic reticulum (ER) quality control. Finally the defective CFTR protein is degraded shortly after synthesis before it can reach the cell surface. F508del, the most common mutation, is among others such as N1303K categorized as a class II defect. In the case of F508del the mutation leads to the loss of phenylalanine at 508<sup>th</sup> position of the protein. N1303K is a substitution at nucleotide position 4041 of the CF gene which causes a change from asparagine (N) to lysine (K) at amino acid position 1303 of the CFTR protein [27].

- Class III mutations are defined by abnormal ion channel activity. The missense mutation G551D for example possesses a diminished ATP binding and hydrolysis through the nucleotide binding domain, resulting in a disordered regulation [28].

- Class IV defects lead to a deficient chloride conductance or channel gating. The R334W mutation belongs to class IV defects in which arginine (R) is changed to tryptophane (W) at codon 334 of the CFTR gene [29].

- Class V mutations are characterized by a reduced number of CFTR transcripts for example due to a promoter or splicing abnormality. For example the missense mutation A455E in the first nucleotide binding domain reveals reduced levels of mature CFTR [30].

It is interesting that the protein level vary amongst patients and even amongst the organs of each patient.

- Class VI mutations cause an accelerated turnover from the cell surface. For instance, the deletion mutant c.120del23 lacks the N-tail which is required for cytoskeleton anchoring because of the absence of a CFTR protein initiation codon [31][32; 25; 33].

The tremendous diversity of mutations in the CFTR gene causes a large variability in disease severity. Patients with two class I, II, or III alleles display the full spectrum of cystic fibrosis characteristics such as serious lung diseases and pancreatic insufficiency. Whereas patients with at least one class IV, V, or VI allele show milder forms of cystic fibrosis up to a complete lack of symptoms in females [34] (Figure 4).

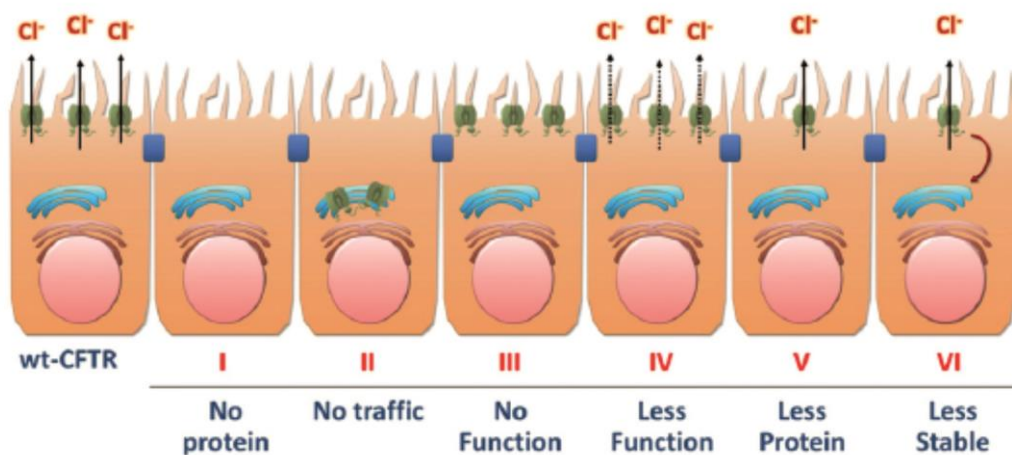


**Figure 4: Categories of CFTR mutations**

Class I mutations are characterized by the absence of synthesis of CFTR. Class II mutations lead to a defective protein maturation and premature degradation. Class III defects result in a disordered regulation, such as a diminished ATP binding and hydrolysis. Class IV mutations cause a defective chloride conductance or channel gating. Class V mutations lead to a reduced number of CFTR transcripts due to promoter or splicing abnormalities. Class VI defects result in an accelerated turnover from the cell surface.

### 3.5 Research and treatment of Cystic Fibrosis

The most serious clinical manifestation of CF is in the lung and it is characterized by airway obstruction, infection and inflammation. Consequently, many treatments target one or more of these symptoms for example antibiotics, mucolytic agents and anti-inflammatory substances. Intravenous and oral antibiotics are the drug of choice in the past to treat chronic manifestation of CF. Many CF patients use one or more antibiotics at all times, even when they are

not infected, to prophylactically suppress infections. But severe side effects caused the development of inhaled antibiotics (Tobramycin, Aztreonam, Colistimethate). Their advantage is that high drug concentrations are restricted in the lung and therefore the side effects are reduced. Furthermore anti-inflammatory drugs such as azithromycin are antimicrobial and anti-inflammatory and cause a decreased production of pro-inflammatory cytokines by monocytes and epithelial cells which finally leads to a reduction in the number of exacerbations in Cystic Fibrosis.

Imbalanced ionic transport leads to an abnormal mucus composition. Mucolytics reduce mucus viscosity in the lung and improve the secretion clearance. Mannitol for example improves mucus clearance, probably by means of changing the mucus' viscosity, increasing the hydration in the airway, or increasing ciliary motility [35; 6].

One of the last therapeutical options in CF is the lung transplantation. Lung transplanted patients with CF show survival rates of between 60 - 70 % 5 - 7 years post transplantation [36].

The therapies mentioned so far treat CF disease manifestations. But there is a different approach that directly targets the CFTR anion channel defect by using two kinds of small molecules: "correctors" and "potentiators".

"Potentiators" such as VX-770 also known as Ivacaftor from Vertex Pharmaceuticals repair the gating and conductance defect of F508del-CFTR Cl<sup>-</sup> channel. VX-770 is able to activate F508del-CFTR chloride conductance and to restore F508del-CFTR open probability to almost that of wild-type CFTR when added together with a cAMP agonist. Ivacaftor is mainly used to correct the defect channel gating of cystic fibrosis caused by mutant G551D-CFTR [16]. There is limited information about the mechanism of action of "potentiators" but a direct interaction with the CFTR is discussed which facilitates the conformation change of the mutated CFTR or the activation of cAMP through activation of phosphodiesterases or inhibition of phosphatases which cause an increase of phosphorylation of protein kinase A (Figure 5).

“Correctors” such as VX-809 also developed by Vertex Pharmaceuticals (in phase II clinical trials) target the F508del-CFTR cellular misprocessing and thus restore the CFTR expression and function in CF mucus producing epithelial cells. The molecular mechanism of “correctors” is similar to those of the “potentiators” poorly understood. A function as a “pharmacological chaperone” seems plausible, the interaction with the mutated channel itself leads to a facilitated folding and cellular processing. “Correctors” could also influence the cellular protein-control machinery to affect mutated-CFTR recognition and processing. CFTR “correctors” and “potentiators” were identified through high-throughput screening. The best treatment of CF is of course a combination of both drugs because in the most cases of CF the patients express a mixture of different kinds of mutations and symptoms [15; 16] (Figure 5).

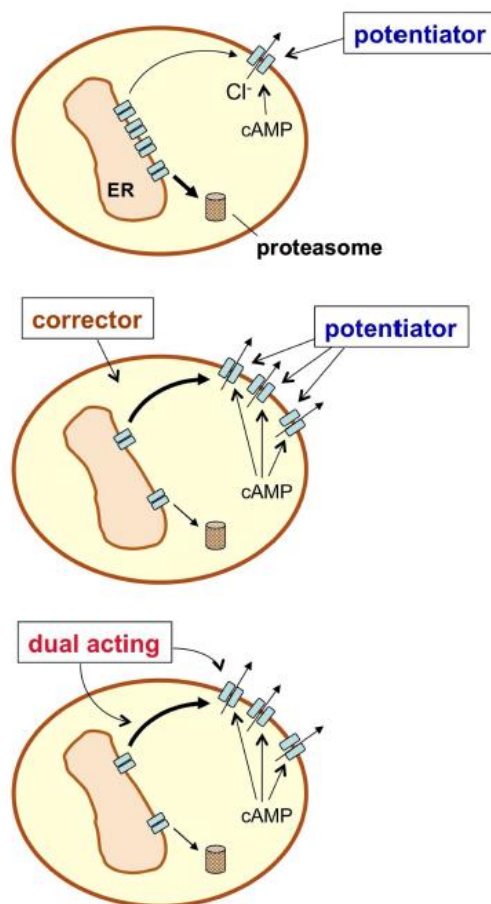


**Figure 5: The underlying principle of “potentiators” and “correctors”**

Two different small molecules are used in the treatment of Cystic Fibrosis.

The gating and conductance defects are treated with “potentiators” which modulate the opening of CFTR channels and thus the  $\text{Cl}^-$  transport. The treatment of CF with “correctors” causes an increase of the amount of CFTR  $\text{Cl}^-$  channels in the cell surface.

The best treatment of CF is with both agents together because most of CF patients suffer from a combination of molecular defects [37].

Another potential cure for cystic fibrosis is via gene therapy which is “The introduction or alteration of genetic material within a cell or organism with the intention of curing or treating a disease”[38]. In the case of cystic fibrosis this



means the insertion of a functional CFTR gene into airway epithelial cells [39]. Different constructs were used such as adenoviral, adeno-associated, lentiviral, cytoplasmic RNA viruses or non viral vectors [40]. 26 clinical trials with 450 patients were performed in the past. But the results showed only limited success. Very few cells internalized the vector and expressed the gene, which could be explained by viscous mucus, cilia beating or nuclear membranes [40].

### 3.6 Targeting the CFTR-CAL interaction to develop new therapeutics

“Correctors” and “potentiators” influence the misprocessing or the gating and conductance defect in Cystic Fibrosis. Another possibility to treat CF is via “stabilizers” that specifically address the half-life deficiency [41]. The key proteins in this research are CAL, NHERF1, and NHERF2. The three proteins regulate the abundance of CFTR proteins in the plasma membrane of mucus producing cells. CAL negatively regulates the cell surface amount of CFTR proteins. NHERF1/2 are able to displace CAL from interacting with the CFTR and improve the activity and the level of CFTR at the apical membranes [9]. Our hypothesis is that an inhibition of CAL activity by binding a short peptide to its PDZ binding domain should prevent the interaction of CAL and CFTR and therefore interrupt the degradation of CFTR. At this point it is important that the inhibitor does not affect the PDZ domains of the NHERF proteins [41] (Figure 6).

For engineering a selective CAL PDZ inhibitor human peptide libraries, substitution analysis and combinatorial libraries were synthesized. The general approach of these arrays is the synthesis of peptides on cellulose membranes based on SPOT technology [42]. As described above PDZ domains interact with the C term of their binding partners. Therefore peptides with a free C term were synthesized through the method of inverted peptides [43]. Finally the goal was the development of C terminal amino acid sequence motifs with affinity for CAL PDZ domain but not for the NHERF PDZ domains. The development of a CAL PDZ inhibitor resulted in the peptide iCAL36 with the amino acid sequence: ANSRWPTSII<sub>COOH</sub> [44].

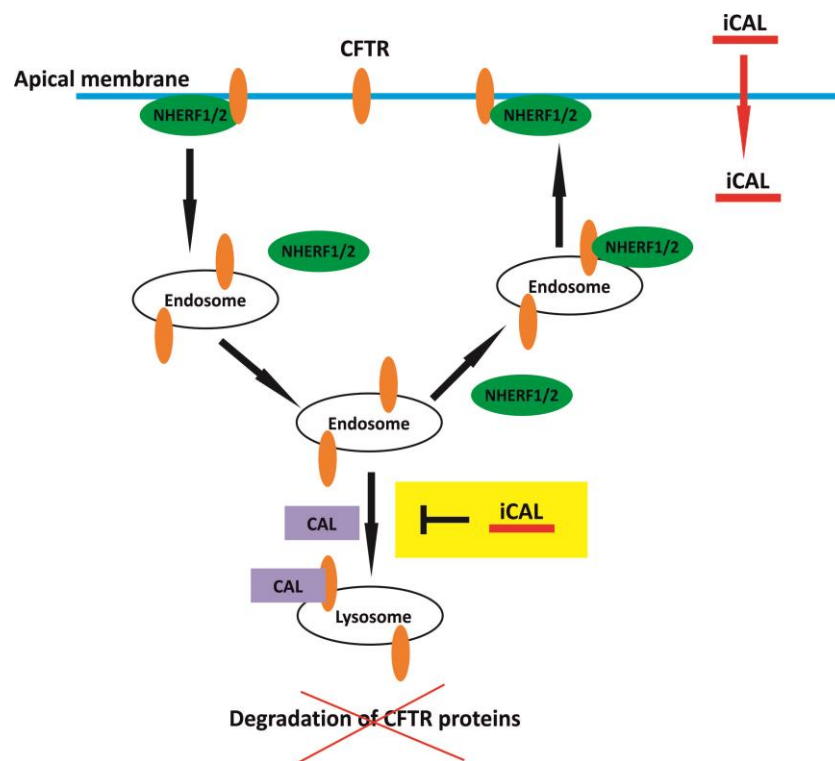


**Figure 6: “Stabilizers” address the half-life deficiency**

NHERF1/2 and CAL regulate the abundance of CFTR proteins in cell membranes of mucus producing cells. If NHERF1/2 interacts with CFTR the Cl<sup>-</sup> channel is transported to the apical membrane and subsequently inserted into the membrane. Furthermore NHERF1/2 stabilize CFTR in the membrane. But if NHERF1/2 dissociate and CAL binds it follows the degradation of CFTR proteins. The inhibition of CAL due to the interaction of iCAL with CAL PDZ should prevent the interaction between CAL and CFTR and interrupt the degradation of CFTR proteins.

To research all PDZ domains inhibited by iCAL36 pull down, mass-spectrometry assays for iCAL36 interactors were performed. To this end iCAL36 was incubated with whole cell lysate from human cystic fibrosis bronchial epithelial cells. Two PDZ proteins that interact with iCAL36 were found. One was CAL and the other one was the Tax-interacting protein-1 (TIP-1) [45]. TIP-1 targets for example regulating proteins which are involved in signaling pathways in cancer and other diseases [46]. To prevent the binding of iCAL36 to TIP-1 ComLib peptide arrays were synthesized varying two positions of the iCAL36 sequence. The peptide arrays were incubated with PDZ domains of either CAL or TIP-1. The result was another CAL PDZ inhibitor, named iCAL42 with single PDZ specificity without affecting NHERF1/2. iCAL42 is created by a single Trp-Leu substitution on position 5 of iCAL36 which leads to the amino acid sequence ANSRLPTSII [45]. On

one hand iCAL36 has a higher binding affinity than iCAL42 (Table 1), but on the other hand iCAL42 has a higher specificity than iCAL36.

The cell internalization of iCAL36 was initially achieved using the commercially available delivery reagent BioPORTER™. An increase in  $\Delta I_{sc}$  values of 25 % was achieved after the treatment of CFBE- $\Delta F$  cell monolayers with F\*-iCAL36 (500  $\mu M$ ):BioPORTER™ compared to the inactive construct F\*-SCR (scrambled version of iCAL36) [41].

### 3.7 Crossing biological membranes

Cell membranes are barriers that protect the cells from pathogens, small molecules, proteins, genetic material, and larger protein complexes in a nonspecific manner [47]. Additionally membranes are needed for the maintenance of the cells inner homeostasis, resulting in well-controlled import and export [48]. Therefore it is very difficult to transport substances such as peptides, proteins, nucleic acids, liposomes or nanoparticles into cells, both for research or medical treatment. Currently there are different ways used to overcome this barrier.

A physical method is electroporation which uses short electric impulses to increase the membrane permeability, thus allowing a transient exchange of matter across membranes [49].

Viral vectors are used to deliver genetic material into cells. Types of viral vectors are retroviruses, lentiviruses, adenoviruses and adeno-associated viruses [50].

Another possibility to overcome cell membranes is via nanoparticles. Various forms of nanoparticles were used including liposomes, polymer particles or micelles. For precise targeting and internalization nanoparticles are usually attached with antibodies, proteins, aptamers, peptides, folate and other small molecules. The surface altered particles enter the cells especially by receptor-mediated endocytosis, caveolae-mediated endocytosis, lipid raft mediated endocytosis and macropinocytosis.

As many other therapeutic agents iCAL can not translocate over cellular membranes without a carrier.

### 3.7.1 Cell penetrating peptides (CPP)

Cell penetrating peptides are a class of diverse peptides which comprise generally 5 - 30 amino acids. The advantage of CPP's is that they are able to translocate over cellular membranes and thus to act as a carrier for siRNA, nucleotides, small molecules, proteins and other peptides, both *in vitro* and *in vivo* [51]. During the last two decades numerous cell penetrating peptides (CPP) were discovered [52]. Frankel and Pabo [53] as well as Green and Loewenstein [54] reported in the same year 1988 the proof of concept of protein transfer into cells. They described that the transactivator of transcription (TAT) protein of HIV can pass cell membranes and is finally internalized by cells. Nine years later Vives *et al* [55] identified a minimal sequence of TAT that enabled cell entry. Another early research of Juliot *et al* revealed in 1991 that the amphiphilic *Drosophila* Antennapedia homeodomain (pAntp) is capable to translocate across neuronal membranes of post mitotic neurons of *Drosophila* [56].

A lot of approaches deal with the classification of cell penetrating peptides. CPP's can be categorized into subgroups according to their origin or amino acid sequence characteristics [57; 58]. Based upon their origin CPPs can be divided into three main classes: peptides derived from proteins such as pVEC with 13 cytosolic and 5 transmembrane residues from VE-cadherin [51], chimeric peptides which are assembled by the fusion of two or more motifs from other peptides such as galparan, a peptide combination of the neuropeptide galanin and the wasp venom peptide mastoparan [59] and synthetic CPP's with rationally developed sequences such as the polyarginine family [60]. Another possibility to classify CPP's is according to their sequence characteristics and the associated physico-chemical features. Cationic peptides such as R9 and Tat show a high positive net charge and few acidic amino acid residues. Peptides including MPG and penetratin which contain polar and nonpolar regions represent the class of amphipathic peptides and peptides which only consist of apolar residue are considered as hydrophobic peptides [57].

The connection between the cell penetrating peptide and its cargo is either through chemical linkage via covalent bond or through non covalent

association. Most CPP's were used in covalently bound form, but the limitation of covalent bounding is that the linkage could disturb the biological activity of the cargo or the protein could be denatured before delivery [61; 62]. The arrangement of the non-covalent complexes of CPP's and their cargos occurs mainly through hydrophobic interaction and ionic binding. One drawback could be that the required minimum tenfold excess of CPP's over the amount of their cargo [61] negatively influences the viability and membrane integrity of the cells.

### **3.7.1.1 Mechanism of CPP cellular internalization**

The mechanism of how CPPs enter cells is not fully understood. But the internalization mechanism is not the same for all CPP families. It seems to be dependent on the type of CPP, the concentration, the cargo and the cell line which is used in research [47]. Additionally most CPPs used two or more pathways to enter the cells. The two main cellular internalization mechanisms are energy independent direct translocation and endocytosis. The mechanisms for direct translocation are inverted micelle formation, pore formation, the carpet like model and the membrane thinning model. They all have in common that the positively charged CPPs interact with the negatively charged elements of the membrane or with the phospholipid bilayer [60]. Ultimately direct translocation leads to a stable or transient membrane destabilization in an energy and temperature independent manner [59] followed by peptide folding on the membrane [60].

The mechanisms for endocytosis are phagocytosis for uptake of large particles and pinocytosis for solute uptake [60]. During these both processes vesicles are formed which is triggered by and dependent on actin-mediated remodeling of the plasma membrane [63]. Pinocytosis is further distinguished in clathrin-mediated, caveolin-mediated, micropinocytosis, and clathrin- and caveolin-independent endocytosis. These processes include different types of receptor-ligand interactions, which are dependent on particle size and membrane chemistry. After internalization the particles can be transferred to different cell organelles such as mitochondria or even nucleus (Figure 7) [64].

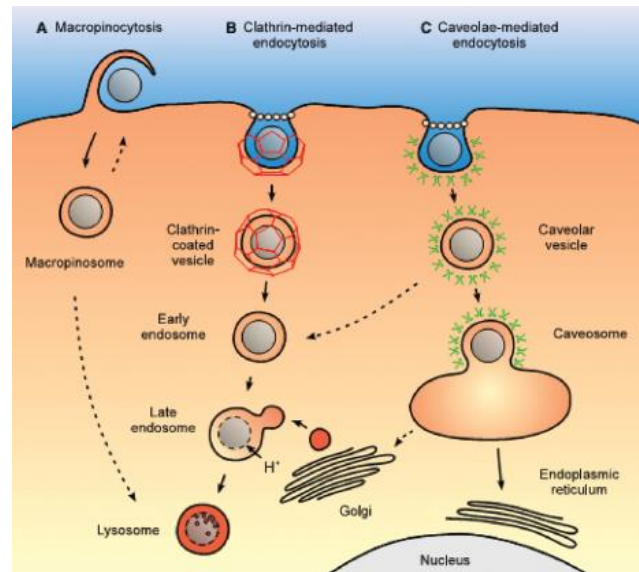


**Figure 7: Endocytosis**

(A) Macropinocytosis cause the formation of a macropinosome. It is supposed that the macropinosome fuse with lysosome or convert its content to the membrane. (B) Clathrin-mediated endocytosis causes the development of an early endosome. The early endosome acidified and fuses with prelysosomal vesicles containing enzymes which generate a late endosome and finally a lysosome. This acidic and enzyme-rich surrounding facilitates the particle and drug degradation. (C) Caveolae-mediated endocytosis leads to a caveosome which prevents a degradative acidic and enzyme-rich environment such as in lysosomes [64].

For efficient optimization of the CPP carrier it is important to investigate its cellular uptake. To identify the different entrance ways there are various tools available. CPP's use translocation and endocytosis but while both pathways work at 37°C only translocation is used at 4 °C [65]. Human transferrin is a marker for clathrin-mediated and lactosylceramide for clathrin-independent endocytosis. Another possibility is via inhibitors such as chlorpromazine and amiloride. Chlorpromazine is an inhibitor of clathrin-mediated endocytosis because it inhibits clathrin-coated pit formation [66]. Amiloride inhibits macropinocytosis by lowering submembraneous pH and blocking Rac1 and Cdc42 signaling [67]. Sodium azide and 2-deoxy-D-glucose (2-DG) were used to deplete the ATP production and thus to investigate the energy dependency of internalization pathways. 2-deoxy-D-glucose is a special glucose molecule in which the 2-hydroxyl group is replaced by hydrogen. Therefore 2-DG cannot undergo further glycolysis and inhibits competitively the production of glucose 6-phosphate from glucose [68]. Sodium azide inhibits the cytochrom-c-oxidase (complex IV), which is the last enzyme in the respiratory electron transport chain of mitochondria [69].

### 3.7.1.2 MPG and penetratin

In our working group we compared the cellular internalization of 22 cell penetrating peptides in 4 different cell lines. Based on this knowledge we decided to use MPG and penetratin as carriers of iCAL36/42 for internalization into the cell. MPG and penetratin belong to the group which shows the highest internalization results without inducing cytotoxicity in Cos-7, HEK293, HeLa and MDCK cells [48].

The group of G. Divita *et al* described in 1997 a new strategy for the delivery of oligonucleotides into cells. They developed and synthesized a peptide vector which they termed MPG. If MPG is mixed with oligonucleotides, they rapidly build a complex with tight non-covalent interactions and it is suggested that the oligonucleotides are coated with several molecules of MPG. The association of MPG and oligonucleotides involves mainly electrostatic interactions in detail between the negative charges of the nucleic acids (mainly phosphate groups) and the positively charged part of MPG (lysine residues of NLS) [71].

MPG is a primary amphipathic peptide which consists of a variable N terminal hydrophobic (GALFLGFLGAAGSTMGA) motif, a hydrophilic (KKKRKV) lysine-rich moiety and a linker (WSQP) domain which connects both domains and promotes the flexibility. The hydrophilic part of MPG is derived from the nuclear localization sequence (NLS) of simian virus 40 (SV40) large T-antigen and is necessary for the interaction with nucleic acid and intracellular trafficking. The hydrophobic component is originated from the fusion sequence of the HIV glycoprotein 41 and is required for the targeting to the cell surface and cellular internalization [72]. It could be shown that MPG associated with or without its cargo is able to interact and to penetrate spontaneously lipid-phase and insert into natural membranes [73]. The interaction between the cell surface and the MPG-cargo complex is due to the electrostatic interaction with proteoglycans and then with the head groups of phospholipids. The Rac1 associated membrane dynamics are involved in the direct contact of the peptide with the lipid phase of

the cell surface and lead to the insertion of the complex into the membrane [74]. The interaction of MPG with phospholipids leads to the folding of the N terminal domain into a  $\beta$ -sheet and an  $\alpha$ -helix structure. Finally the MPG-cargo compound is delivered into the cytoplasm [74, 73].

Penetratin is a protein derived cell penetrating peptide which is originated from the *Drosophila* Antennapedia homeodomain (amino acids 43-58 of the protein) [75]. Homeoproteins represent a large class of transcription factors containing a DNA binding domain, the homeodomain. Homeodomains are involved in the secretion and internalization, thus intracellular trafficking of homeoproteins [76]. It could be shown that penetratin uses different ways to internalize into the cell. At low extracellular concentration penetratin translocates into the cell but at high concentrations for both endocytosis and translocation occur. Endocytosis of penetratin depends on glycosaminoglycans on the cell surface. But also phosphatidylinositol 4,5-bisphosphate (PtdIns(4,5)P<sub>2</sub>) located in the inner cell membrane plays a role in the endocytosis of penetratin and is probably involved in the actin dynamics and endocytosis (Jiao). Beside endocytosis translocation is also a possibility for penetratin to overcome cellular membranes. Different ways are discussed how penetratin and other CPPs internalized into the cell such as tubule formation and fission, inverted micelles and electroporation-like with membrane repair depending on cell membrane formation and amino acid sequence of the CPP [77].

### **3.7.1.3 Cellular internalization *via* N-myristoylation**

CPP's have received the most attention in connection with the transport of molecules into living cells. But at the same time another approach to overcome cellular membranes has been used but is poorly described: covalent attachment of myristate, a 14-carbon saturated fatty acid to the N-terminal glycine of signaling and viral proteins [78, 80].

Yet myristate is very interesting because for example a myristoylated peptide was efficiently internalized into the B lymphocyte cell line BA/F3 while in



contrast a cell penetrating peptide derived from the TAT protein was not able to translocate over the cell membrane of this cell line [62]. N-myristoylation is irreversible and catalyzed co-translational via N-myristoyltransferase [86]. It is one of the most commonly occurring lipid modification of proteins [84] and is generally required for targeting proteins to cellular membranes or proper localization of many proteins [78; 79; 80]. But myristoylation has many other functions besides membrane binding. Examples are its involvement in the enhancement of cSrc kinase activity and the ubiquitination and degradation of the protein and its association with thermal stability of protein kinase A [80]. The presence or absence of specific cell-surface molecules play an important role in the cell membrane association. In contrast, the myristoyl group is known to insert via direct hydrophobic interaction without the need of additional components for attachment to the cell membrane. This characteristic may allow use a greater repertoire of cell types for transport of molecules into the cell by myristoylation [78].

## 4 Objective of the work

The cystic fibrosis transmembrane conductance regulator (CFTR) protein is a chloride channel at the apical surface of secretory epithelial. Mutations in the *CFTR* gene cause cystic fibrosis (CF), the most common autosomal recessive genetic disorder among Caucasian [81].

NHERF proteins increase CFTR activity at the apical membrane, whereas CAL promotes its lysosomal degradation. To explore novel therapeutic strategies for increasing the cell-surface abundance of CFTR, our goal was to design a selective inhibitor of the PDZ binding domain of CAL that does not affect the PDZ domains of the competitors NHERF1 and NHERF2. One part of Lars Vouillème's work was to engineer a selective peptide based inhibitor for CAL PDZ. The resulting decamer peptide iCAL36 (ANSRWPTSII) has a higher affinity but the other designed inhibitor iCAL42 (ANSRLPTSII) has a higher specificity to the CAL PDZ domain.

To continue the project, 6 specific objectives will be presented in the following chapter:

1. We will compare two different kind of carriers (cell penetrating peptides and myristic acid) regarding their capacity to deliver iCAL36/42 into cells. In this context we will investigate the energy and temperature dependency of the MPG-iCAL36/42, Pen-iCAL36/42 and the Myr-iCAL36/42 internalization.
2. We will measure the release of MPG-iCAL42, Pen-iCAL42 and Myr-iCAL42 out of the cell.
3. We will analyze the influence of each construct on the viability of Caco-2 cells and human rectal epithelial biopsies.
4. We will investigate the stability of each construct in 20 % human serum.
5. We will evaluate the direct interaction of our compounds with the CAL PDZ domain. Therefore we will measure the  $K_d$  and  $K_i$  values *in vitro* using the method of fluorescence polarization before we will test the co-localization of the iCAL inhibitor and the CAL PDZ domain *in cellulo*.

6. Finally, we will test the functionality of the constructs in polarized Caco-2 cells and human rectal epithelial biopsies (from CF-patients) by measuring differences in  $\text{Cl}^-$  efflux based on the CFTR accumulation at the apical membrane by Ussing chamber experiments.

All the obtained results will be a step forward in the development of peptide-based “stabilizers” applicable in a combined tri-therapy together with “correctors” and potentiators.

## 5 Material and Methods

### 5.1 Fluorescence anisotropy binding experiments

Fluorescence polarization data were measured on a Spectramax M1000 microplate reader (Molecular Devices) at 24 °C. For  $K_d$  measurements with a given fluorescently labeled peptide, a stock solution of protein was incubated for 10-30 min at room temperature in FP buffer (storage buffer, supplemented to a final concentration of 0.1 mg/mL bovine IgG (Sigma) and 0.5 Mm Thesit (Fluka) containing 30 nM fluorescent peptide). The pre-equilibrated protein:reporter peptide mixture was then serially diluted into FP buffer containing 30 nM fluorescent peptide and allowed to incubate for 10 min. 40  $\mu$ L aliquots were transferred to HE low-volume, black 96-well plates (Molecular Devices). Fluorescence polarization was determined at an excitation wavelength of 485 nm and an emission wavelength of 525 nm as depicted in ref. [59]. For competition experiments, a single stock solution was prepared in FP buffer containing fixed concentrations of both fluorescently labeled reporter peptide and protein. This mixture was allowed to equilibrate for 20-60 min at RT. Unlabeled competitor peptide was dissolved and serially diluted in DMSO (Fluka). Each serial dilution was aliquoted at 1/20 final volume, to which was added 19/20 volume of the protein:reporter mixture. The final reporter peptide concentration was 30 nM and the final protein concentration was 0.25  $K_d$  - 3.0  $K_d$ , depending on the measurement. Plates were mixed by vibration, centrifuged and allowed to incubate for an additional 15 min at 24 °C in the microplate reader before measurement. For weakly interacting peptides,  $K_i$  values were estimated as follows: theoretical fluorescence anisotropy values were calculated for inhibitor  $K_i$  based on the known reporter:peptide fluorescence anisotropy (FPPL), free reporter anisotropy (FPL), and the known  $K_d$  of the reporter:peptide complex. The estimated  $K_i$  value was increased until the theoretical fluorescence anisotropy value (with assumed equal variance) at the 1 mM concentration significantly increased ( $p < 0.05$ ) above experimental fluorescence anisotropy.

## 5.2 Cell culture

### Caco-2 cells

Human epithelial colorectal adenocarcinoma (Caco-2) cells were a generous gift from Prof. Dr. Theuring (Center for Cardiovascular Research – Charité Berlin). Caco-2 cells were cultured in phenol red-free DMEM High Glucose (4.5 g/L) (Life Technologies) supplemented with 20 % fetal bovine serum (Biochrom AG), with L-glutamine (Sigma), non-essential amino acids (Sigma) and 1 % penicillin/streptomycin (PAA). The cells were passaged 3 - 4 times a week and cultured at 37°C and in a humidified 5 % CO<sub>2</sub> atmosphere.

For experiments, cells were seeded either 1000 µL in 12 well culture plates (Falcon) or 1000 or 250 µL in 6 or 12 Transwell culture plates (Costar) with a concentration of  $6 \times 10^4$  cells/mL, respectively. The cells were cultivated for 14 days for differentiated and polarized cells or in the case of 80 % confluent cells for 24 hours. All cells used in experiments were between passages 10 and 70.

### HT29/B6 cells

The cultivation of HT29/B6 cells was performed in the Institut für Klinische Physiologie, Charité - Campus Benjamin Franklin.

The human colon carcinoma cell line HT-29 clone B6 was grown in RPMI 1640 AQMedia (Sigma) supplemented with 10 % fetal bovine serum (Biochrom AG), 100 mg/mL streptomycin and 100 U/mL penicillin (Biochrom). Cells were cultivated at 37°C and 5 % CO<sub>2</sub>. For all Ussing chamber measurements, epithelial cell monolayers were grown on culture plate inserts (pore size 3.0 µm, effective area 0.6 cm<sup>2</sup>, Millicell-PCF, Millipore, Bedford, MA). Confluent cell layers were used on days 6 - 8 after seeding.

### 5.3 Mycoplasmae test

Mycoplasma contamination is a major headache for cell cultures. Mycoplasmae are small, simple bacteria which lack a cell wall and represent one of the most prevalent and serious sources of cell line contamination. Mycoplasma contamination is invisible with no discernible change in turbidity or pH even at densities as high as 10<sup>8</sup> cells/mL. Mycoplasmae are a problem because they can induce changes to the cell cultures which include altered growth rates, morphological changes, chromosomal aberrations, and altered cell metabolism. For these reasons, our cells were tested in regular intervals for contamination using the MycoAlert™ mycoplasma kit from Lonza. The principle of this method is that the released mycoplasmal enzymes in the supernatant of cell culture medium react with the MycoAlert substrate, which catalyzes the conversion of ADP to ATP. By measuring the level of ATP in a sample both before and after the addition of the substrate, a ratio can be obtained which is indicative of the presence or absence of mycoplasmae. If mycoplasmal enzymes are present, the reaction of the enzymes with the substrate leads to elevated ATP levels and the ratio is higher than 1.2. If the mycoplasmal enzymes are not present the ratio is smaller than 1.0.

The ATP in the supernatant can be detected by using the following bioluminescent reaction:



The emitted light intensity is linearly related to the ATP concentration and is measured using a luminometer.

### 5.4 Solubilization of peptides

In order to ensure the reproducibility of our peptide incubations, it is important to control the weighted peptide concentration. Therefore, each peptide was dissolved at a concentration of 1 mM and the concentrations were measured

with NanoDrop (Thermo) following the Beer-Lambert law ( $E = \epsilon cd$ ). Calculation of  $\epsilon$  was done according to the ProtParam tool of the Expasy website (<http://web.expasy.org/protparam/>).

Example Pen-iCAL42:

$$e = 11000 \text{ L/mol*cm}$$

$$d = 1 \text{ cm}$$

$$E = 6.84$$

$$E = e c d$$

$$c = E/(e*d)$$

$$c = 6.84/(1.1*10^{-4}*1)$$

$$c = 6.22*10^{-4} \text{ mol/L} = 0.622 \text{ mM}$$

All analyzed peptides show a solubility of approximately 60 % in this example of 62 %.

## 5.5 Fluorescence measurement

### 5.5.1 Selection of fluorescence dye

To realize our confocal microscopy experiments and our internalization tests we have to select a suitable fluorescence dye. It is important, that the dye is very stable against the used high energetic laser light. In the beginning we coupled 5,6 Carboxyfluorescein (CF, appears in green) to the peptides, but after a single exposure to laser light we observed a strong bleaching effect (Figure 8). The confocal microscopy pictures show Caco-2 cells incubated with CF-MPG-iCAL36 for 1 hour at a concentration of 10  $\mu\text{M}$ . The plane appearance of the 5,6 Carboxyfluorescein (CF) dye is due to the glass bottom attached peptides. The dark areas are exactly the regions, which were exposed to the confocal laser light (Figure 8).

Due to the observed bleaching effect we were looking for an alternative dye. We tested 5(6)-Carboxytetramethylrhodamine (TAMRA) and treated Caco-2 cells at the same conditions as with the 5,6 Carboxyfluorescein labeled peptide (Figure 8). We exposed the samples more than one time to laser light and could not detect a decrease of the intensity of the fluorescence signal. Therefore we labeled our constructs with TAMRA for further microscopy and internalization experiments.

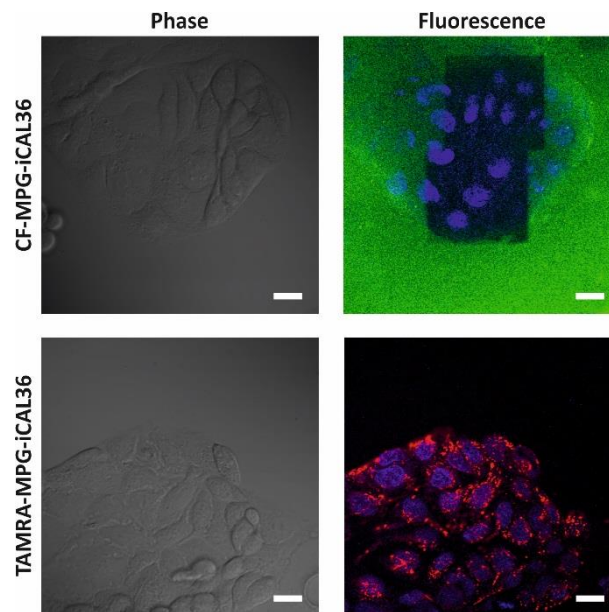


**Figure 8: Bleaching effect**

Caco-2 cells were treated with 5,6 Carboxyfluorescein (CF) labeled MPG-iCAL36 (CF-MPG-iCAL36) or with 5(6)- Carboxytetramethylrhodamine (TAMRA) labeled \*MPG-iCAL36 (TAMRA-MPG-iCAL36) for 1 hour at a peptide concentration of 10  $\mu\text{M}$ . A strong bleaching effect is observable in the case of CF-MPG-iCAL36 after the one time exposure to the confocal laser light. In contrast, after repeated exposure with laser light the \*MPG-iCAL36 sample shows nearly no bleaching effect.

White scale bar=20  $\mu\text{m}$

### 5.5.2 Fluorescence intensities of TAMRA-labeled peptides

All TAMRA-labeled peptides used in this study (Table 1) were dissolved in Ripa lysis buffer at a stock solution of 1 mM. Thereafter, the peptides were serially diluted to concentrations ranging between 2.5  $\mu\text{M}$  and 0.15625  $\mu\text{M}$  in a black 96 well plate (Costar) (100  $\mu\text{L}$ /well). The fluorescence intensities were measured at room temperature (Ex 544 nm / Em 590 nm) with the Fluostar microplate reader (BMG).



MPG-iCAL36 functions as reference value, because it produces the highest intensities. Therefore in this case we normalized all other peptide intensities regarding the MPG-iCAL36 value. We determined for each peptide and concentration the multiplication factor in relation to MPG-iCAL36 and generated the average.

## 5.6 Cellular uptake

We seeded 1000  $\mu\text{L}$  either for differentiated cells in 12 well plates (Falcon) or for polarized cells in 6 well plates (Transwell, Costar) at a density of  $6 \times 10^4$  cells/mL. Differentiated or polarized Caco-2 cells were rinsed twice with PBS (Gibco, Paisley) and incubated with 1000  $\mu\text{L}$  of 10  $\mu\text{M}$  TAMRA labeled peptides in FBS-phenol red free medium for 3 hours at 37°C and 5 %  $\text{CO}_2$ . Afterwards, the cells were rinsed twice with 1 mL PBS to remove the medium completely. To remove peptides that could have adhered to the extra-cellular membrane, cells were incubated for 10 min with 200  $\mu\text{L}$  trypsin (Biochrom) (37°C; 5 %  $\text{CO}_2$ ). Cells were transferred in 2 mL tubes after addition of 800  $\mu\text{L}$  PBS followed by centrifugation for 15 min, 4°C and 3400 rpm. Pellets were washed once with 1000  $\mu\text{L}$  PBS and centrifuged for 15 min, 4°C and 3400 rpm. Subsequently the cells were lysed 1 hour with 500  $\mu\text{L}$  Ripa buffer (50 mM Tris, 1 mM EDTA, 150 mM NaCl, 1 % (v/v) NP40, 0.5 % (v/v) deoxycholat, 0.1 % (w/v) SDS, pH 7.5, Complete Mini, EDTA-free (Roche Diagnostica)). Uptake was determined by measuring TAMRA emission (black Nunc 96 well plates,) on a microplate reader (FLUOstar Optima (Ex 544 nm / Em 590 nm) using 100  $\mu\text{L}$  of lysate (Figure 9).

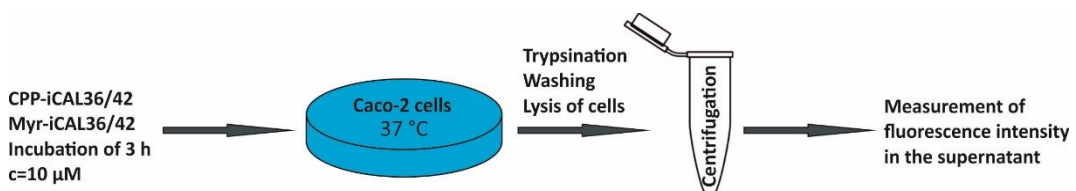


**Figure 9: Cellular internalization**

Differentiated or polarized Caco-2 cells were incubated with Pen-iCAL36/42, MPG-iCAL36/42 or Myr-iCAL36/42 at a concentration of 10  $\mu\text{M}$  for 3 hours. After the incubation the cells were trypsinated, washed with PBS, lysed for 1 hour with Ripa buffer and subsequently centrifuged. The fluorescence intensities were measured in the supernatant and the results were normalized to the total protein concentration.

The results were normalized to the total protein concentration using a BCA (bicinchoninic acid) protein assay.

The BCA reagent was freshly prepared with solution A and B at a ratio of 50:1.

Solution A:

1 % (w/v)	BCA-Na <sub>2</sub>
2 % (w/v)	Na <sub>2</sub> CO <sub>3</sub>
0,16 % (w/v)	Na <sub>2</sub> -Tatrat
0,4 % (w/v)	NaOH
0,95 % (w/v)	NaHCO <sub>3</sub>
pH 11,25	

Solution B: 4 % (w/v) CuSO<sub>4</sub> x 5 H<sub>2</sub>O

After the preparation 200 µL of the AB mixture will be filled in a 96 clear well plate (Falcon). Then 20 µL of the sample will be pipetted to the AB solution. We used two wells without a sample, which serve as the subtracted blank value. After a 30 min incubation time at 37°C and 5 % CO<sub>2</sub> we measured the absorbance at a wavelength of 620 nm and the concentration was calculated using a bovine serum albumin (BSA, Sigma-Aldrich) calibration curve.

### 5.7 The delivery of TAMRA labeled peptides

Caco-2 cells were used after a differentiation of 14 d in 12 well plates. The cells were washed with 1 mL PBS to remove the medium. Than 1 mL peptide medium solution (c = 10 µM) was added to the cells. It was important that the medium is FBS-free to prevent the degradation of our peptides through proteases.

After 1 hour incubation at 37°C and 5 % CO<sub>2</sub> the medium was removed and the cells were washed twice. To detach adhered peptides, which would be falsify our measurements, we treated the cells with 200 µL trypsin. To interrupt the trypsin reaction 800 µL medium with FBS were added and then the cells were transferred in 2 mL reaction tubes (Eppendorf). The cells were centrifuged for 5 min at room temperature and 900 g. The supernatant was removed and the cells were washed and centrifuged again. After the second washing step the cells were dissolved in medium without FBS. Directly afterwards (0 min) and after 10, 30, 60, 120 min and 24 hours 500 µL of the solution was extracted and

centrifuged for 5 min at room temperature and 900 g. In 100  $\mu$ L of the produced supernatant the fluorescence intensities were measured with the microplate reader.

## 5.8 Confocal laser scanning microscopy

### Differentiated Caco-2 cells

$6 \times 10^4$  cells/mL were seeded in glass-bottom dishes (World Precision Instruments) and allowed to differentiate for 14 days. The medium was changed three times a week. 80 % confluent cells were seeded in the same conditions but were microscoped already after 24 hours. The cells were washed twice with PBS, followed by incubation with 1  $\mu$ M or 10  $\mu$ M TAMRA-labeled CPP-iCAL36/42 and Myr-iCAL36/42 constructs in medium without FBS for 60 or 180 min (37°C/5 % CO<sub>2</sub>). 0.5  $\mu$ g/mL Hoechst 333258 was added to the wells after 50 min of incubation to stain cell nuclei. Cells were then washed twice with PBS and imaged without fixation in medium lacking FBS. The internalization of peptides was visualized with an inverted IX81 fluorescence microscope equipped with a Fluoview 1000 scanhead (Olympus, Japan) and a 60 x (N.A. 1.35) oil-immersion objective at 25°C. Fluorescence micrographs were acquired using the following conditions: (i) TAMRA: 543 nm He-Ne laser, (ii) Hoechst and (iii) GFP: 488 nm laser line of an Ar-ion laser. The system was run in sequential scanning mode, where only one laser was active at a time, to avoid spectral overlap. Images were treated with Olympus FluoViewer.

### Biopsies

Freshly extracted human rectal biopsies were washed twice with PBS and incubated with 10  $\mu$ M MPG-iCAL36, Pen-iCAL36 and MPG-iCAL42 in phenol red-free RPMI medium without FBS (1 hour, 37°C/5 % CO<sub>2</sub>). Cell nuclei were stained with 1  $\mu$ g/mL Hoechst 333258. After the incubation the biopsies were washed twice with PBS and afterwards transferred to glass slides.

## 5.9 Cell viability assay

### Differentiated Caco-2 cells

$6 \times 10^4$  cells/mL were seeded in 96-well plates (100  $\mu$ L per well) and cultivated 14 d for differentiation (37°C/5 % CO<sub>2</sub>). After two washing steps with PBS, cells were incubated with different peptide concentrations in 100  $\mu$ L medium without FBS (37°C/5 % CO<sub>2</sub>). After 3 hours, 50  $\mu$ L medium with 20 % FBS was added and cells were further incubated overnight. The next day, 10  $\mu$ L CCK-8 solution (Fluka) were added to each well and incubated for 4 h (37°C/5 % CO<sub>2</sub>). Then, the absorbance was measured using a microplate reader (FLUOstar Optima (absorbance 570 nm)). The results were normalized to the control (without peptide) corresponding to 100 % viability.

### Polarized Caco-2 cells

$6 \times 10^4$  cells/mL were dispensed in 12-transwell plates (250  $\mu$ L) and cultivated 14 d for polarization (37°C/5 % CO<sub>2</sub>). After 4 d the cells on the membrane should be impermeable for basolateral influx of medium. Prior to applying peptides, the medium on the basal side was replaced by medium without FBS, and the medium on the apical side was replaced by 250  $\mu$ L medium without FBS containing 100  $\mu$ M peptide. Furthermore, two control wells were not treated with peptides but were instead incubated on the apical side with medium lacking FBS (untreated cells). After a 3 hours incubation (37°C/5 % CO<sub>2</sub>), 100  $\mu$ L of medium with FBS were added apically, and on the basal site 1/3 medium without FBS were replaced with 1/3 medium with FBS. Cells were further incubated overnight (37°C/5 % CO<sub>2</sub>). The next day, 20  $\mu$ L MTT (Fluka) dye were added to each well and incubated for 4 h (37°C/5 % CO<sub>2</sub>). Then, 160  $\mu$ L of supernatant from each well were transferred to a 96-well plate, and the absorbance was measured using a microplate reader (FLUOstar Optima (absorbance 570 nm)). The results were normalized to the control (without peptide) corresponding to 100 % viability.

### Biopsies

Freshly extracted human epithelium rectal biopsies were washed twice with PBS. Afterwards the biopsies were transferred in 96-well plates and they were incubated with 100  $\mu$ L FBS-free RPMI 1640 AQMedium (Sigma) containing 100  $\mu$ M MPG-iCAL36 and 10  $\mu$ L MTT dye solution. After incubation of 4 h (37°C/5 % CO<sub>2</sub>), the absorbance was measured using a microplate reader (FLUOstar Optima (absorbance 570 nm)). The results were normalized to the control (without peptide) corresponding to 100 % viability. Finally, all results were normalized to the weight of the biopsies.

Calculation of the viability of Caco-2 cells and human rectal Biopsies:

$$\text{viability in \%} = \frac{(\text{value}_{\text{peptide}} - \text{value}_{\text{blank value}})}{(\text{value}_{\text{untreated cells/biopsies}} - \text{value}_{\text{blank value}})} * 100$$

## **5.10 Evaluation of the internalization pathway**

6 x 10<sup>4</sup> cells/mL were seeded in 12-well plates (100  $\mu$ L per well) and cultivated 14 d for differentiation (37°C/5 % CO<sub>2</sub>). Differentiated Caco-2 cells were washed twice with PBS and pre-incubated for 30 min with either 1000  $\mu$ L of 4°C cold OptiMEM (reduced serum media, Gibco) or 1000  $\mu$ L OptiMEM with 200 mM NaN<sub>3</sub> (Sigma-Aldrich) and 120 mM 2'-Deoxy-D-Glucose (2-DG, Sigma-Aldrich). After pre-incubations the NaN<sub>3</sub>/2-DG solution is removed and replaced by 1000  $\mu$ L of 10  $\mu$ M peptide solution containing the same amount of NaN<sub>3</sub>/2-DG. In the case of the 4°C incubation the medium is also removed and the peptide solution was added at a concentration of 10  $\mu$ M. The incubation with peptides took 3 hours either at 37°C or 4°C depending on the condition (Figure 10). After the treatment with the peptides all following steps are the same as described in section "cellular internalization". To compare the consequential results with internalization under normal conditions parallel tests without NaN<sub>3</sub> and 2-DG or 4°C were performed as described in cellular internalization.

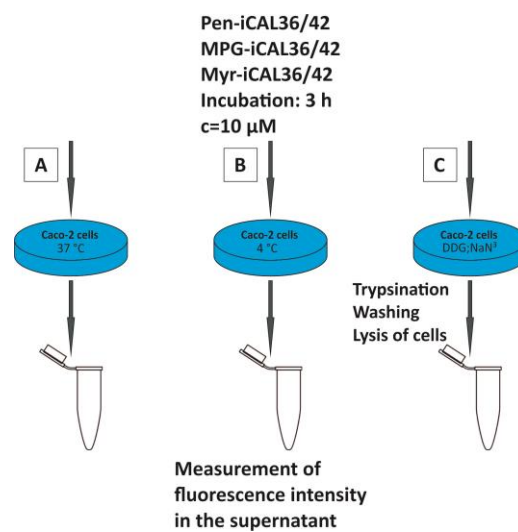


**Figure 10: Test of internalization pathway**

The cells were treated in parallel under normal conditions (see section cellular internalization) (A) at 4°C or (B) with 200 mM  $\text{NaN}_3$  and (C) 2-DG at 37°C. Additionally all samples are treated after pre-incubation with the different peptide constructs at a concentration of 10  $\mu$ M.

### 5.11 Peptide stability in human serum

Generally the stability of CPP-iCAL/Myr-iCAL constructs was tested in 20 % human serum at a concentration of 500  $\mu$ M. The peptides were dissolved and the pure human serum was diluted in Ampuwa Aqua ad injectibilia (Fresenius). 40 % human serum and 1 mM peptide solution were mixed at a ratio of 1:1 which leads to the above specified concentrations. The suitable peptide concentration was tested in several pre-tests. The Myr-iCAL compound is dissolved at the same procedure but with a final concentration of 1000  $\mu$ M.

Finally a 20 % human serum / 500  $\mu$ M CPP-iCAL, iCAL or a 1000  $\mu$ M Myr-iCAL solution was prepared. During the incubation the tubes were shaken at 37°C and after 0, 60, 120, 240, 360, 1440 min 50  $\mu$ L samples were extracted and precipitated with 50  $\mu$ L DCA (final concentration 5 %) in the case of CPP-iCAL and iCAL or with 50  $\mu$ L ethanol (final concentration 10 %) in the case of Myr-iCAL on ice. The precipitated samples were centrifuged for 10 min and 14,000 rpm at room temperature. The supernatants were analyzed by RP-HPLC (Waters, Eschborn, 1.2 mL/min, 40  $\mu$ L injection volume). The HPLC measured the amide bonding at a wavelength of 214 nm and detected the time point when a substance is

dissolved in a H<sub>2</sub>O-acetonitrile-gradient. We used a HPLC column C18 Vydac® (Grace, Deerfield, USA) (Figure 11). The HPLC documented this process as a graph over a time period. The area under the peak was integrated and changes were blotted over the incubation time to evaluate the CPP-iCAL/Myr-iCAL degradation.

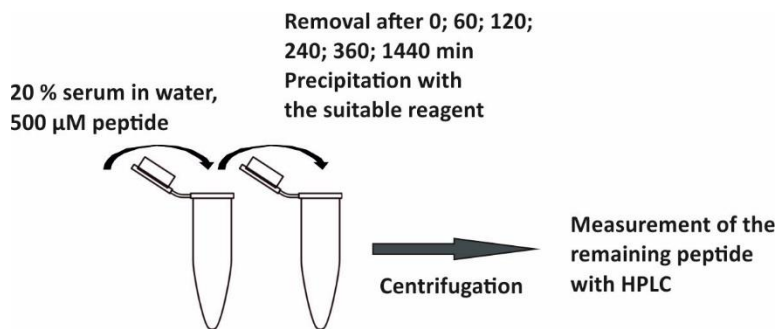


**Figure 11: Measurement of the protease stability**

500 μM peptide was dissolved in 20 % serum. After the indicated time points the serum peptide solutions were precipitated and afterwards centrifuged. The remaining peptide was detected in the supernatant with the HPLC as described above.

## 5.12 Co-localization of CAL PDZ and iCAL

### 5.12.1 Production of competent cells

*E. coli DH5α* cells were used as competent bacterium. 100 μL competent cells were grown in lysogeny broth (LB) medium (2.5 L Aqua dest., 25 g Trypton (Sigma-Aldrich), 12.5 g yeast extract (Sigma-Aldrich), 25 g NaCl) until they reach OD<sub>600</sub> = 0.3 (this needs 3-4 h; 220 rpm; 37°C). Then the cells were centrifuged for 10 min; 4°C and 4000 rpm. The supernatant was removed and the bacteria were resuspended in 10 mL 0.1 M CaCl<sub>2</sub> (5 min on ice). The cells were centrifuged again for 10 min; 4°C and 4000 rpm and the bacteria were resuspended in 2 mL 0.1 M CaCl<sub>2</sub>. 10-25 % glycerol (Thermo Fischer scientific) as anti-freezing agent was added to the cells and the cells were stored at -80°C (Figure 12).

### 5.12.2 Transformation of *DH5α* bacteria

Full length GFP-CAL (CFTR associated ligand) cloned into pEGFP-N1 with a kanamycin resistance was a generous gift from Jie Cheng, PhD (Department of Physiology, Johns Hopkins University School of Medicine, Baltimore,). The construction of the plasmid was described in *J Biol Chem.* 2002 Feb 1;277(5):3520-9.

40 ng of GFP-CAL plasmid were pipetted to 100  $\mu$ L of competent *DH5α* cells and incubated for 30 min on ice followed by a heat shock for 45 s at 42°C. Then 1 mL LB medium were added. Afterwards the cells were incubated for 1 hour, 220 rpm and 37°C. Thereafter the treated cells were spread to LB agar plates (1.5 % agar) containing kanamycin (50  $\mu$ g/lm) to distinguish transformed *E. coli* bacteria. The plates were incubated over night at 37°C and 5 % CO<sub>2</sub>.

Separated colonies were transferred to 4 mL LB medium with kanamycin (50  $\mu$ g/mL) and incubated over night at 37°C, 220 rpm and 5 % CO<sub>2</sub>. This bacteria culture was used to perform a minipreparation (Quiagen) according to the manufacturer's instructions. 10 - 25 % glycerol as anti-freezing agent was added to the remaining cells. Cells were stored at -80 °C.

The plasmid was confirmed with appropriate restriction enzymes NotI (Promega) and Sall (Thermo Fischer scientific).

For the maxipreparation (Quiagen) the frozen transfected cells were used. The cells were spread to LB agar plates containing kanamycin and afterwards incubated overnight at 37°C. Some material of a separate colony was taken again and transferred to 4 mL LB medium with kanamycin. This solution was cultivated over night at 37°C. 250  $\mu$ L of this culture were dissolved in 250 mL LB medium with kanamycin followed by an incubation over night at 37°C, 220 rpm. Then we performed the maxipreparation (Quiagen) to augment the plasmids for the transfection as recommended by the manufacturer and the plasmid was confirmed again with the restriction enzymes NotI and Sall.



### 5.12.3 Transfection of Caco-2 cells for microscopy experiments

$1 \times 10^5$  Caco-2 cells/mL were seeded in glass-bottom dishes (World Precision Instruments) and grown at 37°C/5 % CO<sub>2</sub>. After 24 hours, Caco-2 cells were transfected using Lipofectamine (Invitrogen) according to the manufacturer's declaration. 24 hours after the procedure the transfection medium was removed and the cells were washed two times with PBS. Then the cells were incubated with CPP-iCAL or Myr-iCAL at concentrations of 1 or 10  $\mu$ M in medium without FBS for 1 or 3 hours (37°C, 5 % CO<sub>2</sub>). Additionally the cells were treated with 0.5  $\mu$ g/mL Hoechst 333258 to stain cell nuclei. Specifications are described above in the section microscopy (Figure12).

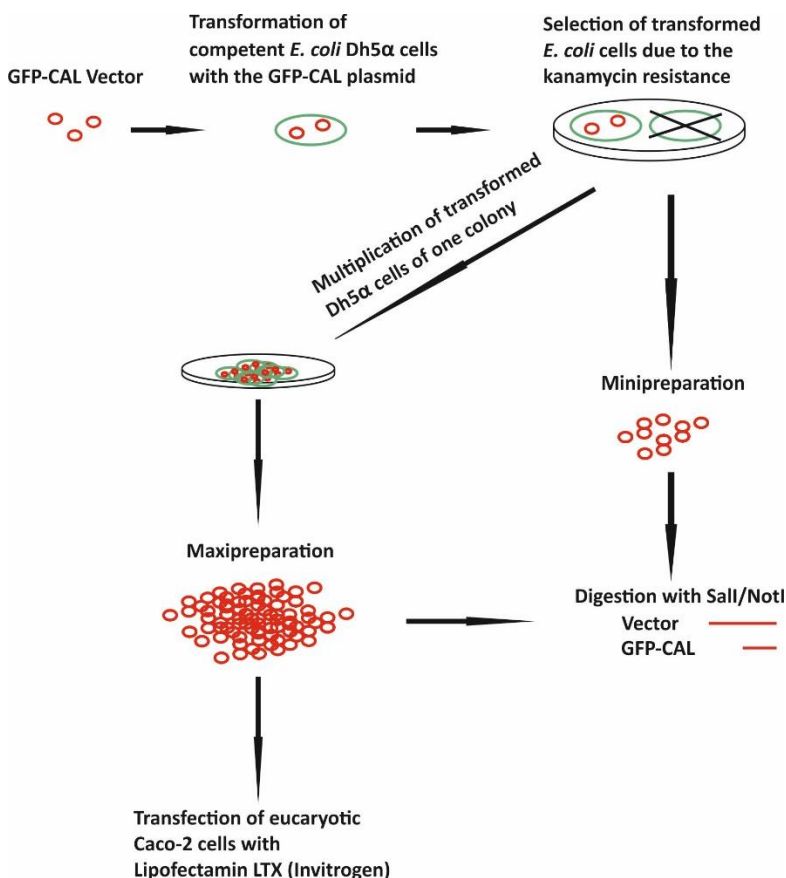


**Figure 12: Transformation of *E. coli* Dh5 $\alpha$  cells and Transfection of eucaryotic Caco-2 cells**

Competent *E. coli* Dh5 $\alpha$  cells were transformed with the GFP-CAL plasmid. Transformed *E. coli* cells were selected due to the kanamycin resistance which is a component of the pEGFP-N1 plasmid. After a miniprep the isolated DNA was digested with the restriction enzymes Sall and NotI. The digested DNA was analyzed through gel electrophoresis. If the right fragments were detectable a multiplication of transformed Dh5 $\alpha$  cells of one colony was performed. After the maxiprep the right fragments were proved again through the digestion with Sall and

Notl. The transfection of eukaryotic Caco-2 cells with Lipofectamin LTX (Invitrogen) occurs according to the manufacturer's declaration.

### 5.13 Ussing chamber measurement

Due to the inhibition of CAL PDZ through iCAL36 should increase the CFTR proteins in the membranes of mucus producing cells. This leads to an enhanced chloride secretion and thus to a change in current, which was measured with Ussing chambers (Physiologic Instruments). A schematic representation of an Ussing chamber is depicted in figure 13. The inserts were mounted in Ussing chambers which are especially designed for insertion of Millicell filters (a). Both chambers were filled with 5 mL standard bath solution, which contains: 137.6 mM NaCl, 2.4 mM Na<sub>2</sub>HPO<sub>4</sub>, 0.6 mM NaH<sub>2</sub>PO<sub>4</sub>, 5.4 mM KCl, 1.2 mM CaCl<sub>2</sub>, 1.2 mM MgCl<sub>2</sub>, 10 mM HEPES, and 10 mM D(+)-glucose (b). The solution was aerated constantly with 95 % O<sub>2</sub> and 5 % CO<sub>2</sub> and was continuously heated to receive a temperature of 37°C. Ion transport produces a potential difference (PD, voltage difference) across the epithelium. The voltage is detected by Agar-Ringer bridges placed near the cells (c). The Agar-Ringer bridges are in contact with two electrodes (h). The electrodes are connected with the volt meter (i), which measures the voltage. Another pair of electrodes (e) placed away from the cells are also in contact with the solution by Agar-Ringer bridges (d). The electrodes are attached to a variable DC (direct current) source (f) and additionally an ampere meter (g) is connected in series.

The ion transport across the membrane produces a potential difference between both halves. Both electrodes placed near the cells record the PD across the tissue. The set of two other electrodes (e) allows the injection by the variable DC source of a current (short-circuit current or I<sub>sc</sub>) to nullify the PD. The intensity of the current, which is necessary to clamp the PD at 0 mV is monitored by an ampere meter. Finally we measured a current with the ampere meter in  $\mu\text{A}/\text{cm}^2$ .

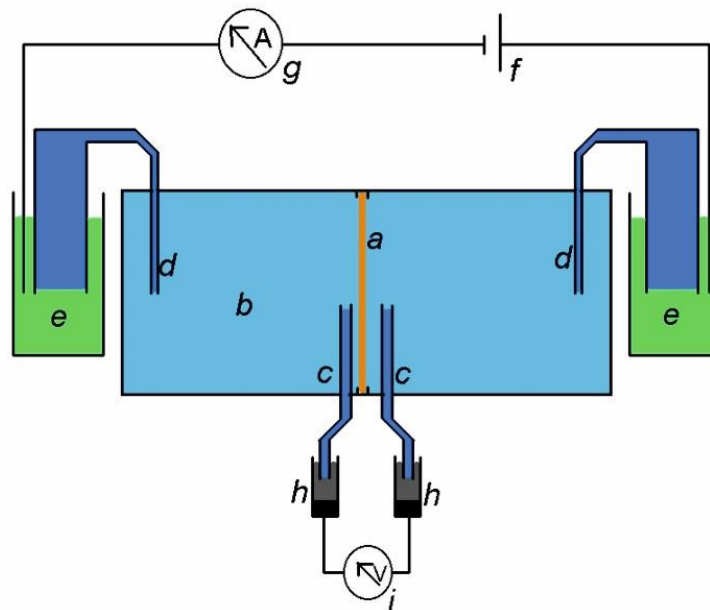


**Figure 13: Schematic representation of an Ussing chamber**

Cells grown on permeable supports (a). Bath solution is filled in both chambers (b). Two agar ringer bridges near the cells (c) are in contact with two electrodes (h). The electrodes are connected with a volt meter (i). Two other electrodes (e) which are placed away from the cells are in contact with the bath solution by agar ringer bridges (d). The electrodes are attached to a variable DC source and an amper meter (g). [[https://en.wikipedia.org/wiki/Ussing\\_chamber](https://en.wikipedia.org/wiki/Ussing_chamber)]

#### Caco-2 and HT-29/B6 cells

Caco-2 or HT-29/B6 cells were seeded on culture plate inserts. The confluent cell layer was used on days 6 - 8 in the case of HT-29/B6 cells and on days 12 - 14 in the case of Caco-2 cells after seeding. If the confluent cell layer produces minimum resistance values of 200 Ohm/cm<sup>2</sup> the cells were incubated with different MPG-iCAL36 concentrations. The peptides were dissolved in RPMI 1640 AQMedium (Sigma) (HT29/B6 cells) or in DMEM High Glucose (4.5 g/L) (Life Technologies) (Caco-2 cells) without FBS at a concentration of 1 mM or 100 µM. To reach the suitable concentration for the experiment the peptide stock solution was diluted in RPMI or DMEM medium, which was then added to the cells. The cells were incubated with the peptide solution for 3 hours at 37°C and 5 % CO<sub>2</sub>.

For electrophysiological measurements, inserts with cells were mounted in Ussing chambers especially designed for insertion of Millicell filters. Both chambers were filled with 5 mL standard bath solution, which was aerated

constantly with 95 % O<sub>2</sub> and 5 % CO<sub>2</sub>. The bath solution was continuously heated to keep the temperature constantly at 37°C.

Additionally, different substances were added into the bath solution of both chambers during the Ussing chamber measurement of peptide incubated cells to stimulate ion channels for a more detailed analysis. Therefore amiloride (100 µM) was initially applied apically to inhibit epithelial sodium channel (ENaC) activity. I<sub>SC</sub> was stimulated with forskolin (10 µM) which was added to the apical and basolateral bath solution to increase cellular cAMP levels followed by genistein (25 µM) (Sigma) which was added only to the apical bath solution to increase the open probability of ΔF508-CFTR Cl<sup>-</sup> channels. CFTR-specific chloride efflux was computed as the I<sub>SC</sub> current change (ΔI<sub>SC</sub>) following application of CFTR<sub>inh</sub>-172 (10 µM) which reversibly inhibits CFTR I<sub>SC</sub>.

First experiments were performed with Caco-2 cells, however, these cells are not the best candidate for this measurement due to the minimal change of ΔI<sub>SC</sub> values after treatment with amiloride (0.69 µA/cm<sup>2</sup>), forskolin (1.87 µA/cm<sup>2</sup>), genistein (0.6 µA/cm<sup>2</sup>) and the CFTR<sub>inh</sub>-172 (1.17 µA/cm<sup>2</sup>) (Figure 14).

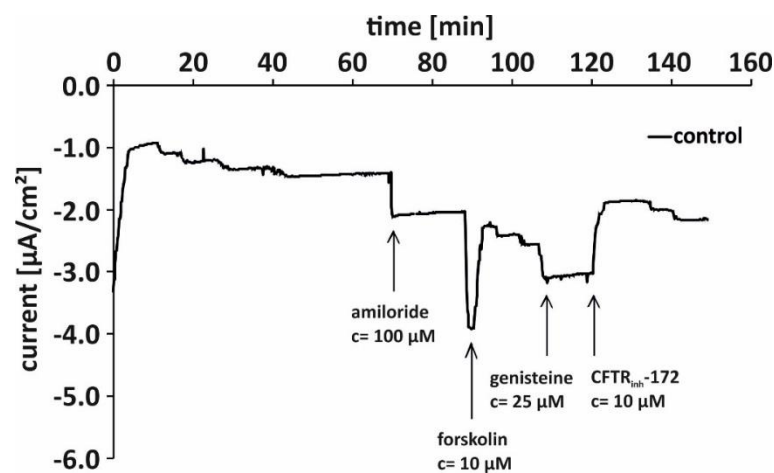


**Figure 14: Current values of Caco-2 cells after treatment with different ion channel stimulators**

We treated polarized Caco-2 cells consecutively with amiloride, forskolin, genistein, and CFTR<sub>inh</sub>-172 and measured the course of current in µA/cm<sup>2</sup> with Ussing chamber measurement. The change of current values was very small and was between 0.6 µA/cm<sup>2</sup> after treatment with genistein and 1.87 µA/cm<sup>2</sup> after treatment with forskolin.

Therefore we decided to use HT29/B6 cells for further experiments. The changes of currents of HT29/B6 cells are shown in figure 15. The cells show also small

changes in currents after treatment with amiloride and genistein, but react tremendously after treatment with forskolin ( $70 \mu\text{A}/\text{cm}^2$ ) and  $\text{CFTR}_{\text{inh-172}}$  ( $40 \mu\text{A}/\text{cm}^2$ ) (Figure 15).

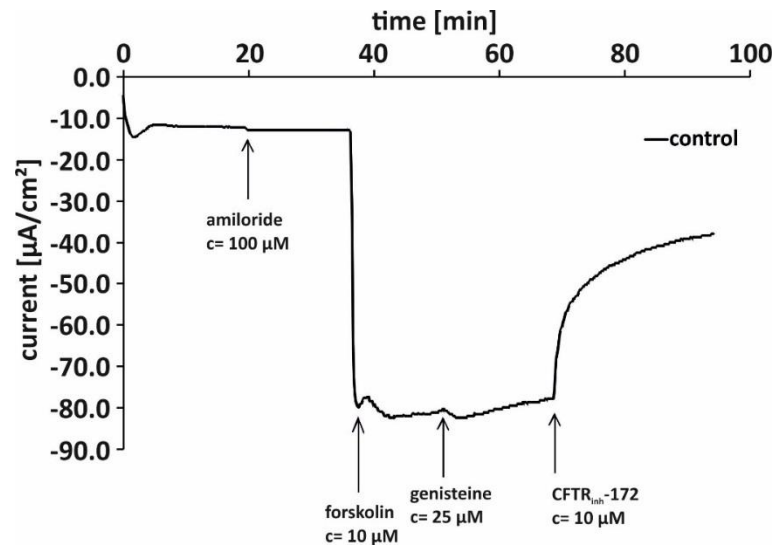


**Figure 15: Current values of HT29/B6 cells after treatment with different ion channel stimulators**

We treated HT29/B6 cells consecutively with amiloride, forskolin, genistein, and  $\text{CFTR}_{\text{inh-172}}$  at the dedicated concentrations. We measured the current change with using chambers.

We detected a dramatically change after treatment with forskolin and the  $\text{CFTR}_{\text{inh-172}}$ . The average values were about 25-fold higher than the results of Caco-2 cells after the same treatment.

### Biopsies

Freshly obtained rectal suction biopsies of patients or healthy donors (diameter of 2 - 3 mm) were immediately transported on ice to the ion transport lab (AG Derichs) in ice-cold PBS buffer solution. The biopsies were incubated with MPG-iCAL36 (active compound) or MPG-SC (negative control) and/or with VX-809 ("corrector"). The peptide compounds were used at a concentration of  $100 \mu\text{M}$  and the "corrector" at a concentration of  $10 \mu\text{M}$ . After the incubation with these constructs for 12 hours the biopsies were spanned in a 2 mm dia circular aperture slider which is designed to hold biopsy specimens (P2307, physiologic instruments). This creates an area of  $0.031 \text{ cm}^2$ , which could be examined. The slider with the fixed biopsy was clamped between the two halves of the Ussing chamber (P2300, physiologic instruments). The chambers were filled with 5 mL buffer ( $128.0 \text{ mM NaCl}$ ,  $0.3 \text{ mM Na}_2\text{HPO}_4$ ,  $0.4 \text{ mM NaH}_2\text{PO}_4$ ,  $4.7 \text{ mM KCl}$ ,  $1.3 \text{ mM CaCl}_2$ ,  $1.0 \text{ mM MgCl}_2$ ,  $10 \text{ mM HEPES}$ ), heated to  $37^\circ\text{C}$  and aerated with  $\text{N}_2$ . The basic principle of biopsy Ussing chamber measurements is the same as of cell

lines. During the measurement biopsies were additionally treated at first with forskolin/IBMX (10/100  $\mu\text{M}$ ), then with carbachol (100  $\mu\text{M}$ ) and last with histamine (500  $\mu\text{M}$ ). The three substances were added on the basal and apical side of the biopsies. In general the short-circuit measurements on transepithelial ion transport (Intestinal current measurements, ICM) were performed according to a standardized procedure (ECFS ICM SOP, Derichs/de Jonge 2011).

## 6 Results

### 6.1 Characterization of different iCAL vehicles

As mentioned in the introduction, Lars Vouillème has developed during his PhD thesis in our laboratory two CAL inhibitors named iCAL36 and iCAL42. To evaluate and characterize the internalization of both peptides, we decided to couple both peptides either to cell penetrating peptides (CPP) or to the myristic acid. We selected MPG and penetratin based on previous results [70] as well as the myristic acid each covalently coupled to the N-terminus of iCAL36/iCAL42 [MPG-iCAL36/42, Pen-iCAL36/42 (CPP-iCAL) and Myr-iCAL36/42 (Myr-iCAL)]. Additionally we synthesized a scrambled version of iCAL36 as a control sequence which we coupled covalently to penetratin and MPG (MPG-SC and Pen-SC). For uptake and cellular localization experiments we labeled the peptides with 5(6)-Carboxytetramethylrhodamine (TAMRA).

#### 6.1.1 Affinity measurements of the iCAL constructs and CAL PDZ

Before we tested our constructs *in vitro* we analyzed their ability to target the CAL PDZ domain by fluorescence polarization (FP) measurements (Table 1).

Interestingly, iCAL36 has a more than 4-fold higher affinity to the PDZ domain of CAL than iCAL42 although the difference between the two peptides is only one amino acid in position 5. When we coupled penetratin or MPG covalently to iCAL36 or iCAL42 we observed a clear affinity improvement of minimum 3.3-fold in the case of Pen-iCAL36 and even a 22.8-fold increase in the case of MPG-iCAL42. The coupling of myristic acid to iCAL36 and iCAL42 also had a positive impact on the interaction with the CAL PDZ domain. The values are at  $2.7 \pm 0.5 \mu\text{M}$  (Myr-iCAL36) and  $2.2 \pm 0.4 \mu\text{M}$  (Myr-iCAL42) in the same range as after the coupling with the cell penetrating peptides. The coupling of TAMRA to MPG-iCAL36/42 and Pen-iCAL36/42 yielded another interesting result. After labeling MPG-iCAL36/42 with TAMRA the affinity to CAL PDZ was clearly reduced (9.6 and

15.5-fold decrease). But in contrast when we labeled Pen-iCAL36/42 with TAMRA we achieved either a further decrease from  $3.6 \pm 0.4$  to  $0.6 \pm 0.1$  in the case of Pen-iCAL36 or nearly no change in the case of Pen-iCAL42 (from  $3.3 \pm 0.4$  to  $4.2 \pm 1.1$ ) compared with their unlabeled counterparts. Additionally the results of the TAMRA labeled peptides showed an unusually high standard deviation which is why their validity is doubtful. The FP measurements were performed by Prof. Dean R. Maddens lab at the Dartmouth Medical School in Hanover.

**Table 2:** Evaluation of  $K_i$  /  $K_d$  values (in  $\mu\text{M}$ ) - influence of a N-terminal MPG, penetratin sequence and myristic acid moiety on CAL PDZ binding affinity

ID	Peptide sequences	$K_i$ [ $\mu\text{M}$ ]	$K_d$ [ $\mu\text{M}$ ]
iCAL36	ANSRWPTSII	$11.9 \pm 4.3$	/
*iCAL36	*ANSRWPTSII	/	$7.0 \pm 0.7$
MPG-iCAL36	GALFLGWLGAAGSTMGAWSQPKKKRKV-ANSRWPTSII	$1.1 \pm 0.4$	/
MPG-SC	GALFLGWLGAAGSTMGAWSQPKKKRKV-SPTINSAIWR	NB	
Pen-iCAL36	RQLIWFQNRMMKWKK-ANSRWPTSII	$3.6 \pm 0.4$	/
Pen-SCR	RQLIWFQNRMMKWKK-SPTINSAIWR	NB	
Myr-iCAL36	C <sub>14</sub> H <sub>27</sub> O-ANSRWPTSII	$2.7 \pm 0.5$	/
*MPG-iCAL36	*GALFLGWLGAAGSTMGAWSQPKKKRKV-ANSRWPTSII	/	$10.6 \pm 8.3$
*Pen-iCAL36	*RQLIWFQNRMMKWKK-ANSRWPTSII	/	$0.6 \pm 0.1$
*Myr-iCAL36	C <sub>14</sub> H <sub>27</sub> O-K(*)-ANSRWPTSII	/	n.d.
iCAL42	ANSRLPTSII	$49.8 \pm 9.7$	/
*iCAL42	*ANSRLPTSII	/	$21.7 \pm 0.5$
MPG-iCAL42	GALFLGWLGAAGSTMGAWSQPKKKRKV-ANSRLPTSII	$2.2 \pm 0.3$	/
Pen-iCAL42	RQLIWFQNRMMKWKK-ANSRWPTSII	$3.3 \pm 0.4$	/
Myr-iCAL42	C <sub>14</sub> H <sub>27</sub> O-ANSRWPTSII	$2.2 \pm 0.4$	/
*MPG-iCAL42	*GALFLGWLGAAGSTMGAWSQPKKKRKV-ANSRLPTSII	/	$33.82 \pm 19.5$
*Pen-iCAL42	*RQLIWFQNRMMKWKK-ANSRLPTSII	/	$4.2 \pm 1.1$
*Myr-iCAL42	*C <sub>14</sub> H <sub>27</sub> O-K(*)-ANSRLPTSII	/	n.d.

\* = 5(6)-Carboxytetramethylrhodamine (TAMRA), NB = no binding to CAL PDZ, n.d. = not determined, Pen = penetratin, Myr = myristic acid. Mean values  $\pm$  SD (n=2)

### 6.1.2 Viability assay with Caco-2 cells

MPG-iCAL36/42, Pen-iCAL36/42 and Myr-iCAL36/42 are meant for the future treatment of CF patients, therefore one of the first necessary steps should be to test the cytotoxicity of the constructs.



To analyze the cytotoxicity we used the Cell Counting Kit-8 from Sigma which utilizes the highly water-soluble tetrazolium salt (WST-8). WST-8 is reduced by dehydrogenases in cells to give a yellow colored product (formazan), which is soluble in the culture medium. The amount of the formazan dye generated by the activity of dehydrogenases in cells is directly proportional to the number of living cells.

We used Caco-2 cells, because they are a heterogeneous human epithelial colorectal adenocarcinoma cell line, which expresses wild type CFTR proteins in their apical membranes [82; 83]. The advantage of this cell line is that although derived from colon carcinoma when cultured, the cells become differentiated and polarized as their original phenotype [84]. On cell culture insert filters (Transwell) they built single confluent monolayers [85].

To determine possible dose-dependent effects of our conjugates on the viability of the Caco-2 cells, we decided to facilitate the assay by using differentiated cells growing on conventional 24-well plates for 14 days. Cells were treated with the CPP-iCAL conjugates at the indicated concentration (from 1  $\mu$ M up to 100  $\mu$ M) for 180 minutes. As controls and for the 100 % reference value we used untreated cells. All tested conditions revealed no significant cytotoxic effects ( $100 \% \pm 20 \%$ ) even at high concentrations (Figure 16 A).

Therefore, the highest concentration of 100  $\mu$ M was used to incubate polarized Caco-2 cells and to analyze the potential effect of all conjugates (CPP-iCAL and Myr-iCAL). As expected we could not detect a decrease of viability of polarized Caco-2 cells at the highest concentration of 100  $\mu$ M either. The results ranged from  $103 \pm 12.5 \%$  (iCAL36) to  $93 \pm 7 \%$  (Myr-iCAL42) (Figure 16 B).

Simultaneously with the viability assay, we monitored the cells by microscope and again we could not detect any indications of a reduced viability such as cell detachment or morphology changes (data not shown).

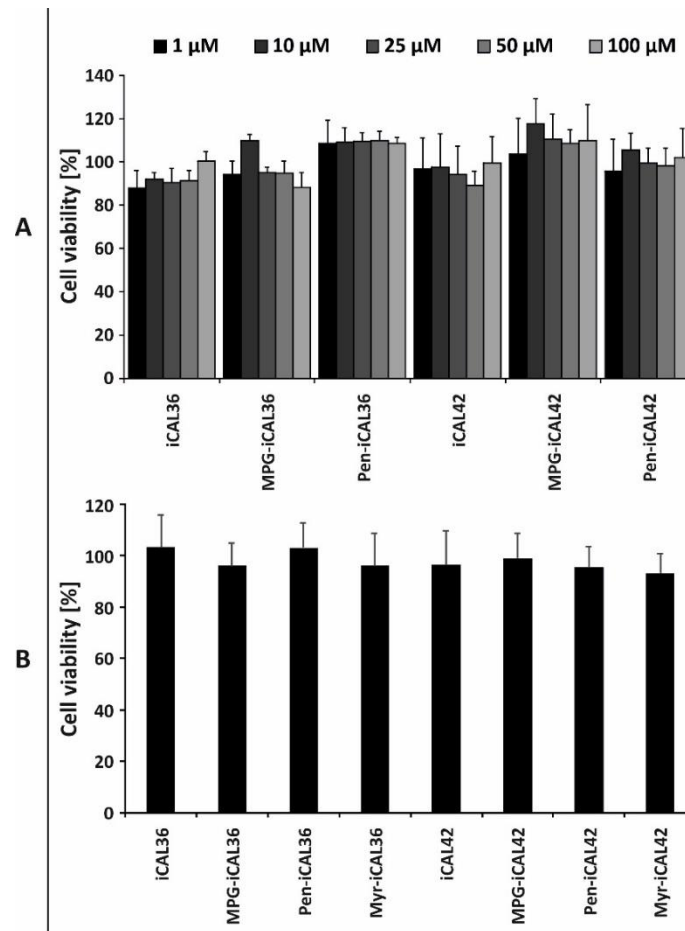


**Figure 16: Influence of CPP/Myr-iCAL36/42 to the viability of Caco-2 cells**

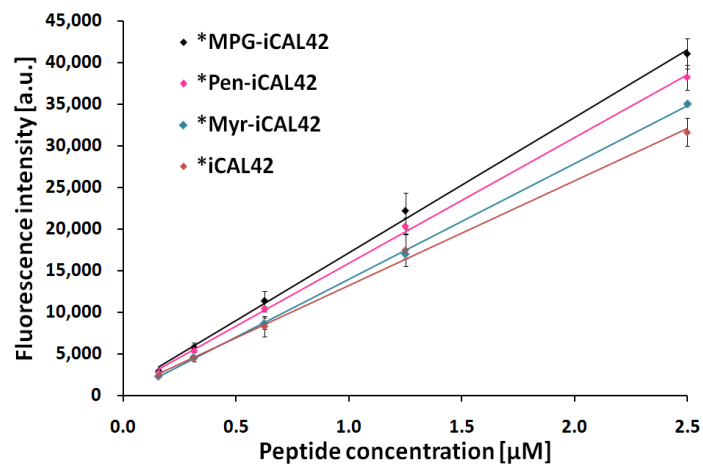
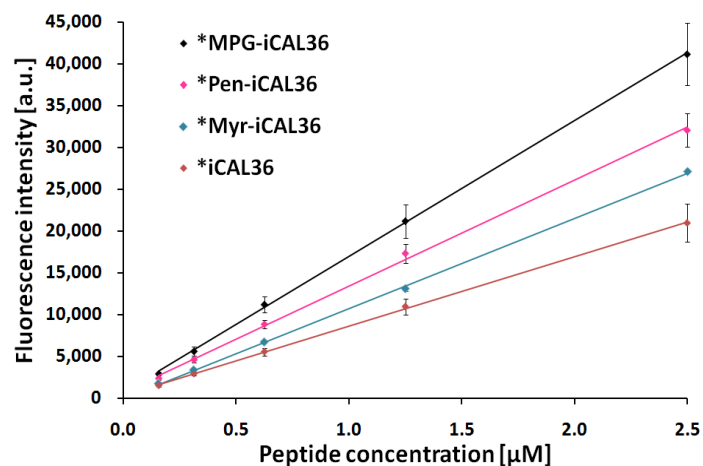
(A) Confluent Caco-2 cells were treated with MPG-iCAL36/42, Pen-iCAL36/42 and iCAL36/42 at different concentrations of 1  $\mu\text{M}$ , 10  $\mu\text{M}$ , 25  $\mu\text{M}$ , 50  $\mu\text{M}$  and 100  $\mu\text{M}$  for 3 hours and subsequently the viability was determined with (B) polarized Caco-2 cells treated with MPG-iCAL36/42, Pen-iCAL36/42, Myr-iCAL36/42 and iCAL36/42 only at a concentration of 100  $\mu\text{M}$ . Neither the confluent nor the polarized Caco-2 cells show any cytotoxicity even with concentrations up to 100  $\mu\text{M}$ . Mean values  $\pm$  SD with  $n = 3$  independent measurements.

In conclusion, the addition of MPG, penetratin, and myristic acid to the N terminus of iCAL36 and iCAL42 increased the CAL PDZ binding affinity of both inhibitors. The three iCAL modifications did not induce any cytotoxic effect at concentrations between 1  $\mu\text{M}$  and 100  $\mu\text{M}$  in confluent or polarized Caco-2 cells. This range was used for our further experiments with Myr-iCAL and CPP-iCAL conjugates.

## 6.2 Variability of the fluorescence intensity of the iCAL peptides

During our first experiments, we had observed variations in the TAMRA intensities depending on the coupled entities (peptide sequence or Myr-peptide). To allow the comparison of the fluorescence values of the different

compounds used in this study, we decided to normalize the differences between the intensities. Therefore we dissolved all TAMRA-labeled peptides at the same concentration (10  $\mu\text{M}$ ) in the RIPA lysis buffer which was used to lyse the cells and to measure the intracellular peptide. After a serial dilution from 2.5  $\mu\text{M}$  to 0.15625  $\mu\text{M}$ , we measured the different intensities in constant volumes of 100  $\mu\text{L}$  for each sample with a fluorescence spectrometer (Figure 17 A, B ).

**A****B**

**Figure 17: The fluorescence intensities of TAMRA are dependent on coupled peptides**

All TAMRA-labelled peptides (\*) were dissolved in lysis buffer and a serial dilution from 2.5  $\mu\text{M}$  to 0.15625  $\mu\text{M}$  was performed. Afterwards the fluorescence intensities of each sample was measured and depicted in dependency of concentration. (A) Fluorescence intensities of MPG-iCAL42, Pen-iCAL42, Myr-iCAL42 and iCAL42 (B) Fluorescence intensities of MPG-iCAL36, Pen-iCAL36, Myr-iCAL36 and iCAL36, Mean values with  $n \geq 3$ .

Although using the same concentration \*MPG-iCAL36 showed a 2-fold higher intensity compared to \*iCAL36. That clearly demonstrates that fluorescence intensities are influenced by the peptide sequence and the length of the peptide.

MPG-iCAL36 functions as reference value, because it produces the highest intensities. Therefore we used factor one here and normalized all other peptide intensities regarding the MPG-iCAL36 value. This results in the following multiplication factors (Table 2) which were applied in all of our further experiments.

**Table 2:** Multiplication factors of different fluorescence intensities of TAMRA

Construct	Multiplication factor
*MPG-iCAL36	1.0
*Pen-iCAL36	1.3
*Myr-iCAL36	1.6
*iCAL36	2.0
*MPG-iCAL42	1.0
*Pen-iCAL42	1.1
*Myr-iCAL42	1.2
*iCAL42	1.3

\*=TAMRA

In summary, the TAMRA fluorescence moiety is an optimal dye to measure the CPP-iCAL and Myr-iCAL internalization by fluorescence spectroscopy and the cellular localization by confocal microscopy. However, results obtained by fluorescence spectroscopy should be corrected by an experimentally determined factor due to the peptide sequence dependency of the TAMRA fluorescence signal.

### 6.3 Internalization of \*CPP/ \*Myr-iCAL in Caco-2 cells

To find the best carrier for transporting our inhibitor peptides into Caco-2 cells we performed internalization tests as described in Figure 18. We treated polarized Caco-2 cells with \*CPP-iCAL, \*Myr-iCAL and \*iCAL using a constant concentration of 10  $\mu$ M. After treatment, we trypsinated, washed and lysed the cells and after a final centrifugation step, we measured the fluorescence in the supernatant of the different samples using a microplate reader (for details see Materials and Methods).

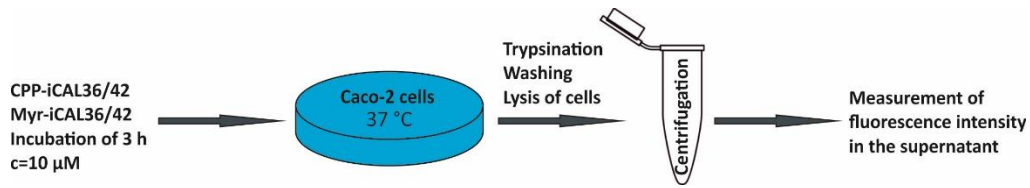


**Figure 18: Experimental setup for internalization tests**

Caco-2 cells were seeded in transwells and grown up for 14 d. Then the cells were treated with the different peptides for 3 hours and at a concentration of 10  $\mu\text{M}$ . After trypsination, washing, lysis and centrifugation the different fluorescence intensities were measured in the supernatant.

### 6.3.1 Time dependent internalization of \*CPP-iCAL42 and \*Myr-iCAL42

In a first experiment the time dependency of the internalization process was investigated using \*MPG-iCAL42, \*Pen-iCAL42 and \*Myr-iCAL42. We were interested in the internalization rate over a determined time period, also in order to find a suitable standard treatment for further experiments.

We treated Caco-2 cells for 10, 30, 60, 120 and 180 minutes with the respective peptide construct (Figure 19) according to the experimental setup described in figure 18. We set the values after the incubation of 180 minutes as equivalent to 100 %. Both CPP and myr constructs were continuously internalized over the complete time period of 180 minutes but not in a linear manner. After 10 minutes already  $22 \pm 6$  % (\*Pen-iCAL42);  $15 \pm 4$  % (\*MPG-iCAL42) and  $30 \pm 9$  % (\*Myr-iCAL42) were absorbed. The observed curves seem to follow roughly an asymptotic pattern. Due to the asymptotic increase of the CPP-iCAL and Myr-iCAL internalization, reaching more or less a plateau at 180 minutes we decided to use this incubation time in all experiments (if not otherwise denoted). Furthermore, this incubation time corresponded to the one used previously for the Bioporter iCAL36 internalization [41].

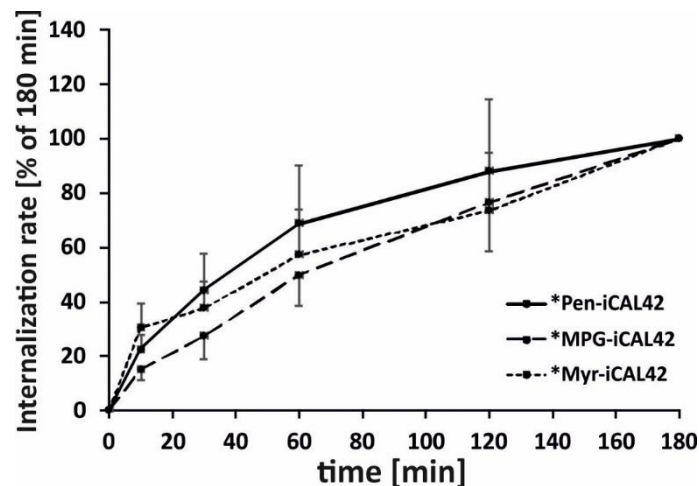


**Figure 19: Internalization rates of \*MPG/\*Pen-iCAL42 and \*Myr-iCAL42**

The internalization of the different peptides was measured after 10; 30; 60; 120 and 180 minutes according to the above (Figure 18) described experimental setup. The internalization rate is markedly higher between 0 and 10 minutes compared with the rate between 120 and 180 minutes. This is also recognizable by comparing the slopes in the beginning and the end of each curve. Mean values  $\pm$  SD with  $n = 5$  independent measurements. (\*) TAMRA

In conclusion, we did not observe a significant difference in the internalization between the three compounds \*MPG-iCAL42, \*Pen-iCAL42 and \*Myr-iCAL42 after 180 minutes. However, the internalization rate is faster in the first 10 minutes than in the remaining incubation time.

### 6.3.2 Internalization of \*iCAL36/42 and \*CPP/Myr-iCAL in comparison

To compare the internalization potential of the 8 iCAL compounds used in this study, we incubated polarized Caco-2 cells for 180 minutes using a constant concentration of 10  $\mu$ M. As expected, non-vectorized \*iCAL36/42 showed the same fluorescence intensities as the untreated cells (Control) in Caco-2 cells. Interestingly, the internalization of both \*CPP-iCAL36 was more efficient than the internalization of both \*CPP-iCAL42 constructs. That is a remarkable result as the structural difference is only one amino acid within the iCAL sequence (W $\rightarrow$ L mutation).

Furthermore, our results demonstrated that myristic acid acts also as an effective carrier for the iCALs. Remarkably, the above observed internalization difference between \*CPP-iCAL36 and \*CPP-iCAL42 constructs could not be observed in either Myr-iCAL construct (Figure 20).

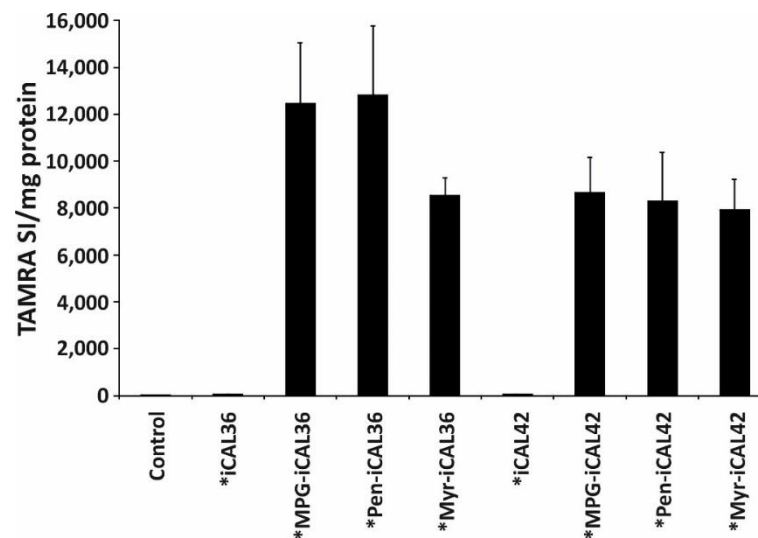


**Figure 20: Internalization with \*CPP/Myr-iCAL and \*iCAL treated Caco-2 cells**

Polarized Caco-2 cells were seeded 14 d before the experiment. The cells were treated apical with 10  $\mu$ M of each construct for 3 hours at 37  $^{\circ}$ C and 5 % CO<sub>2</sub>. Untreated cells serve as the control. After the treatment the cells were trypsinated, washed and lysed. Afterwards the fluorescence intensity was analyzed in 100  $\mu$ L of the supernatant of each sample.

iCAL36 coupled to \*CPP shows higher internalization results than iCAL42. \*Myristic acid coupled to iCAL36/42 is also an effective carrier. A carrier is necessary for an efficient transport, because both “stabilizers” without any carrier show signals in the range of the untreated control cells.

Graph represents an values  $\pm$  SD with n = 4 independent experiments. (\*) TAMRA

### 6.3.3 Peptide release after cellular internalization

Another question that we tried to address is to determine whether peptides after their internalization into the cell the peptides would be released and if this would be the case, how quick this process would be? This could be relevant because if the peptides remain inside the cell only for a short time their effect could be remarkably decreased. Unfortunately, we could find no publication answering these questions and therefore we had to develop a new experimental setup. We incubated differentiated Caco-2 cells with \*CPP-iCAL42 and \*Myr-iCAL42 at a concentration of 10  $\mu$ M for 60 minutes. After the trypsination and washing steps for removing extracellular attached peptides, the cells were transferred in a medium without FBS. At defined time points (30, 60 and 120 minutes), we measured the fluorescence intensities of both the supernatant (peptide release) and the cell lysate (peptide internalization). Thereafter, we calculated the percentage of released peptide compared to the total internalization.

The fluorescence values of released \*MPG-iCAL42 were  $14.0 \pm 4.1$  % (after 30 minutes);  $13.0 \pm 5.1$  % (after 60 minutes) and  $17.0 \pm 5.3$  % (after 120 minutes) of the respective internalization which was in the same range as \*Pen-iCAL42 with results of  $6.9 \pm 1.4$  % (30 minutes),  $8.1 \pm 0.9$  % (60 minutes) and  $12.1 \pm 1.5$  % (120 minutes). In contrast the delivery of \*Myr-iCAL42 in the supernatant is very low compared to \*MPG/\*Pen-iCAL42. The amounts are only  $1.4 \pm 0.5$  % (30 minutes),  $1.1 \pm 0.2$  % (60 minutes) and  $1.7 \pm 0.3$  % (120 minutes) of the respective internalization values (Figure 21). This phenomenon was surprising and should be elucidated using other experiments as described in the next chapters.

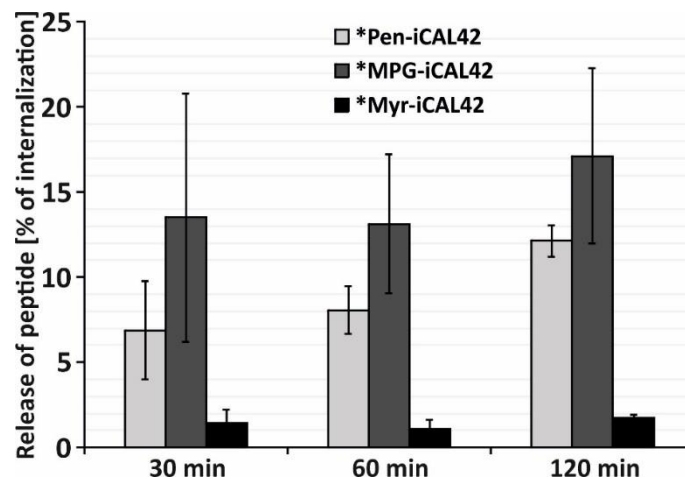


**Figure 21: The release of \*Pen/\*MPG-iCal42 and \*Myr-iCal42**

Caco-2 cells were incubated with \*Pen/\*MPG-iCAL42 and \*Myr-iCAL42 at a concentration of 10  $\mu$ M at 37°C and 5 % CO<sub>2</sub>. The constructs are labeled with TAMRA and the analysis occurs due to the measurement of the fluorescence of TAMRA. After the incubation the cells were washed and trypsinated for removing attached peptides, which falsify the results. Then the cells were dissolved in 1 mL medium without FBS. After 30; 60 and 120 minutes a sample is extracted from the supernatant and the fluorescence is measured with the microplate reader. The % values refer to the internalization values after 30; 60 and 120 minutes. \*MPG-iCAL42 shows the highest release values (14; 13 and 17 %) and \*Pen-iCAL42 are approximately in the same range (7; 8; and 12 %) whereas the myristic acid samples show a nearly 10-fold lower release (1.4; 1.1 and 1.7 %) after the declared time points.

Graph represent mean values  $\pm$  SD with n = 3 independent experiments. (\*) TAMRA

In conclusion, the internalization rate of \*MPG, \*penetratin or \*myristic acid coupled to iCAL42 over a time period of 180 minutes did not follow a linear but an asymptotic pattern. We measured the highest internalization values after 180 minutes (Figure 19). Therefore we used the same time frame in our further internalization experiments.



The internalization experiments revealed that there is no uptake of \*iCAL without a CPP or Myr, which shows the necessity to use a vectorization mode. In addition, we observed that the internalization of \*CPP-iCAL36 was significant higher than for their \*CPP-iCAL42 counterpart, although there was only one amino acid substituted in the iCAL sequence. The \*Myr-iCAL compound also showed remarkable internalization results in the range of \*CPP-iCAL42 (Figure 20). In contrast, the intracellular release of \*Myr-iCAL42 is nearly 10-fold lower than that of \*CPP-iCAL42 (Figure 21).

#### **6.3.4 Cellular iCAL localization depending on the used carrier**

To confirm the results of our internalization tests and to see the cellular localization of our compounds, we performed microscopy analyses of \*iCAL and \*CPP-iCAL incubations (60 minutes) on confluent Caco-2 cells.

First we had to find the optimal peptide concentration regarding intensity, amount and peptide distribution in the cell. Therefore we incubated Caco-2 cells with TAMRA labeled \*MPG-iCAL36 and \*Pen-iCAL36 at peptide concentrations of 1  $\mu\text{M}$  and 10  $\mu\text{M}$  for one hour. With 10  $\mu\text{M}$  we received a strong and well distinguishable TAMRA fluorescence signal (red) whereas at 1  $\mu\text{M}$  there were significantly less fluorescence spots in the cytosol. So we decided to use the higher peptide concentration of 10  $\mu\text{M}$  for our further experiments (Figure 22).

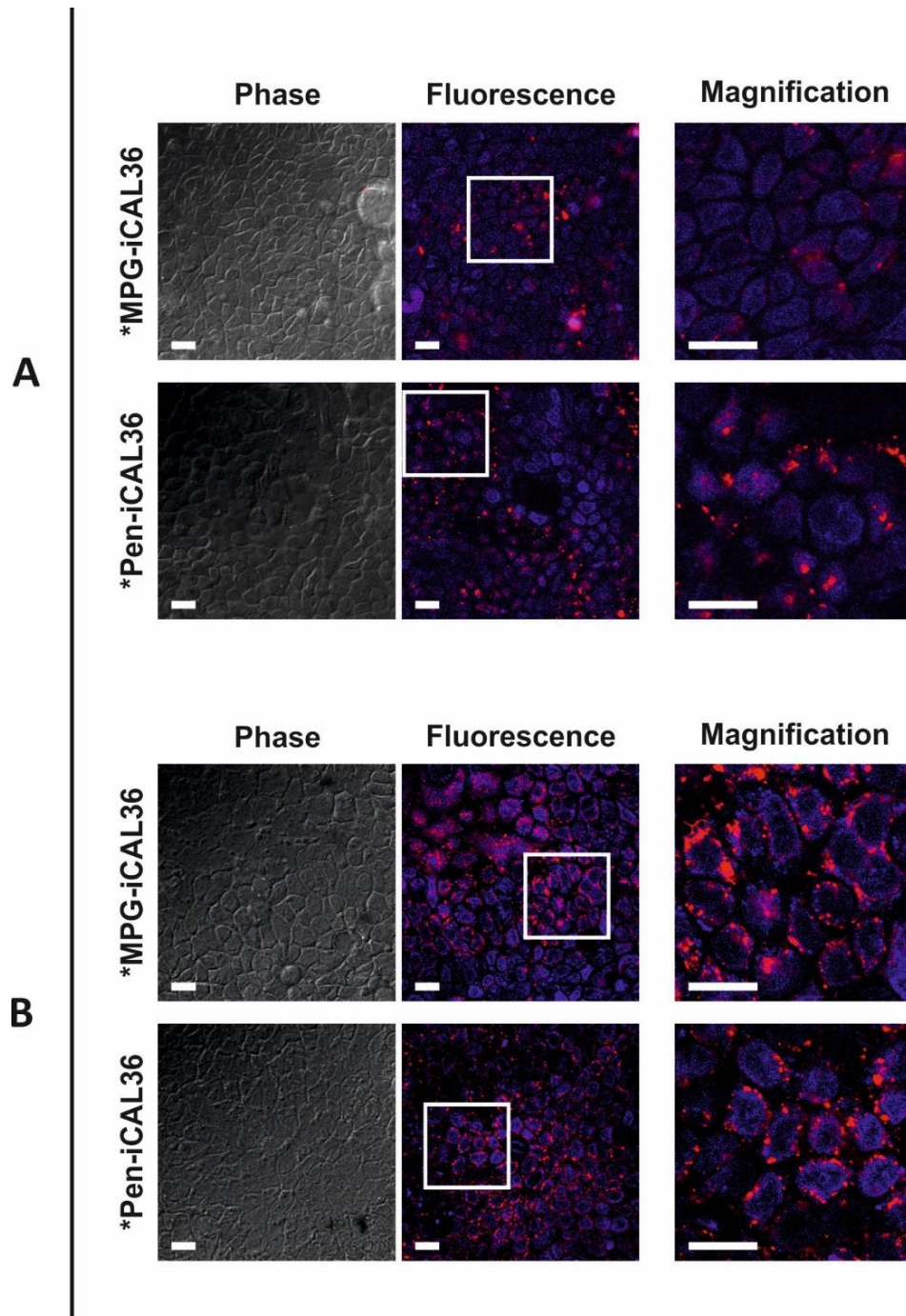


**Figure 22: Dose-dependent intracellular distribution of \*CPP-iCAL36 in Caco-2 cells**

Representative images of confluent Caco-2 cells which were incubated with (A) 1  $\mu\text{M}$  or (B) 10  $\mu\text{M}$  \*MPG/\*Pen-iCAL36 for 1 hour. Cell nuclei were labeled with Hoechst dye and appear in blue. \*MPG/\*Pen-iCAL36 distributions were evaluated in living, unfixed cells by fluorescence microscopy. (A) The fluorescence intensities are obviously lower in the cells which are treated with (A) 1  $\mu\text{M}$  peptide concentration compared with the higher intensity of the (B) 10  $\mu\text{M}$  incubated cells. White scale bar = 20  $\mu\text{m}$ , (\*) TAMRA

Based on the results of our preliminary tests we incubated confluent Caco-2 cells with MPG/Pen-iCAL36/42 and iCAL36 at a peptide concentration of 10  $\mu\text{M}$  for one hour. The picture of the inhibitor alone did not show any red signal (Figure

23, bottom panel), which is in accordance with our internalization tests by fluorescence spectroscopy. This demonstrates the necessity of a carrier for an efficient internalization.

The incubation with the inhibitors coupled to the CPPs revealed dotted patterns in the cytosol and a complete absence of nuclear localization (labeled in blue), regardless which CPP was used. This is shown particularly well in the magnification. One should note that a large proportion (> 90 %) of the total cell population was successfully transfected (Figure 23).

Interestingly, the fluorescence signals of the \*CPP-iCAL36 constructs were stronger than signals given by the \*CPP-iCAL42 constructs. This confirms our internalization results measured in the supernatant of lysed Caco-2 cells (see Figure 20).

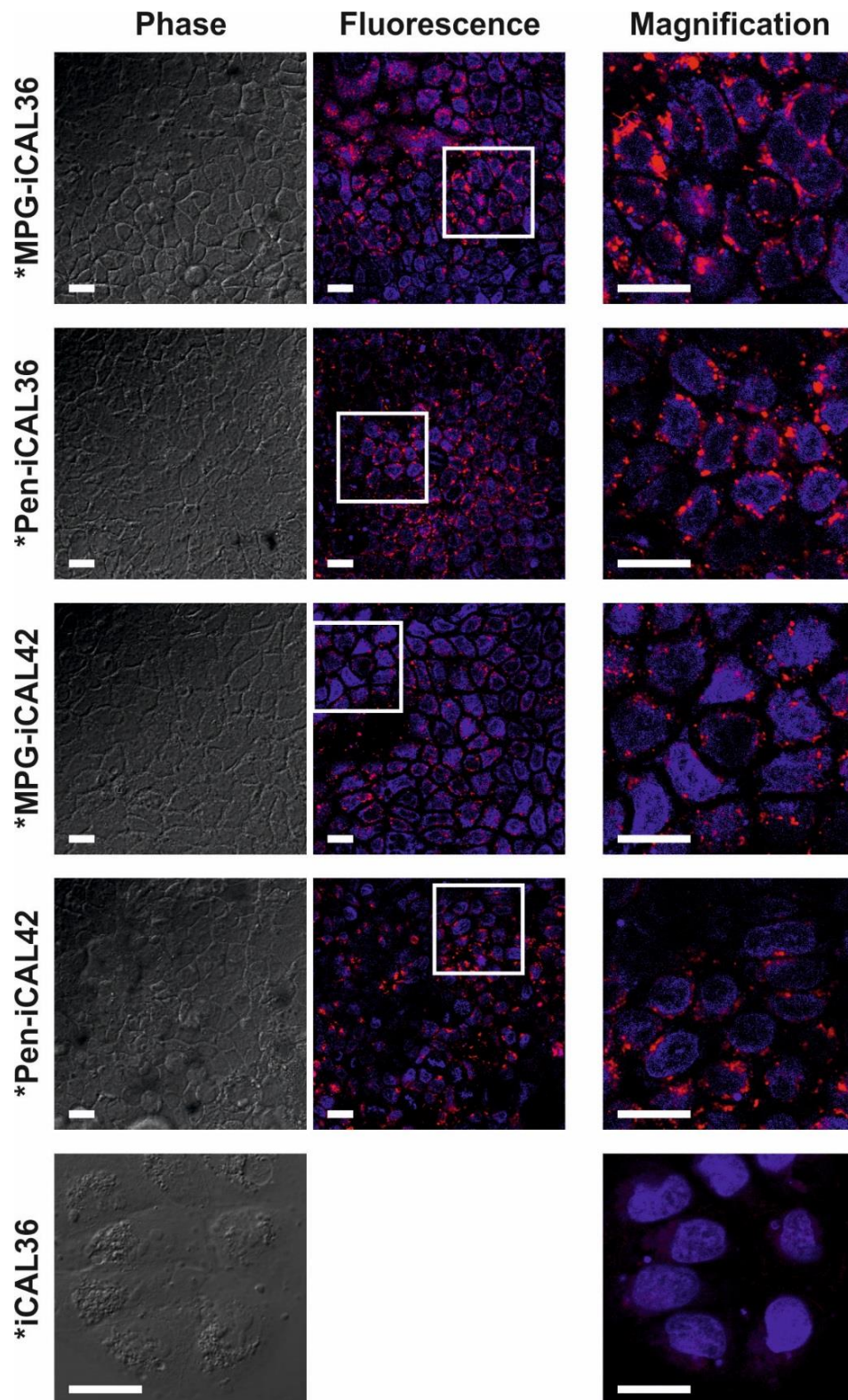


**Figure 23: Representative images of the internalization of \*CPP-iCAL in Caco-2 cells**

Caco-2 cells were treated with \*Pen-iCAL36/42, \*MPG-iCAL36/42 and \*iCAL36 at a concentration of 10  $\mu\text{M}$  for 1 hour. All peptides are labeled with TAMRA and appear in red and the nuclei are dyed with Hoechst and appear in blue. The internalization is clearly visible. The TAMRA signal is distributed around the nuclei and is complete absent in nuclei. The inhibitor \*iCAL36 alone is not able to translocate over cellular membranes, which is an obvious indication for the necessity of a carrier for an efficient internalization. White scale bar = 20  $\mu\text{M}$ , (\*) TAMRA

#### 6.3.4.1 \*Myr-iCAL internalization and cellular localization

At the same time we analyzed the internalisation efficiency of Myr-iCAL by confocal microscopy. To this end we incubated Caco-2 cells for 1 hour with \*Myr-iCAL42 (1  $\mu$ M). We chose the concentration of 1  $\mu$ M because when we tested Myr-iCAL at a concentration of 10  $\mu$ M the fatty acid remained on the cell membranes and negatively influenced the picture quality. Conspicuously, after an incubation of 1 hour \*Myr-iCAL appeared to be stuck within the cellular membrane (Figure 24 A). To test whether the fatty acid is able to translocate into the cytoplasm after a longer incubation time, we treated Caco-2 cells with \*Myr-iCAL42 for 3 hours. After the longer incubation time the distribution of \*Myr-iCAL is similar to that of their \*CPP-iCAL counterparts. We could also detect the complete absence of nuclear localization. The red fluorescence signal was dispersed around the nuclei and is now not located in the cell membranes. It is reasonable to suggest, that myristic acid needs a longer incubation time for an efficient translocation into the cytoplasm of Caco-2 cells.

To further compare the different internalization rates of the CPP's and Myr in detail, we performed internalization tests with \*MPG-iCAL, \*Pen-iCAL and \*Myr-iCAL over 1 hour and 3 hours respectively as described in Figure 18.

We could not detect the expected significant differences between the internalization of CPP's and the myristic acid after an incubation time of one hour. The lowest value showed \*MPG-iCAL42 with  $53 \pm 14$  % and the highest \*Pen-iCAL36 with  $76 \pm 11$  %. \*Myr-iCAL36 and \*Myr-iCAL42 showed values of  $63 \pm 14$  % and  $70 \pm 16$  % which were in the same range (Figure 24 B), although our microscopy results had suggested that the CPP's were internalized while the myristic acid remained in the cell membranes and should not have been detectable in the cytoplasm.

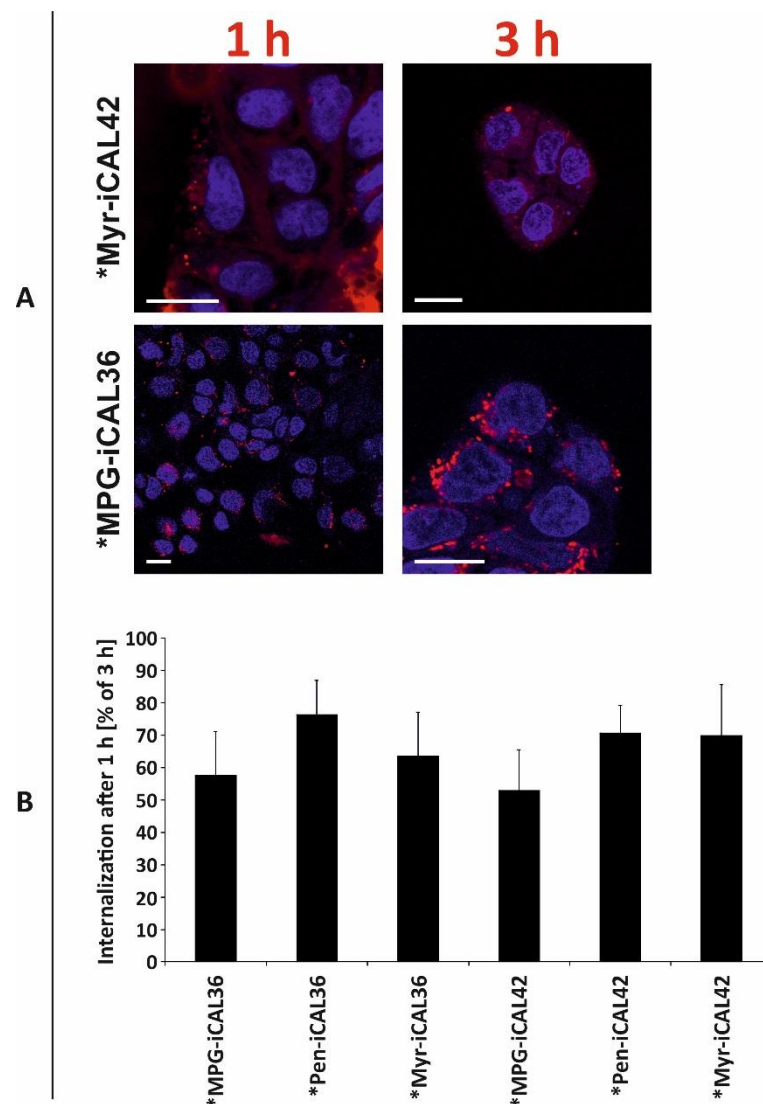


**Figure 24: The internalization efficiency of \*Myr-iCAL42 depending on the incubation time**

(A) Confluent Caco-2 cells were treated with \*Myr-iCAL42 for 1 and 3 hours at a concentration of 1  $\mu$ M. The myristic acid appears in red and the nuclei in blue. After 1 hour the fatty acid is to be arranged in the cell membranes but after the longer treatment of 3 hours the \*Myr-iCAL42 compound is distributed in the cytoplasm of the cells around the nuclei. It might be assumed, that the \*myristic acid needs a longer incubation time for an efficient internalization. White scale bar = 20  $\mu$ M (B). To investigate the difference of internalization between CPP's and the myristic acid we compared the internalization values after treatment for 1 hour and 3 hours at the same concentration of 10  $\mu$ M. The values are between 53  $\pm$  14 % (\*MPG-iCAL42) and 76  $\pm$  11 % (\*Pen-iCAL36) of the 3 hours results. \*Myr-iCAL36 and \*Myr-iCAL are intermediate with values of 63  $\pm$  14 % and 70  $\pm$  16 % and thus did not show the expected results of significant lower internalization values after 1 hour incubation. Graphs represent mean values  $\pm$  SD with n = 4 independent experiments. (\*) TAMRA

In summary, the microscopy pictures of Caco-2 cells treated with \*CPP-iCAL showed a significant internalization and the fluorescence signals of \*CPP-iCAL36 were higher than those of their iCAL42 counterparts. We also observed that a carrier was necessary for an efficient internalization because \*iCAL36 treated cells did not show any TAMRA signal (Figure 23) in the cytosol.

Microscopy experiments revealed that the \*Myr compounds needed a longer incubation time than their CPP counterparts for an optimal delivery into the cell (Figure 24 A), while our internalization experiments did not confirm these differences (Figure 24 B). See details in the discussion.

### 6.3.5 Temperature and ATP dependency of internalization

As the next step in our research we looked at the mechanism behind the translocation of CPP-iCAL and Myr-iCAL across the cytoplasm. The mechanisms of cellular internalization of CPPs and/or CPP-cargoes as well as those of fatty acids (such as myristic acid) and their covalently bound cargo are not fully understood, although there are different models discussed [60; 80; 86]. For all these reasons, it is important to elucidate the uptake mechanism of our analyzed \*CPP-iCAL and \*Myr-iCAL constructs. In this context the question arose whether it is a direct translocation or an ATP (energy) dependent endocytosis.

Therefore we incubated confluent Caco-2 cells with \*MPG-iCAL, \*Pen-iCAL or \*Myr-iCAL at a concentration of 10  $\mu$ M for 3 hours simultaneously in three different settings (Figure 25). In the first setting the cells were treated under standard conditions at 37°C according to our reference (Figure 25 A); in the second setting the cells were incubated at 4 °C to inhibit the endocytosis and to lower the entire cell metabolism (Figure 25 B); in the third setting the cells were incubated at 37°C in the presence of sodium azide and 2-deoxy-D-glucose (2-DG) which prevent the production of ATP [69] and inhibit the glycolysis pathway [68] subsequently resulting in a reduction of the cellular energy ATP levels (Figure 25 C). Finally we measured the fluorescence intensity by means of fluorescence spectroscopy.

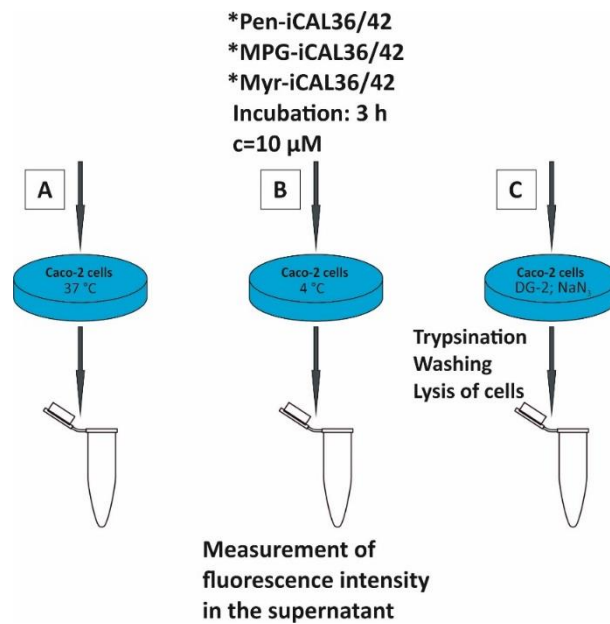


**Figure 25: Experimental setup for analyzing ATP dependency**

Three different preparations were performed. Common to all three is, that they are treated with 10  $\mu$ M \*Pen-iCAL36/42, \*MPG-iCAL36/42 and \*Myr-iCAL36/42 for 3 hours. (A) Additionally the first preparation serves as the 100 % reference value which means that Caco-2 cells are incubated by 37 °C under normal internalization conditions as described in figure 18. (B) The second variation is that the cells were incubated at 4°C, and (C) the last version is the additional treatment of the cells with NaN<sub>3</sub> and DG-2. After incubation we trypsinated and washed the cells several times followed by lysis. After a last centrifugation step we measured the fluorescence in the supernatant. (\*) TAMRA

Neither the 4°C nor the ATP-depletion treatment showed a remarkable effect on the \*Pen-iCAL or \*MPG-iCAL internalization in Caco-2 cells (Figure 26). We observed only a slight reduction of 20 % of the internalization with \*MPG-iCAL42 ( $79 \pm 6$  %) at a temperature of 4°C and of 15 % with \*Pen-iCAL46 ( $86 \pm 14$  %) under ATP inhibition. This leads to the conclusion that the uptake of \*Pen-iCAL and \*MPG-iCAL is ATP-independent and it seems that CPP's needed almost no other driving forces because even at a temperature of 4°C we could observe an uptake relatively close to our reference values (37°C condition).

In contrast to \*Pen-iCAL or \*MPG-iCAL the internalization of the \*Myr-iCAL showed a reduction of ~50 % in the 4°C incubation while under conditions of ATP inhibition with NaN<sub>3</sub> and DG-2 the uptake values were in the same range as its untreated references. The results were  $106 \pm 11$  % in the case \*Myr-iCAL36 and  $95 \pm 17$  % in the case of \*Myr-iCAL42 (Figure 26).



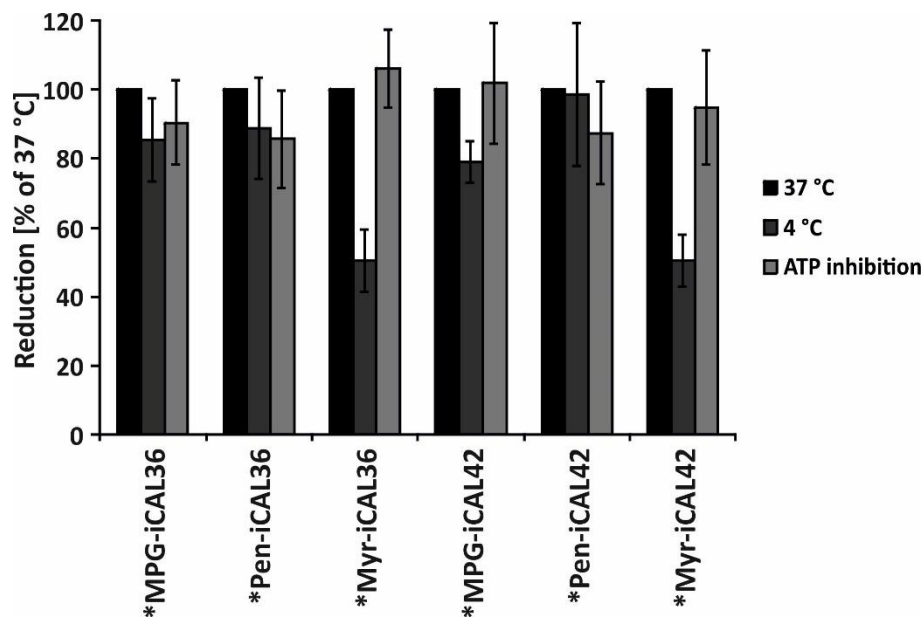


**Figure 26: Evaluation of the internalization mechanism of \*CPP-iCAL and \*Myr-iCAL**

The experimental setup is as described in figure 18. Neither the inhibition of ATP production of the cells nor the 4°C treatment shows any effect to the internalization of \*MPG and \*penetratin. \*CPPs are able to translocate over cellular membranes without ATP consumption. The \*myristic acid is halved after the treatment at a temperature of 4°C, but we could not detect an effect after blocking the ATP production.

Graphs represent mean values  $\pm$  SD with n = 3 (Myr-iCAL36/42) n = 5 (Pen/MPG-iCAL36/42) independent experiments. (\*) TAMRA

In summary, the energy dependency experiments revealed that the energy reduction did not show any effect to the internalization of all \*CPP-iCAL constructs which is a sign for an energy independent transduction of \*CPP-iCAL. In contrast, the internalization of \*Myr-iCAL is clearly reduced during the treatment at 4°C signifying a temperature dependence.

### 6.5 Evaluation of the stability of iCAL, CPP-iCAL and Myr-iCAL

With regard to a future application, the iCAL inhibitor should be nebulized for lung administration, should be able to pass the mucus and to internalize the lung epithelial cells. Therefore, it is important to estimate the stability of our compounds towards proteases.

To this end the CPP-iCAL and Myr-iCAL constructs were dissolved in 20 % human serum, sampled probes were collected at defined time points and analyzed by RP-HPLC (Figure 27 A). This process resulted in a graph over a time period (Figure

27 B and C). The curve or the peak was integrated and the changes in these values were compared and analyzed.

For a better visualization without disturbances caused by the serum figure 27 B and C show Myr-iCAL42 and MPG-iCAL42 dissolved in water at a concentration of 500  $\mu\text{M}$ . The spectra in figure 27 show differences between myristic acid (B) and CPP-iCAL (C). The area of myristic acid is 10-fold lower than of CPP-iCAL although we used the same concentration. The reason for this phenomenon could be, that we detected UV-adsorption at 214 nm which is the optimal wave length of amide bonds. The cell penetrating peptides consisted of 26 (MPG) or 16 (penetratin) amino acids and just as many amide bonds. The myristic acid coupled to iCAL36/42 contained only one additional amide bond. Probably these differences between CPP's and the myristic acid lead to the varying spectra in figure 27 B and C. Therefore we used Myr-iCAL in the 2-fold higher concentration of 1000  $\mu\text{M}$  in the stability experiments in order to reach a meaningful evaluation.

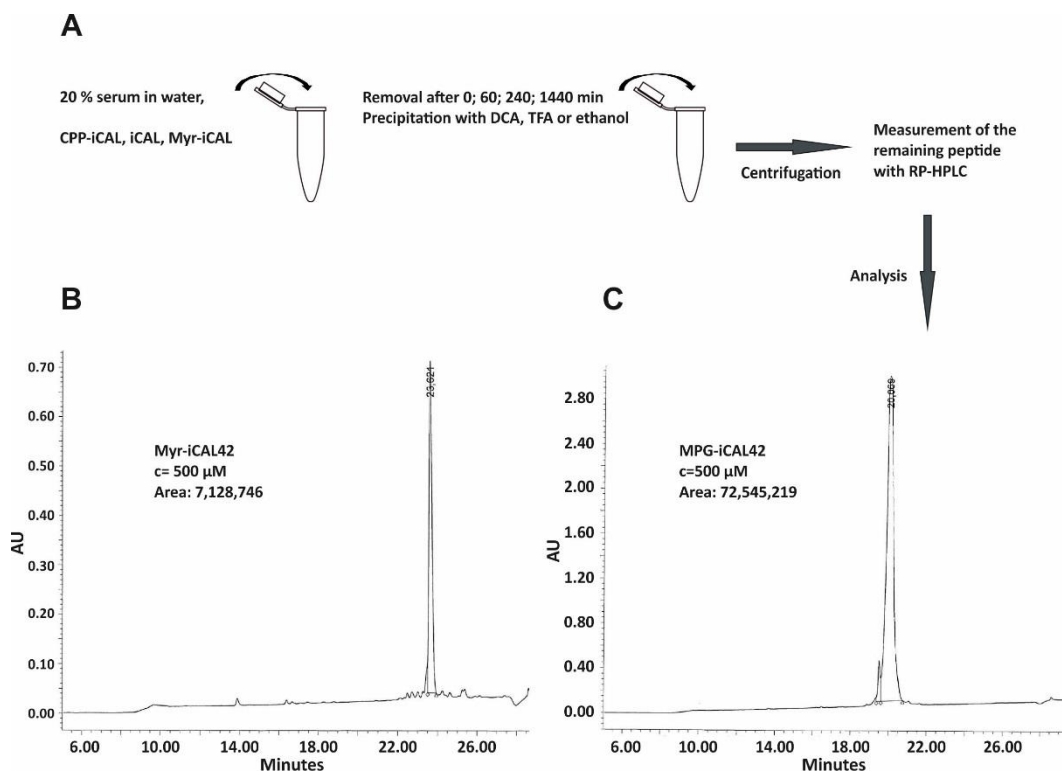


**Figure 27: General procedure of stability tests and comparison of two different spectra**

(A) CPP-iCAL, iCAL and Myr-iCAL were dissolved in 20 % human serum. After defined time points 50  $\mu\text{L}$  were removed and precipitated. After centrifugation the samples were analyzed with RP-HPLC and the area under the curve is integrated. (B, C) RP-HPLC spectra of Myr-iCAL and MPG-iCAL42 dissolved in water as examples for the difference of myristic acid and CPP. The peak of MPG-iCAL42 is more than 4-fold and the area under the curve is 10-fold higher than under Myr-iCAL42 although we used the same concentration.

### 6.5.1 Improvement of precipitation conditions

One critical step in the presented analysis of the protease stability of our compounds is the optimal precipitation procedure to remove cell compounds and proteins which can impair the HPLC analyses. We tested 500  $\mu\text{M}$  Pen-iCAL42 and 1000  $\mu\text{M}$  Myr-iCAL36 in 20 % human serum as examples for CPP-iCAL and Myr-iCAL. After an incubation time of 240 minutes 50  $\mu\text{L}$  were removed and precipitated. Because of the practical experience of our group regarding the behavior of peptides in presence of acids or alcohol we decided to test 5 % DCA, 6.7 % DCA and 14.3 % TFA in the case of Pen-iCAL42 and 5 % DCA, 10 % ethanol and 5 % TFA for Myr-iCAL36, respectively (Figure 28). The highest results were reached by the precipitation of Pen-iCAL42 with 5 % DCA (Figure 28 A) which is why we used this condition for our further degradation experiments with iCAL and CPP-iCAL. Furthermore the RP-HPLC spectra of Pen-iCAL42 precipitated with 5 % DCA showed the smallest disturbances through proteins and cell compounds (data not shown).

For our further protease stability tests with Myr-iCAL we decided to use 10 % ethanol because this precipitation procedure produced the highest values after precipitating Myr-iCAL36 (Figure 28 B).

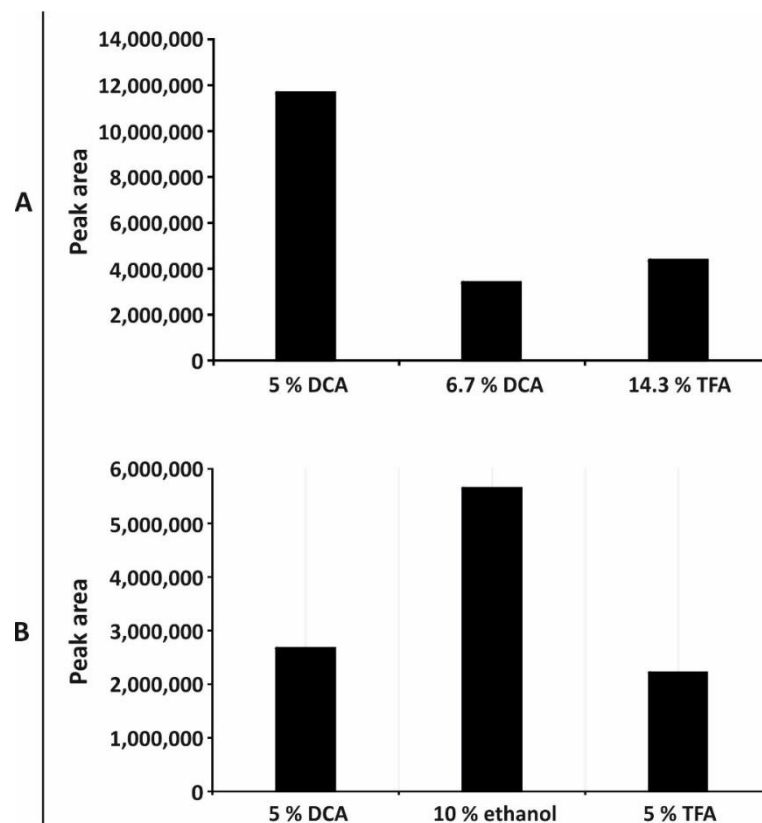


**Figure 28: Different precipitations to find the suitable procedure**

The degradation of (A) Pen-iCAL42 and (B) Myr-iCAL36 in 20 % human serum is measured after a time period of 240 minutes and is shown as absolute values. Different precipitation variants were tested. Finally 5 % DCA (iCAL, CPP-iCAL) and 10 % ethanol (Myr-iCAL) were used for further precipitation experiments because both substances lead to the highest amounts.

### 6.5.2 Comparison of the protease stability of iCAL compounds

We probed the degradation of iCAL, CPP-iCAL and Myr-iCAL in 20 % human serum over a time period of 24 hours. For this purpose we took samples directly after dissolving (= 0 minutes), after 60 minutes, 120 minutes, 240 minutes, 360 minutes, and 24 hours. Then we precipitated and centrifuged the samples and measured the remaining peptide in the supernatant with the RP-HPLC which was generally the same procedure as described in figure 27 A.

The values of MPG/Pen-iCAL36, iCAL36 (Figure 29 A) and MPG/Pen-iCAL42, iCAL42 (Figure 29 B) were approximately in the same range. It should be noted that the MPG compounds were degraded faster than the penetratin compounds. For a better demonstration we calculated the half-lives based on the resulting curve of each peptide. For realization we generated a function of each curve and computed the time point in which 50 % of the peptides remain. After 128

minutes respectively 153 minutes the calculated half of MPG-iCAL42 and MPG-iCAL36 is degraded. In contrast degradation of Pen-iCAL36, Pen-iCAL42, iCAL36 and iCAL42 took place more slowly. The calculated half-lives of these peptides are 427 minutes (Pen-iCAL42 and iCAL42), 360 minutes (Pen-iCAL36) and 407 minutes (iCAL36) (Figure 29 A and B). Pen-iCAL36, Pen-iCAL42, iCAL36 and iCAL42 showed a nearly three times longer half-life than the MPG-iCAL conjugates. After 24 hours no intact iCAL nor iCAL-conjugate could be detected by RP-HPLC (data not shown).

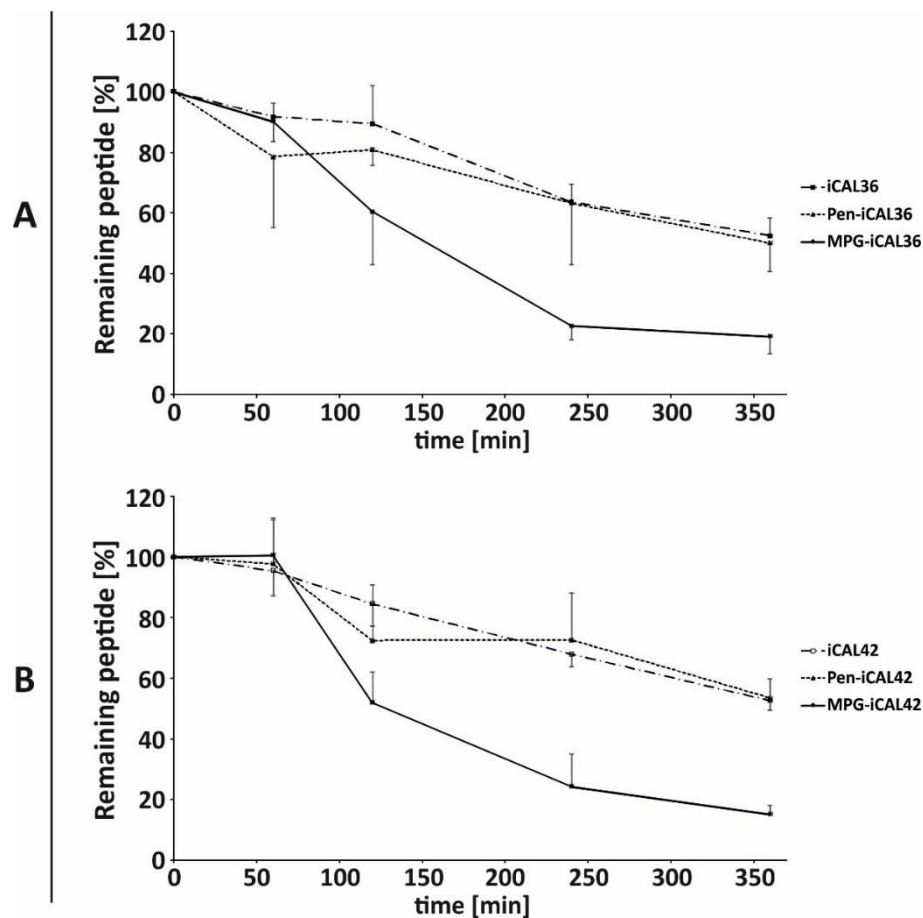


**Figure 29: Degradation of Pen-iCAL36/42; MPG-iCAL36/42 and iCAL36/42 in human serum**

All peptides were tested at a concentration of 500  $\mu$ M in 20 % human serum. During the whole experiment the samples were shaken at a temperature of 37 °C. The samples were precipitated with 5 % DCA on ice.

The MPG constructs were most rapidly degraded. Already after 120 minutes the half of the peptide was degraded. In contrast penetratin coupled to both “stabilizers” and iCAL36/42 without a cell penetrating peptide was degraded after 360 minutes. All peptides are disappeared at the latest after 1440 minutes.

Graphs represent mean values  $\pm$  SD with  $n = 3$  (Myr-iCAL36/42)  $n = 5$  (Pen/MPG-iCAL36/42) independent experiments. Graph represent mean values  $\pm$  SD with minimum  $n = 3$

Next we tested the protease stability of Myr-iCAL36 and Myr-iCAL42 in 20 % human serum over a time period of 24 hours. During the incubation at a temperature of 37 °C the probes were shaken continuously. Directly after dissolving and then after 240 minutes, 360 minutes and 24 hours samples were taken, centrifuged and analyzed by RP-HPLC. The degradation of Myr-iCAL36 and Myr-iCAL42 was shown in figure 30. After 240 minutes already 60.3 % of Myr-iCAL36 was degraded. In contrast Myr-iCAL42 nearly completely withstood the degradation process within the first 24 hours (16 % degradation). Therefore we tested the protease stability of Myr-iCAL36 and Myr-iCAL42 over an extended time period of 72 hours. Both compounds Myr-iCAL36 as well as Myr-iCAL42 were still detectable even after 72 hours (Myr-iCAL36 with  $17 \pm 2$  % and Myr-iCAL42 with  $63 \pm 20$  %, data not shown).

In comparison, every CPP-iCAL and iCAL conjugate tested before was completely degraded after 24 hours. Myr-iCAL42 is more stable than Myr-iCAL36 over a time period of 72 hours although they are only different in one amino acid.

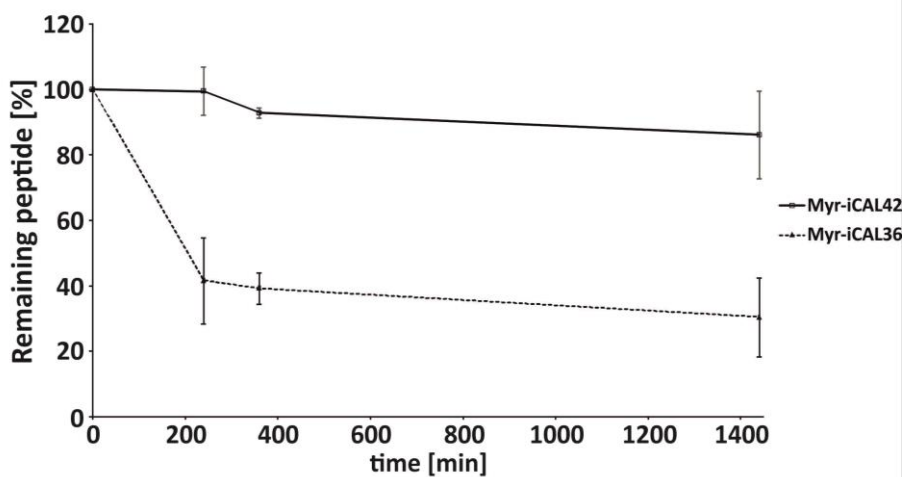


**Figure 30: Protease stability of Myr-iCAL36 and Myr-iCAL42 in human serum**

The protease stability of Myr-iCAL36/42 was tested in 20 % human serum at a myristic acid concentration of 1 mM. The degradation is shown over a time period of 24 hours. In the beginning Myr-iCAL36 is fast diminished but after 240 minutes the degradation rate is significantly reduced. In contrast the Myr-iCAL42 reduction is over the whole time period decelerated. Particularly interesting is that Myr-iCAL36 as well as Myr-iCAL42 after 72 hours is not completely degraded.

Graphs represent mean values  $\pm$  SD with minimum  $n = 3$

In conclusion our preliminary experiments established 5 % DCA and 10 % ethanol as optimal precipitation for CPP-iCAL and iCAL (Figure 28 A) and for Myr-iCAL

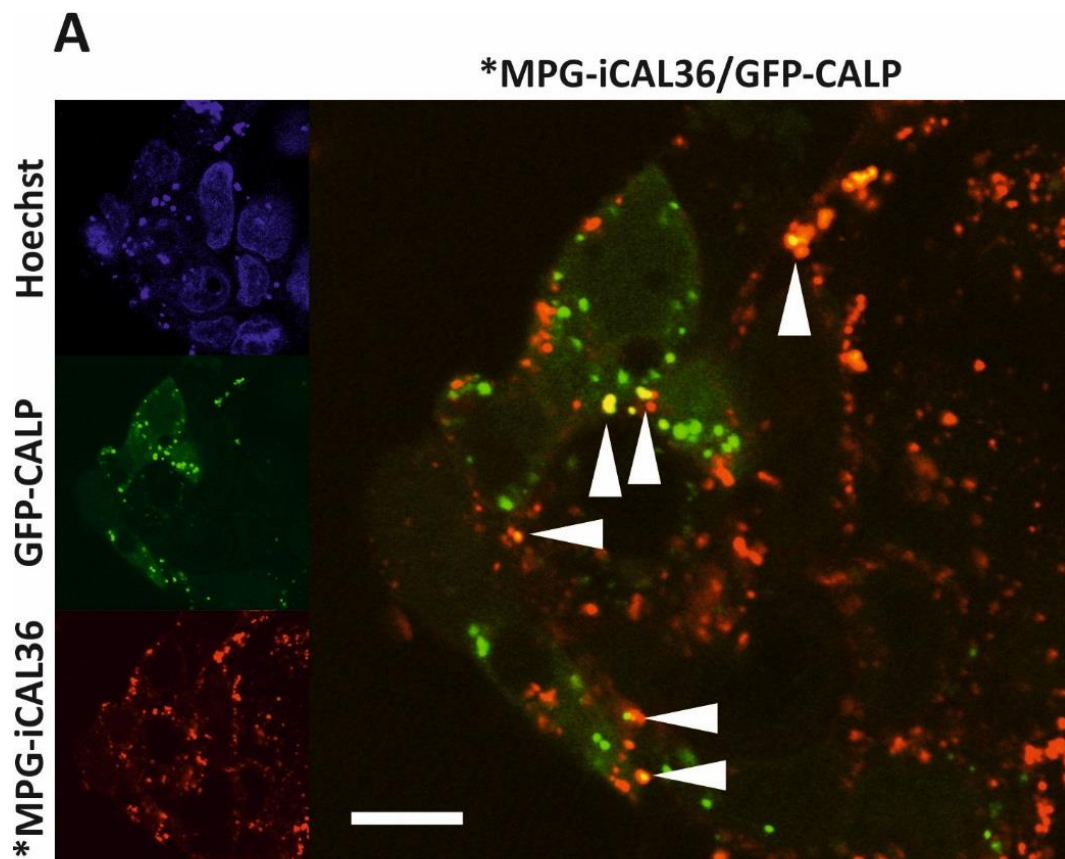
(Figure 28 B) respectively. MPG-iCAL was degraded most rapidly while its Pen-iCAL and iCAL counterparts were more stable with a nearly three times longer half-life. None of them were detectable after 24 hours.

Both Myr-iCAL compounds showed better protease stability with large amounts still detectable even after 72 hours, but Myr-iCAL42 was more stable than Myr-iCAL36.

## 6.6 Co-localization of \*MPG-iCAL36 and CAL PDZ *in cellulo*

In an earlier cooperative publication with Prof Dean R. Madden's group we could demonstrate by NMR measurements that iCAL36 occupies the CAL PDZ peptide-binding cleft [41]. But until now, the co-localization of the vectorized iCAL peptide and the PDZ domain of the CAL protein had not been demonstrated in a biological system. Therefore, we performed a transient transfection of Caco-2 cells using a plasmid encoding the green fluorescence protein (GFP) tagged full length GFP-CAL plasmid. After 24 hours, the transfected cells were incubated with \*MPG-iCAL36 as well as \*MPG-SC as negative control for 1 hour. In contrast to the previous incubation, the concentration of the TAMRA labeled peptides was decreased to 1  $\mu$ M to adjust the TAMRA fluorescence intensity to the GFP fluorescence intensity. To avoid any artifact by peptide degradation, the cells were incubated with the vectorized iCAL compounds for only 1 hour (nearly no degradation at all as shown in Figure 29). As shown before Myr-iCAL would not internalize in such a short time period and thus would not be able to co-localize with the CAL PDZ domain. Because it has the highest affinity to the CAL PDZ domain *in vitro* (see Table 1 in Chapter 6.1) we finally selected MPG-iCAL36 as the sequence to verify the co-localization *in cellulo*. The representative picture obtained by confocal microscopy revealed a red \*MPG-iCAL36 and a green GFP-CAL PDZ fluorescence signal (Figure 31 A). The overlay is depicted on the right hand side. The merged signals of \*MPG-iCAL36 and GFP-CAL-PDZ appear in yellow and are marked by white arrows. To confirm the specificity of the co-localization experiments with \*MPG-iCAL36, we performed the same experiment setting using \*MPG-SC. The SC sequence is the scrambled version of iCAL36.

Here again, the representative picture obtained by confocal microscopy revealed a red \*MPG-SC and a green GFP-CAL PDZ fluorescence signal (Figure 31 B). However, the overlay of GFP-CAL PDZ domain and \*MPG-SC fluorescence signal on the right hand side shows no co-localization signal (no yellow signal). This is a robust argument for the specific co-localization of \*MPG-iCAL36 peptide with the GFP-CAL-PDZ domain.





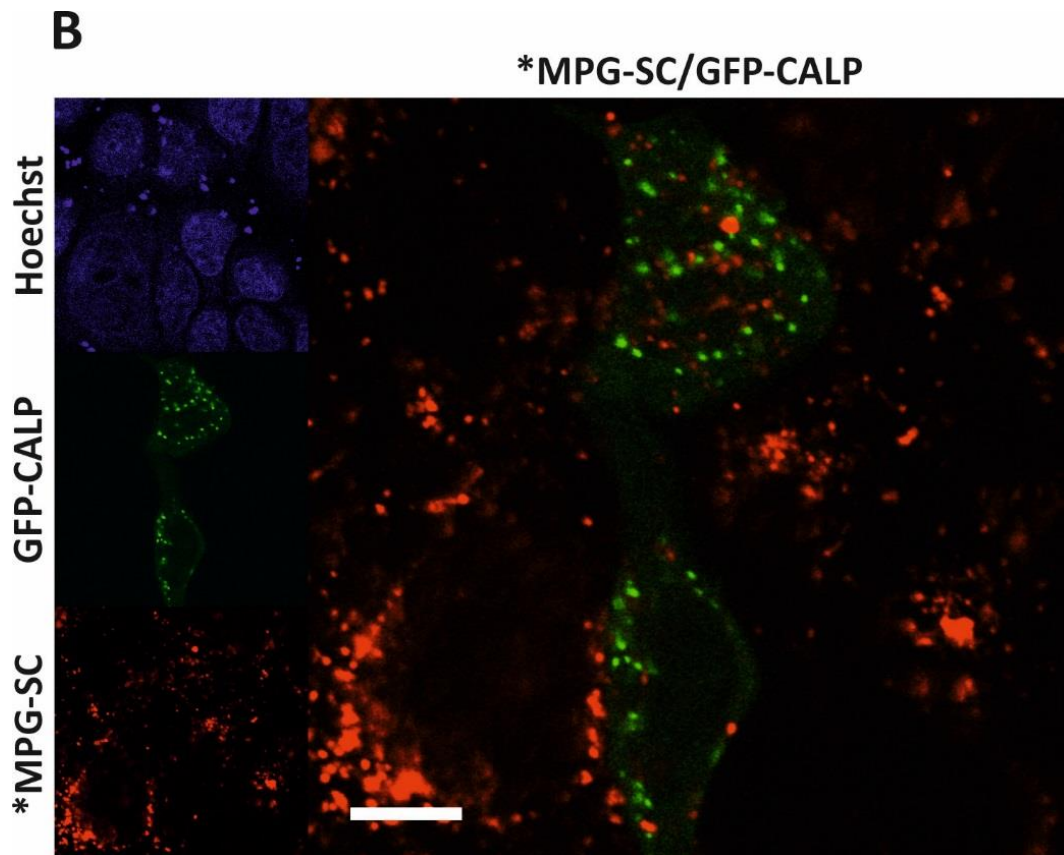


**Figure 31: Co-localization experiments of \*MPG-iCAL36 and MPG-SC with GFP-CAL**

GFP-CAL transfected Caco-2 cells were incubated with (A) \*MPG-iCAL36 and (B) MPG-SC which is a scrambled version of MPG-iCAL36 at a concentration of 1  $\mu$ M for 1 hour. The TAMRA labeled peptides appear in red, the GFP-CAL protein appear in green and the Hoechst dyed DNA appear in blue. The separately stainings are shown on the left hand side of A and B. The overlay of \*MPG-iCAL36 or \*MPG-SC and the GFP-CAL construct are depicted on the right hand side. (A) The co-localization of \*MPG-iCAL36 and CAL-PDZ is marked by the white arrows and are clearly visible. (B) In contrast there is no co-localization in the case of MPG-SC. (\*) TAMRA

In conclusion the experiments reveal a co-localization efficiency of CAL-PDZ transfected cells treated with \*MPG-iCAL36. The results of overlay signals are clearly different to the MPG-SC control with no overlay signals. These findings are strong hints that iCAL36 binds specifically the CAL PDZ domain in a biological system.

### 6.7 Measuring the biological effect of iCAL36 on CFTR activity

The cystic fibrosis transmembrane conductance regulator associated ligand (CAL) provokes the depletion of CFTR proteins [58]. The binding of iCAL36 to CAL's PDZ domain should prevent the interaction between CAL and CFTR and thus the

degradation of CFTR. The consequence should be an increase of CFTR proteins in the apical membranes of mucus producing cells, which in turn would lead to an enhanced secretion of  $\text{Cl}^-$  ions. As reported previously by our group in collaboration with Prof. D.R. Madden, Ussing chamber measurements will be used as a standard method to investigate ion transport over cellular membranes [41; 44]. At this point we decided to use MPG-iCAL36 for the functionality tests because of the successful co-localization experiments. For this purpose, cells were cultured on specially designed Millicell filters which were inserted vertically between the two halves of the Ussing chamber. This allows the separate treatment of the apical and basal side of the cell layer. Both chamber halves were filled with heated bath solution.

The basic principle of the Ussing chamber is that the ion transport produces a potential difference (voltage difference) across the epithelium. The potential difference (PD) is detected by two electrodes placed near the cells on both sides (apical and basal) and is measured by a volt meter. Another pair of electrodes is placed away from the cells and attached to a variable direct current (DC) source and an ampere meter (connected in series). These electrodes allow the injection of a current from the variable DC source (short-circuit current or  $I_{sc}$ ) to nullify the PD. The intensity of the current that is necessary to clamp the PD at 0 mV is monitored by an ampere meter ( $\Delta I_{sc}$ ) which is placed into relation to the area covered by the cell layer as  $\mu\text{A}/\text{cm}^2$  (Figure 32). Due to the treatment with iCAL36, the  $\text{Cl}^-$  secretion mediated through the CFTR should increase and therefore also the measured current. Additionally we could calculate the resulting resistance of the different samples with Ohm's law. The resistance plays an important role in proving the stability and the integrity of the cellular monolayer.

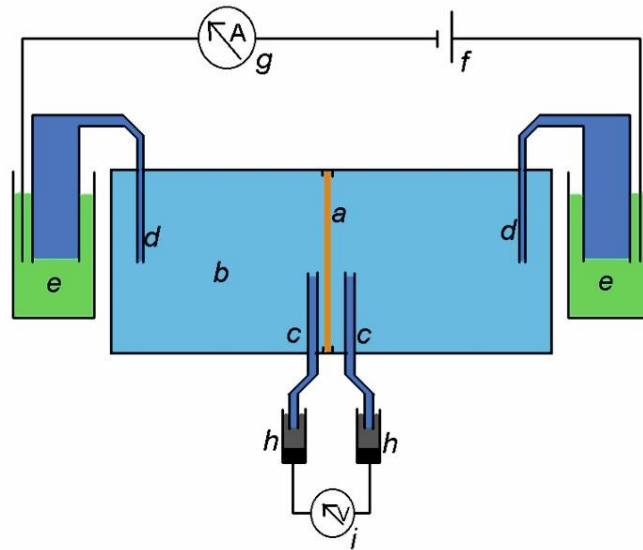


**Figure 32: Schematic representation of an Ussing chamber**

Cells grown on permeable supports (a). Bath solution is filled in both chambers (b). Two agar ringer bridges near the cells (c) are in contact with two electrodes (h). The electrodes are connected with a volt meter (i). Two other electrodes (e) which are placed away from the cells are in contact with the bath solution by agar ringer bridges (d). The electrodes are attached to a variable DC source and an ampere meter (g). [[https://en.wikipedia.org/wiki/Ussing\\_chamber](https://en.wikipedia.org/wiki/Ussing_chamber)]

### 6.7.1 The suitable cell line and MPG-iCAL36 concentration

In a first experiment setup, we tested the efficacy of MPG-iCAL36 to increase CFTR mediated  $\text{Cl}^-$  efflux on Caco-2 cells. For this purpose we incubated polarized Caco-2 cells with MPG-iCAL36 at different concentrations for 3 hours. After the incubation we measured the current change with an Ussing Chamber. During these measurements the cells were additionally treated with amiloride, forskolin, genistein and the CFTR<sub>inh</sub>-172 to stimulate different ion channels to reach a more detailed analysis. Amiloride was initially applied apically to inhibit epithelial sodium channel (ENaC) activity.  $I_{\text{SC}}$  was stimulated with forskolin added to the apical and basolateral bath solution to increase cellular cAMP levels followed by genistein added only to the apical bath solution to increase the open probability of F508del-CFTR  $\text{Cl}^-$  channels. CFTR-specific chloride efflux was inhibited by the application of CFTR<sub>inh</sub>-172. The change of ion transport during the measurement was computed as the  $I_{\text{SC}}$  current change ( $\Delta I_{\text{SC}}$ ).

One usability problem of Caco-2 cells was the minimal change of  $\Delta I_{\text{SC}}$  values after treatment with the denoted substances. In view of the very high standard

deviation and the expected small 5 - 10 % increase in  $\text{Cl}^-$  secretion due to the MPG-iCAL36 treatment it is arguable whether we could detect a significant increase in  $\text{Cl}^-$  transport through the CFTR caused by iCAL36 (for further details see chapter Material and Methods). Therefore we looked for another cell line that would show high reactions after treatment with amiloride, forskolin, genistein and the  $\text{CFTR}_{\text{inh}}-172$  in order to generate suitable results (for details see chapter Material and Methods). We chose HT29/B6 cells, a human colon carcinoma cell line that expresses CFTR channels in their apical membranes [87]. To test the characteristics of HT29/B6 cells regarding the change of current values after the treatment with the same substances that we had used in the Caco-2 cell experiments we treated polarized HT29/B6 cells successively with amiloride, forskolin, genistein and  $\text{CFTR}_{\text{inh}}-172$ .

The HT29/B6 cells reacted tremendously to the treatment with both forskolin and  $\text{CFTR}_{\text{inh}}-172$ . The  $\Delta I_{\text{SC}}$  values were nearly 25 times higher than the respective  $\Delta I_{\text{SC}}$  values in Caco-2 cells and therefore should allow for a reasonable analysis with significant results.

In addition to the aforementioned results the tests with Caco-2 cells showed a significant decrease of resistance values after the incubation with MPG-iCAL36 at a concentration of 100  $\mu\text{M}$ . We tested with 100  $\mu\text{M}$  at first because we had shown that this concentration did not induce any cytotoxic effect in polarized Caco-2 cells. But the problem was that too low resistances disturb the current and thus the  $\Delta I_{\text{SC}}$  values. Furthermore the cell layer or the cells itself could be damaged. Therefore we decided to use lower peptide concentrations in the case of HT29/B6 cells to prevent the negative influence of MPG-iCAL36 to the resistance.

Consequently we tested MPG-iCAL36 at peptide concentrations of 75  $\mu\text{M}$  and 50  $\mu\text{M}$ . Unfortunately, as with the Caco-2 cells we observed a drastic decrease of resistance despite using a lower concentration. The measured values were between 10 and 25  $\Omega/\text{cm}^2$  (Figure 33) while generally a minimum of 200  $\Omega/\text{cm}^2$  is required. Therefore we reduced the peptide concentration further. Now we investigated MPG-iCAL36 at concentrations of 10  $\mu\text{M}$  and 25  $\mu\text{M}$ , respectively.

The control showed an optimal resistance of 430  $\Omega/\text{cm}^2$ . But in the case of the incubated cells appeared a huge decrease in resistance again. The highest values (135  $\Omega/\text{cm}^2$ ) were achieved when the cells were incubated with MPG-iCAL36 at a concentration of 10  $\mu\text{M}$  (Figure 33). Due to these results we further decreased the MPG-iCAL36 concentration to 5  $\mu\text{M}$  and only at this low concentration could we reach suitable resistances above 200  $\Omega/\text{cm}^2$ . It was clearly evident that the resistance values increase if the peptide concentration were reduced. Consequentially we reached the highest resistance results after the incubation with the lowest peptide concentration of 5  $\mu\text{M}$ .

The same reduced resistances appeared after the treatment with the MPG-SC peptide which ruled the iCAL36 compound out as the cause of these resistance complications.

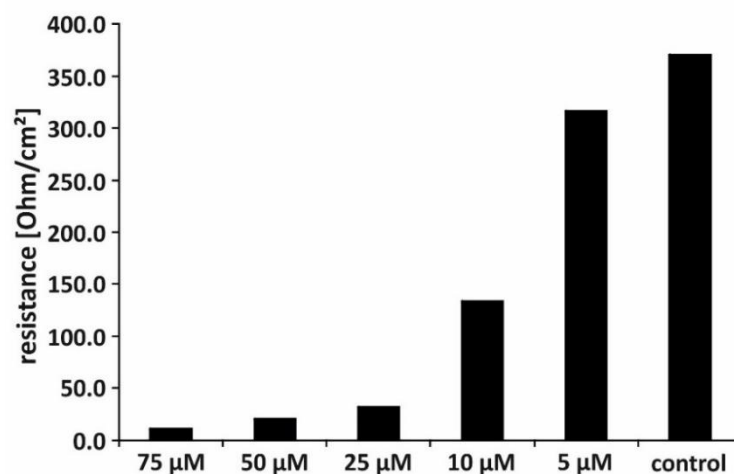


**Figure 33: The dependency of resistance of the concentration of MPG-iCAL36**

7 days polarized HT29/B6 cells were incubated with MPG-iCAL36 at concentrations 75  $\mu\text{M}$  to 5  $\mu\text{M}$  respectively for 3 hours. The goal was to find the appropriate concentration which does not affect the resistance values of the cells. The cells incubated with the lower peptide concentration show higher resistances. Interesting is the stepwise increase in dependency of the peptide concentration. The lowest resistance values were reached at the highest concentration and vice versa.

### 6.7.2 Functionality tests with MPG-iCAL36

Finally we tested the functionality of MPG-iCAL36 at a concentration of only 5  $\mu\text{M}$  because of the aforementioned resistance complications (Figure 33), although this posed the risk of yielding no measurable effect.

We used HT29/B6 cells incubated with MPG-iCAL36 and with the associated scrambled (MPG-SC) version at a concentration of 5  $\mu\text{M}$  for 3 hours at 37  $^{\circ}\text{C}$  and 5 %  $\text{CO}_2$  and evaluated the results after the treatment with forskolin (Figure 34). Untreated cells served as control.

Unfortunately we could not detect any significant effect caused by MPG-iCAL36. The values are in the same range as those of the untreated control or the probe incubated with the scrambled version of MPG-iCAL36 (MPG-SC). As we had expected the peptide concentration was probably too low to evoke a significant effect.

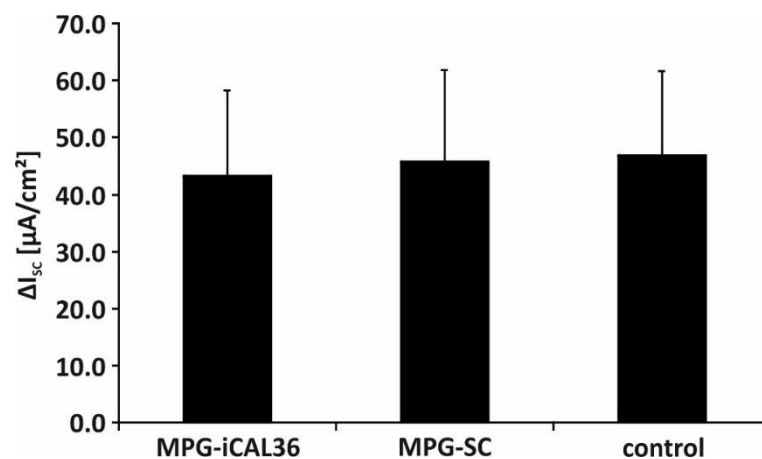


**Figure 34: Influence of MPG-iCAL36 to the  $\text{Cl}^-$  secretion of CFTR**

We incubated polarized HT29/B6 cells with MPG-iCAL36 and the associated scrambled version. After the incubation time of 3 hours we measured the current and treated the cells with amiloride, forskolin, genistein and  $\text{CFTR}_{\text{inh-172}}$ . The diagrams show the change in current after the treatment with  $\text{CFTR}_{\text{inh-172}}$ . We could not detect an increase of  $\text{Cl}^-$  secretion of the incubated cells compared with the control or the cells incubated with the scrambled version of iCAL36. Data represent the mean  $\pm$  SD;  $n \geq 4$

In conclusion at first we used Caco-2 cells for our Ussing chamber measurements. But due to the low reaction after stimulation of different ion channels and a decreased resistance after treatment with MPG-iCAL36 we decided to test HT29/B6 cells. We reached a distinct increase of current after the treatment with forskolin and  $\text{CFTR}_{\text{inh-172}}$  but the diminished resistance results (Figure 33) could not be prevented by the use of HT29/B6 cells. It was necessary to reduce the MPG-iCAL36 concentration to 5  $\mu\text{M}$  to reach resistance values in the range of the untreated control. Probably as a result of this low concentration we could not detect the expected increase of current of MPG-iCAL36 incubated HT29/B6 cells.

## 6.8 Human rectal epithelial suction biopsies

Next we aimed to test MPG-iCAL36 internalization, cytotoxicity and efficacy (CFTR chloride efflux) on human rectal suction biopsies to gain a closer insight into the biological processes. Based on the cellular results and due to limited access of biopsies, we performed all experiments only with MPG-iCAL36. The human rectal biopsies from Cystic Fibrosis patients and healthy donors were provided by Dr. N. Derichs (Christiane Herzog Cystic Fibrosis Centre) who also collaborated with us in the biopsy analysis.

### 6.8.1 Influence of MPG-iCAL36 on viability

Based on our previous cellular experiments, the potential cytotoxic effects of MPG-iCAL36 (100  $\mu$ M, 3 hours incubation) were measured under the same condition using the CCK-8 viability assay (Figure 16). The biopsies showed only a slight susceptibility for cytotoxic effects of MPG-iCAL36. The results showed only a low decrease in viability to 81 % compared to the untreated controls. The wide range of possible peptide concentrations leaves scope for following biopsy experiments.

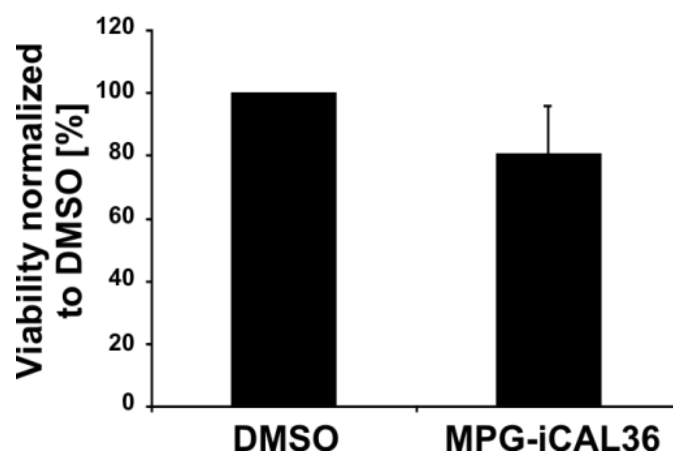


**Figure 35: Cytotoxic effect of MPG-iCAL36 to rectal epithelial biopsies**

Rectal biopsies incubated with 100  $\mu$ M MPG-iCAL36 for 3 hours to evaluate the potential toxic effect. Cell viability determined by MTS assay shows no toxic effect. Shown data were normalized to 100 % DMSO. Graphs represent mean values  $\pm$  SD (n = 6 experiments).

### 6.8.2 Internalization of MPG-iCAL36

We have already shown with confocal microscopy that \*MPG-iCAL36 is able to translocate into the cytoplasm of Caco-2 cells (Figure 23). The next step should be to test the internalization efficiency of \*MPG-iCAL36 into the cells of human rectal biopsies. We performed confocal microscopy tests in accordance to the cell line experiments because of the positive results. We incubated freshly extracted human rectal epithelial biopsies for 1 hour at a peptide concentration of 10  $\mu$ M. Then we transferred the biopsies to glass slides and examined the samples with confocal microscopy (Figure 36). The red signal was distributed in the cells and surprisingly the fluorescence intensities of the TAMRA labeled peptides appeared stronger than in Caco-2 cells under the same conditions. The discrete nuclei were an indication of viable epithelial cells. In a similar way as observed for the Caco-2, no nuclear localization of \*MPG-iCAL36 was observed.

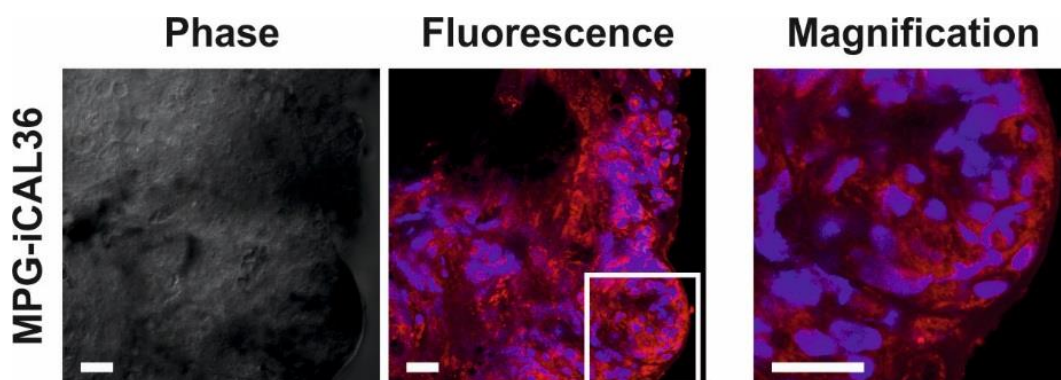


**Figure 36: Internalization of \*MPG-iCAL36 in cells of human rectal epithelial biopsies**

Freshly obtained human rectal mucosa tissues from a healthy control were incubated at 37°C in culture medium with 10  $\mu$ M \*MPG-iCAL36 for 1 hour. The peptides appear in red and the cell nuclei were labeled with Hoechst dye and appear in blue. The optical microscopy pictures are depicted on the left hand side and the fluorescence pictures and their magnifications are shown on the right hand side. A robust internalization of \*MPG-iCAL36 is in both probes clearly visible. White scale bar = 20  $\mu$ m.

### 6.8.3 Effect of MPG-iCAL36 and VX-809 on CFTR function

We could confirm low cytotoxicity as well as successful internalization in human rectal biopsies and the next necessary step in therapeutic drug development should be the proof of biological functionality. In this context it is important that



most Cystic Fibrosis patients having the F508del mutation suffer from pancreatic insufficiency cystic fibrosis (PI-CF) only 15 % retain sufficient exocrine pancreatic function cystic fibrosis (PS-CF) with a milder clinical phenotype [88]. We tested the stabilizing effect of MPG-iCAL36 on the CFTR Cl<sup>-</sup> efflux with both forms of Cystic Fibrosis. For this purpose we performed functional CFTR analysis in a total of 64 native human rectal biopsies from 3 adult subjects (PI-CF F508del/F508del n=1, PS-CF F508del/3849+10kbC-T n=1, healthy control n=1). We transported freshly obtained rectal suction biopsies (diameter of 2-3 mm) immediately to the ion transport lab (AG Derichs) in ice-cold PBS buffer solution and measured the short-circuit on transepithelial ion transport in Ussing chambers at 37°C according to a standardized procedure. Additionally we co-incubated the rectal tissues for 12 hours with MPG-iCAL36 and the F508del-CFTR “corrector” VX809 in a subgroup of biopsies from CF patients. The goal was to allow a partial correction of defective F508del-CFTR expression at the apical membrane and thus to assess the potential synergistic effects of CFTR “correctors” and CAL PDZ inhibitors. The optimal incubation time of VX-809 is 24 hours (according to data sheet) but of MPG-iCAL36 and MPG-SC only 3 hours. Because of that and in order to achieve a sufficient comparability we decided to use an adapted incubation time of 12 hours for VX-809 (10 μM) and MPG-iCAL36 (100 μM) alone as well as both substances together. Although we used a MPG-iCAL36 concentration of 100 μM, we could not detect a reduction in resistance as monitored on Caco-2 or HT29/B6 cells. All Ussing chamber measurements on biopsies and the associated evaluation were performed by Dr. N. Derichs.

As expected the PS-CF rectal biopsies showed remarkable residual CFTR ion channel function of  $4.5 \pm 2.4 \mu\text{A}/\text{cm}^2$  (Figure 37). The value of non-CF healthy control amounted to  $24.9 \pm 8.0 \mu\text{A}/\text{cm}^2$  (data not shown), whereas no CFTR chloride secretion was found in the PI-CF tissues (Figure 37).

For the PI-CF rectal biopsies, we could not detect a positive effect in Cl<sup>-</sup> secretion after the incubation with MPG-iCAL36 alone. The results are similar to the untreated control or the effectless MPG-SC. But we could observe a robust increase of CFTR chloride channel function after the incubation with VX-809 “corrector”, which was additionally increased by co-incubation with the active peptide MPG-iCAL36 (Figure

37). In the PS-CF tissues (expressing CFTR with class II and class V mutation) we could achieve an increase of existing residual CFTR activity with MPG-iCAL36 alone and a further positive effect due to the co-incubation of MPG-iCAL36 and VX-809 (Figure 37) (for further information see chapter Discussion).

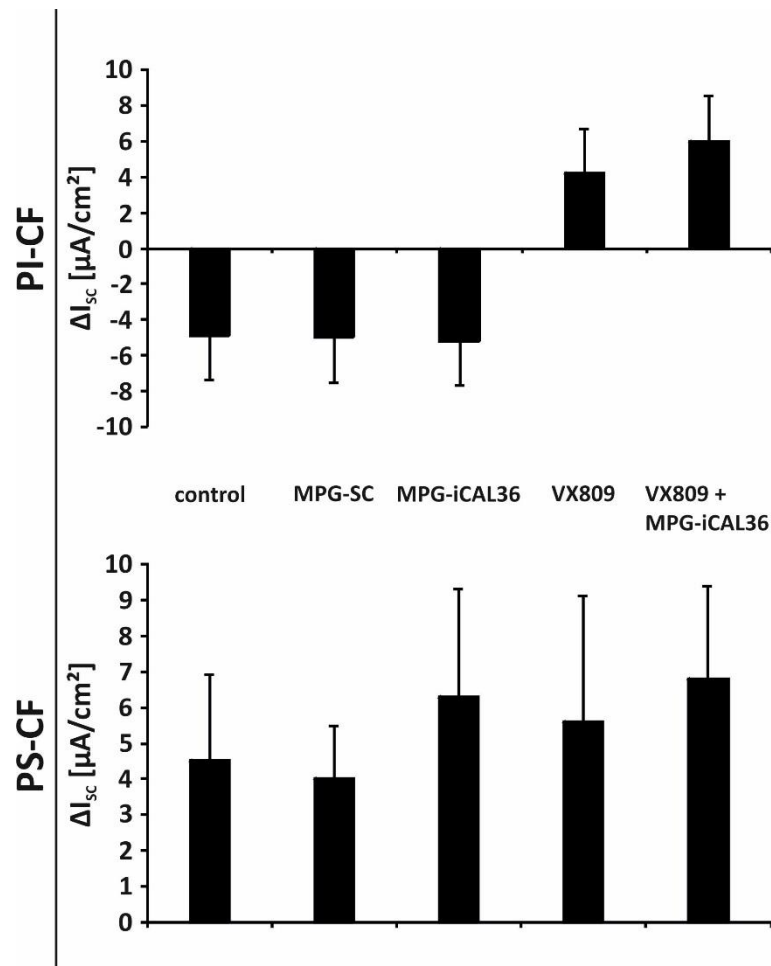


**Figure 37: Effect of MPG-iCAL36 and VX-809 on Cl<sup>-</sup> secretion of human rectal biopsies**

Functional CFTR chloride channel activity in freshly obtained human rectal suction biopsies was registered by transepithelial short-circuit current measurements in Ussing chambers (P2400, Physiologic Instruments, USA). The exposed tissue surface area was 1.8 mm<sup>2</sup>. All data in the presence of 10  $\mu$ M indomethacin (> 60 minutes). After assessment of CFTR function at baseline, rectal tissues were incubated for 12 hours with different combinations of DMSO (0.1 %), MPG-iCAL36 (100  $\mu$ M), MPG-SC (100  $\mu$ M) and VX-809 (10  $\mu$ M). After incubation, measurement was repeated and  $\Delta I_{sc}$  Forsk/IBMX as the most specific readout for cAMP-mediated CFTR function was compared between the biopsies of PI-CF and PS-CF. Data represent the mean  $\pm$  SD; n  $\geq$  2 biopsies.

In summary, MPG-iCAL36 induced a negligible cytotoxicity in human rectal suction biopsies. With confocal microscopy experiments we could also show a strong internalization of \*MPG-iCAL36 in cells of rectal biopsies. We reached an increase in Cl<sup>-</sup> secretion of PS-CF biopsies after the incubation with MPG-iCAL36 alone and furthermore we could show a synergistic effect of MPG-iCAL36 and

---

VX-809 to CFTR Cl<sup>-</sup> channel function in PI-CF and PS-CF biopsies. However, more experiments on human rectal biopsies should be performed to obtain a statistical relevant effect of MPG-iCAL36/VX-809 on CFTR mediated Cl<sup>-</sup> efflux.

## 7 Discussion

Cystic Fibrosis (CF) is the most common life-threatening autosomal recessive disorder among Caucasian population with an incidence around 1 in 3000 individuals. The mutation affects the gene of the cystic fibrosis transmembrane conductance regulator (CFTR) chloride ion channel [1; 2; 3]. Until recently, medical therapies such as clearance therapies to dislodge airway mucus or antimicrobial medicines could only address the symptoms of CF. In contrast, small molecules such as potentiators and “correctors” act on CFTR basic defects (folding and gating) which represent an extensive progress in CF treatment [89]. Until now the potentiator Ivacaftor (Kalydeco, Vertex Pharmaceuticals) is the only FDA-approved CFTR modifier but other agents are in development [89].

Additionally, because of the fact that CF is caused by a multitude of different mutations within a single gene it is considered as an ideal candidate for mutation-targeted therapy. Therefore, extensive investigations are directed on agents that can affect CF at the genetic level. Different vectors were used to transport the functional wild-type CFTR gene into airway epithelial cell such as adeno-viral, adeno-associated, lentiviral or cytoplasmic RNA viruses but the results show only limited success [40]. Another study regarding gene therapy investigated the use of a non-viral plasmid in a randomized, double blind, placebo-controlled phase 2b trial. CF patients received nebulized plasmid DNA encoding the CFTR gene complexed with a cationic liposome (pGM169/GL67A) or a placebo for one year. Alton et al. noted a stabilization of forced expiratory volume (FEV) in the pGM169/GL67A group whereas the placebo group shows a reduction in FEV. However, further work will be needed to prove if this stabilization is significantly maintained [90].

The published data from the Guggino lab show that the CFTR-associated ligand (CAL) mediates post-endocytic degradation of mature CFTR [91; 92]. CAL-specific knockdown extends the apical half-life of F508del-CFTR, quadrupling its cell-surface abundance and tripling its net chloride-channel activity in polarized, CF patient-derived airway epithelial cells (CFBE- $\Delta$ F) [93]. The inhibitor of CAL

peptide iCAL36 (sequence: ANSR**W**PTSII) blocks the CAL PDZ binding site, extends CFTR apical half-life, and increases F508del-CFTR chloride currents alone and in concert with a CFTR “corrector” [57; 58]. By further investigation, we designed a second generation CAL inhibitor (iCAL42, sequence: ANSRL**P**TSII) which has no off-target interaction with other PDZ domains (e.g. TIP-1) [45].

To evaluate the therapeutic potential of our bio-available CAL inhibitors (iCAL36/iCAL42) *in cellulo* (Caco-2 cells) and *ex vivo* (rectal biopsy samples), we functionalized the iCAL N-terminus with the cell-penetrating peptide (MPG-iCAL or Pen-iCAL) or with a fatty acid such as the myristic acid (Myr-iCAL).

### **7.1 Cellular internalization of CPP-iCAL and Myr-iCAL Caco-2 cells and biopsy samples**

As mentioned before, cell penetrating peptides (CPPs) are one of the most promising non-viral strategies to overcome both extracellular and intracellular limitations of various large biomolecules and to improve their intracellular routing [94; 95]. Therefore, we decided to avoid the use of the BioPorter transfection reagent and to couple the iCAL peptide the MPG and penetratine (Pen).

In the process of therapeutic development, it is essential to estimate the possible cytotoxicity of the constructs at an early stage of research. For that reason we analyzed the potential cytotoxic effect on polarized Caco-2 cells reflecting the phenotype of epithelial cells. Based on previously performed pretests on differentiated Caco-2 cells (Figure 16 A), we tested our CPP-iCAL and Myr-iCAL constructs at the highest tolerated concentration of 100  $\mu$ M. We detected no reduction in cell viability after the incubation with all of our constructs over a period of 3 hours (Figure 16 B). Simultaneously, we tested the cytotoxicity of MPG-iCAL36 on human rectal suction biopsies. Here, we used exemplarily only one peptide to investigate the cytotoxicity due to the restricted availability of human biopsies. We detected a non-significant decrease of the tissue viability to approximately 80 % (Figure 35) with MPG-iCAL36 *versus* the untreated control. A possible explanation of this decline could be that the Caco-2 cells were treated

only from the apical side while the biopsies are surrounded by the peptide solution.

To evaluate the internalization property of the fluorescence labeled constructs (\*MPG/\*Pen/\*Myr-iCAL42) we examined them time-dependently in Caco-2 cells by measuring the intracellular fluorescence intensities using a microplate reader. For all three compounds used, we generated three curves with an asymptotic pattern reaching more or less a plateau after 180 min (Figure 19). Therefore and because we observed no significant cytotoxicity in this time frame, we used 180 min as standard incubation time for our further internalization experiments. Without any carrier neither \*iCAL36 nor \*iCAL42 could overcome cellular membranes (Figure 20), which was further confirmed by confocal microscopy experiments (Figure 23) showing no measurable fluorescence within the cells. All other carrier-cargo constructs showed robust internalization values (> 8,000 SI/mg proteins) after an incubation time of 180 min. However, we should pointed out, that iCAL36 coupled to both CPPs showed significantly higher internalization values (> 12,000 SI/mg protein) than iCAL42 under the same conditions (Figure 20). It is interesting that the substitution of one amino acid (W → L) within the cargo has such a relevant impact on the internalization. In contrast, the amino acid exchange within the iCAL sequence has no influence on the cellular internalization when the peptide is coupled to myristic acid. The internalization values of \*Myr-iCAL36 and \*Myr-iCAL42 were in the same range (Figure 20). In order to get more information on the process of cellular membrane crossing, we evaluated not only the cellular internalization (fluorescence measured in the cytosol) but also the cellular release (fluorescence in the supernatant after washing steps). In this context, it is very interesting that Myr-iCAL42 showed around 10 times lower results for the release out of the cells compared to Pen/MPG-iCAL42 (Figure 21). Two hypotheses could explain these results: 1) \*Myr-iCAL stuck into the cell membrane or 2) \*Myr-iCAL was not released. Indeed, confocal microscopy experiments on Caco-2 cells revealed that Myr-iCAL42 stuck into the cellular membrane during the first hour of incubation, but was released in the cytoplasm of the cells over the time (3 hours). One biological function of myristoyl moiety is to mediate membrane binding [95] but the

hydrophobicity is not sufficient to maintain long-term association [96]. This delay in the internalization process could explain the lower values of cellular releasing. In contrast, \*CPP-iCAL was already uniformly distributed in the cytoplasm around the nucleus after 60 min as exemplified by MPG-iCAL36 (Figure 23).

At present, assays attempting to evaluate the different \*CPP-iCAL or \*Myr-iCAL locations (membrane *versus* cytosol) by measuring the fluorescence intensities for Caco-2 cell lysates at different time points (1 hour *versus* 3 hours) failed. To detect the cellular internalization of the constructs, we used a lysis buffer with strong detergent (Triton X-100 and SDS) to disrupt the cell membranes. During this process the membrane-trapped \*Myr-iCAL were also released resulting in falsified results. This experiment should be repeated using milder lysis conditions or specific kits which allow the extraction of the cytosol *versus* the membrane fractions.

Finally, we were able to show an impressive internalization of MPG-iCAL36 in human rectal biopsies kindly provided by Dr. N. Derichs by confocal microscopy (Figure 36). Compared to the dotted patterns observed in Caco-2 cells, representative images revealed a homogenous cytosolic localization in nearly 100 % of the analyzed tissue. These results are encouraging for the further application of the CPP-iCAL conjugates as therapeutics.

## **7.2 First insight in the internalization mechanism of \*CPP-iCAL and \*Myr-iCAL in Caco-2 cells**

For more than two decades, the scientific community has debated the internalization mechanism used by CPPs or CPP-cargoes: direct membrane translocation or the energy dependent endocytosis [60]. Furthermore, the internalization of myristic acid-coupled peptides is not fully understood and we were very interested in comparing the uptake mechanism of CPP-iCAL and Myr-iCAL conjugates in Caco-2 cells. The internalization rates of all conjugates at 37°C (standard condition) were evaluate in parallel at 4°C or at 37°C in the presence of sodium azide (NaN<sub>3</sub>) and 2-deoxy-D-glucose (2-DG). Both direct translocation and endocytosis, took place at 37°C but at 4°C or under ATP depletion (NaN<sub>3</sub> + DG-2)

only direct translocation worked [65]. Endocytosis is an energy-dependent process requiring the invagination of the plasma membrane which is drastically reduced at low temperatures. At 4°C or under ATP-depletion, the CPP-iCAL constructs internalized in the same manner as at 37°C. No significant decrease in the uptake property was observed (Figure 26). This suggests, that our CPP-iCAL constructs entered the cell via a temperature and ATP independent direct translocation pathway.

In contrast to the \*CPP-iCAL conjugates, we observed a different uptake property of the \*Myr-iCAL36/42 compounds: 1) under the condition of ATP depletion the internalization occurred to 100 % compared to 37°C and 2) at 4°C we could detect a 50 % reduction in uptake compared to 37°C. These data indicate that the cellular uptake of the Myr-iCAL compounds is more temperature dependent than an energy-dependent process. In 2007, Nelson et al. reported a  $\approx$  60 % internalization rate reduction of a myristoylated peptide at 4°C in HeLa cells compared to the 37°C condition [78]. Furthermore, it has been shown that palmitoylated peptides are able to use a flip-flop mechanism from the inner to the outer face of synthetic palmitoyl-oleoyl-phosphatidylcholine lipid vesicles [97]. Flip-flop diffusion of the myristoylated peptides is one potential mechanism for the translocation into the cytoplasm of the cell. The process is affected at low temperature (below 20°C) due to reduced fluid-gel transition of mammalian plasma membranes [78].

To investigate the uptake mechanism of the CPP-iCAL or Myr-iCAL conjugates in detail it would be interesting to test different endocytotic inhibitors. Endocytosis can be divided into pinocytosis and phagocytosis. Pinocytosis can be subdivided in clathrin dependent (clathrin-mediated endocytosis, CME) and clathrin independent (CIE) endocytosis [64]. Different endocytotic inhibitors are available such as classical chemical inhibitors (chloroquine or monensin) which have been used mainly to block CME, pharmacological inhibitors (Dynasore, Pitstop 2) and genetic approaches (siRNA of clathrin, siRNA of AP2). Another possibility to visualize whether the CPP-iCAL uptake in Caco-2 cells is dependent from endocytosis or direct translocation is to use specific endocytosis markers (FM4-64 [98], transferrin, etc.) by confocal laser scanning microscopy. By combining



the different methods, it will be possible to deduce the putative internalization pathway of the analyzed molecules.

### **7.3 Detailed evaluation of CPP(/Myr)-iCAL interaction with the CAL PDZ domain *in vitro* and *in cellulo*.**

Knowing that our compounds are able to internalize cells, it was of great interest to evaluate their direct interaction with the CAL PDZ domain. For that reason, we first decided to measure the  $K_d$  and  $K_i$  values *in vitro* using the method of fluorescence polarization (FP) before going *in cellulo* to perform co-localization experiments.

FP measurement allows the quantification of the interaction between two interacting partners in solution, however one of the binding partners needs a fluorescence labeling (normally the small molecule ligand). The fluorescence-labeled ligand is then excited with polarized light which leads to a fast rotation causing a depolarization of the emitted light. Due to the binding to a larger partner, the fluorophore rotation is slowed down by steric hindrance resulting in polarized emitted light [38].

Comparing first the CAL inhibitors alone, we could observe that the substitution of one amino acid from ANSRWPTSII (iCAL36) to ANSRLPTSII (iCAL42) reduced the affinity of the peptide to the CAL PDZ domain by a factor of five (Table 1). Tryptophan is a more spacious amino acid than leucine which could be the reason for a higher affinity and a more robust interaction to the PDZ domain of CAL.

Furthermore if iCAL36 or iCAL42 were prolonged with MPG or penetratin the  $K_i$  values were drastically decreased, up to about 20-fold. For example the prolongation of iCAL42 with MPG leads to a 22-fold enhancement of the affinity results. The CPPs MPG and penetratin have many hydrophobic amino acids (e.g. W, I, L) as well as positive charges (R and K). Therefore, it is possible that the increased  $K_i$  values were due to unspecific hydrophobic or electrostatic interactions of the CPP with the CAL PDZ domain. A similar phenomenon of additional hydrophobic interactions could be observed by coupling of the

myristic acid to iCAL. To verify the observed unspecific binding of the vectors (CPP or Myr) to the PDZ domain, it could be helpful to test another measurement technique such as the microscale thermophoresis (MTS). The underlying principle of this method is the thermophoresis which is the directed movement of molecules along a temperature gradient. Thermophoresis is highly sensitive to binding induced changes of molecular properties such as size, charge or conformation. By using this approach, we will be able to determine if the measured  $K_i$  values of the CPP-iCAL constructs are real or unspecific. In the case of an unspecific interaction, we will measure the same  $K_i$  values as for iCAL36/iCAL42 alone.

In a second step, we wanted to visualize the interaction of iCAL with the CAL PDZ domain in a more complex and biological environment by proving the co-localization of both *in cellulo*. For this purpose, we transiently transfected Caco-2 cells with a green fluorescence protein (GFP)-labeled full length CAL protein. After 24 hours, the transfected cells were incubated with \*CPP-iCAL (or \*CPP-SCR as negative control) for 1 hour to avoid artifacts due to putative peptide degradation. We selected the MPG-iCAL36 sequence to perform this co-localization experiments because this peptide has the highest affinity to the CAL PDZ domain of all our CPP-iCAL conjugates (Table 1) and because the \*Myr-iCAL constructs had stayed trapped in the cell membranes after 1 hour incubation. After merging the green fluorescence signal of the GFP-CAL protein with the red fluorescence signal of TAMRA-MPG-iCAL36, we could observe that yellow signal corresponding to the co-localization of \*MPG-iCAL36 and the CAL protein (Figure 31). A further indication for veracity of our results was shown by the evaluation of co-localization signals between the inactive scrambled version \*MPG-SCR and the CAL protein. In this case, we could not detect any yellow fluorescence signals.

Despite the obvious results from affinity and co-localization measurements, it was difficult to prove the “real” iCAL36:PDZ domain interaction in a biological context. FP measurements are performed out of the cellular context in an artificial environment. On the other hand, co-localization experiments are performed in a cellular context, but it is not clear if the fluorescence-labeled

peptides/proteins are visualized or the fluorescence dye alone. Therefore, it will be of great interest to perform additional experiments such as Pull-downs or co-immunoprecipitation (co-IP) experiments to further validate these interactions.

#### **7.4 Ussing chamber experiments: The challenge to measure the biological activity MPG-iCAL36 as a “stabilizer”.**

The one of main aims of this PhD work was to compare the CFTR-stabilizing activity of CPP-iCAL and/or Myr-iCAL based on previous results obtained using BioPorter as transfection agent (Cushing 2010). The stabilizing properties of our peptides were analyzed by measuring the increase of Cl<sup>-</sup> efflux in two different cell lines and in human rectal suction biopsies with Ussing chambers. Based on the above mentioned results showing no cytotoxicity, good internalization, high affinity to CAL PDZ domain and co-localization with the CAL protein, we decided to use the MPG-iCAL36 peptide to perform the proof of concept study.

In a first step, we decided to use polarized Caco-2 cells for the Ussing chamber experiment, because even the half time of wild-type CFTR at plasma membrane should be increased by the stabilizing effect of our peptides. However, first assays revealed rapidly, that this cell line is unfavorable due to the fact, that in general minimal changes in current values were observed after treatment with different stimuli such as amiloride as ENaC inhibitor, forskolin to increase cAMP level and genistein to boost the delF-CFTR open probability. Thereafter, we switched to HT29/B6 cells which showed – contrary to the Caco-2 cells – huge physiological reactions due to the different channel stimuli as mentioned above. Unfortunately, during the HT29/B6 cell incubation with 75 μM MPG-iCAL36 we noticed a drastic decrease of the epithelial resistance from 370 Ω/cm<sup>2</sup> to 11 Ω/cm<sup>2</sup>. Even the scrambled version (MPG-SCR) caused the same reduction of the epithelial resistance which is an indication that the event is not caused by the iCAL compound itself but probably by the CPP. Stepwise reduction of the MPG-iCAL36 concentration (75 μM and 50 μM) did not show any improvement in terms of a constant epithelial resistance. Only at a 5 μM concentration of the peptide, we were finally able to maintain a constant epithelial resistance of at

least 200  $\Omega/\text{cm}^2$ . To verify if this problem of epithelial resistance persisting with a different compound, we tested Pen-iCAL36 (data not shown). Here again we monitored the same resistance problems revealing a putative contribution of the CPPs to this phenomenon.

How could we explain this impressive decline in epithelial resistance making the Ussing chamber measurements unfeasible? As demonstrated above, MPG/Pen-iCAL36 internalized via an ATP and temperature independent direct translocation mechanism. The direct translocation could include the mechanism of transient pore formation in the cell membrane [60]. The HT29/B6 (as well as Caco-2 cells) formed polarized monolayers and if pores were induced at the apical and basal membrane of this monolayer it could provoke a short circuit resulting in a complete decrease in epithelial resistance. If the transient pore formation is rapid enough, this event could not be detected by conventional cytotoxicity assays. However, as demonstrated it can influence the epithelial resistance.

Finally, because the 5  $\mu\text{M}$  MPG-iCAL36 concentration had no influence on the epithelial resistance, we tried to measure an increase in  $\text{Cl}^-$  efflux on HT29/B6 cells. Unfortunately, we could not determine any effect on chloride secretion during the performed experiments. This could have many reasons such as the incubation time, the low MPG-iCAL36 concentration or the used cell lines.

In parallel to our cellular experiments, Ussing chamber tests were performed in collaboration with Dr. N. Derichs on human rectal suction biopsies of healthy donors (as control), on a CF-patient with a milder pancreas sufficient form (PS-CF, F508del/3849+10kbC-T) and a CF-patient with the very severe mutation F508del on both alleles which caused the pancreas insufficient implementation (PI-CF; F508del/F508del). Most CF-patients suffer from the serious PI-CF form and only 15 % retain a sufficient pancreatic function [88].

First of all, we should mention here, that we could not detect a decrease in epithelial resistance after MPG-iCAL36 incubation of biopsies of CF-patients or healthy donors even at 100  $\mu\text{M}$ . The reason for this difference is probably due to the fact that the human rectal biopsies are multilayered and robust tissue in contrast to the very sensitive cell monolayer of Caco-2 or HT29/B6 cells.

The untreated PS-CF biopsies showed as expected remarkable residual CFTR ion channel function but in the PI-CF biopsies there wasn't any chloride secretion to be found.

At first we treated the biopsies with MPG-iCAL36 and MPG-SC as the control at a peptide concentration of 100  $\mu$ M. In the case of PI-CF biopsies we could not observe an effect after the incubation with MPG-iCAL36 alone. The iCAL36 inhibitor is able to prevent the degradation of functioning CFTR proteins but a characteristic of PI-CF is the complete absence of functioning CFTR chloride channels. Therefore it was expectable that MPG-iCAL36 alone did not produce an effect. In contrast, in the case of PS-CF we reached an increase in chloride secretion after the incubation with MPG-iCAL36 alone because the PS-CF biopsies on the other hand carry functional CFTR proteins so the iCAL36 inhibitor can serve its purpose to bind the CAL PDZ domain and subsequently prevent the degradation of the CFTR. Therefore we could observe a remarkable increase in chloride secretion compared to the untreated control.

Next we tested the synergistic effect of MPG-iCAL36 and the "corrector" VX-809 from VERTEX Pharmaceuticals. VX-809 targets the F508del-CFTR misprocessing and restores the CFTR expression and function in the lung epithelial cells. A possible mode of action is as a "pharmacological chaperone" due to its interaction with the damaged channel itself [15; 16]. We treated PI-CF and PS-CF biopsies with MPG-iCAL36 or VX-809 or with both substances together.

The chloride secretion of the PS-CF biopsies was increased after the incubation with VX-809 alone and we could detect a further enhancement of chloride secretion and thus a synergistic effect after the treatment with VX-809 and MPG-iCAL36 together. The treatment of PI-CF biopsies with VX-809 alone leads also to an increase of chloride secretion and furthermore we could also observe a synergistic effect after the incubation with VX-809 and MPG-iCAL36 together. As expected VX-809 alone caused an increase in chloride secretion in PI-CF as well as in PS-CF biopsies because the "corrector" affects the mutated CFTR channel itself. We could confirm our conclusion that the iCAL36 inhibitor needs functioning CFTR proteins to serve as a "stabilizer" of CFTR channels through the further improvement due to the treatment of the PI-CF biopsies with MPG-

iCAL36 and VX-809 together. Due to the treatment with the “corrector” the PI-CF biopsies produced intact CFTR proteins and now the iCAL36 inhibitor was able to follow its determination and thus prevents the degradation of CFTR proteins. But finally more experiments with human rectal suction biopsies are necessary to deduce a statistically relevant effect of the iCAL inhibitor to the CFTR mediated chloride secretion.

### **7.5 Protease stability of the CPP/Myr-iCAL conjugates as prerequisite for a long-term “stabilizer” effectivity.**

The idea for the future is to administer the iCAL inhibitor as an aerosol. But its pharmacological target is in the cytoplasm of lung epithelial cells and therefore inhibitor must be able to pass the mucus of the lung. That’s why it is necessary to estimate the stability of the compounds regarding proteases. Furthermore, the rapid degradation of the CPP-iCAL compounds could be an explanation for negative results of the Ussing chamber experiments at 5  $\mu$ M.

To address this issue, we incubated all constructs used in this study in 20 % human serum and evaluated their possible degradation over the time by RP-HPLC. All CPP-iCAL36/42 compounds were constantly degraded over a time period of 6 hours and after 24 hours neither a CPP-iCAL36/42 nor iCAL36/42 compound could be detected by RP-HPLC anymore. It is interesting that both MPG peptides (MPG-iCAL36/42 -  $\approx$  20 % of the initial concentration; after 6 hours) were degraded faster than their penetratin counterparts ( $\approx$  50 % for Pen-iCAL36/42; after 6 hours) or the iCAL peptides alone ( $\approx$  50 % for iCAL36/42; after 6 hours) (Figure 29 A and B). It is difficult to explain the rapid degradation of MPG-iCAL. Maybe, one reason could be the length (36 amino acids) which gives a larger contact surface for proteases compared to the others.

Additionally it is important to consider that while the CPP-iCAL constructs were degraded the iCAL36/42 part of the whole peptide may well have been intact and active, but we could not distinguish the remaining fractions of MPG/Pen-iCAL36/42 by the RP-HPLC method.

The degradation behavior of the myristic acid compounds in contrast to that of the CPP-iCAL conjugate was especially interesting because neither Myr-iCAL42 nor Myr-iCAL36 were fully degraded after 24 hours ( $84 \pm 13\%$  and  $28 \pm 6\%$ , respectively). Their main advantage is that the myristic acid protects the N-terminal amino acids of iCAL36/42 against exopeptidases. These results are very encouraging concerning the development of new CF-therapeutics. However, more experiments should be performed especially in terms of possible steric hindrance of the myristic acid during iCAL:CALPDZ interaction (FP measurements).

## 8 Conclusion

The treatment of cystic fibrosis is no longer restricted to the manifestation of the disease but also the basic defect is targeted to minimize the symptoms of CF patients. The research generated CFTR modifiers which addresses the folding (“corrector”) or the conductance and gating defect (potentiator) of the mutated CFTR [15; 16]. Our working group developed an iCAL inhibitor as a “stabilizer” of the CFTR which belongs to the same scientific area. The data presented here deliver a closer insight into aspects of the inhibitor such as protease stability, co-localization, internalization or functionality especially in connection with different iCAL carriers. These investigations show amongst others that the treatment of human rectal epithelial biopsies with the inhibitor and a “corrector” together leads to a synergistic effect. Therefore the iCAL inhibitor is a potential drug for combination with other therapeutics to improve the CF associated disorders.

However, additional work is necessary to forward the development of iCAL inhibitors future therapeutic molecules. For example, modulation of the peptide to obtain a more protease stable candidate could definitely increase its effectivity. An improvement of the iCAL inhibitor could be reached through the introduction of D-amino acids. However, it is important that the function of the inhibitor is not affected by the different substitutions. For examples for L- to D-isoform substitution are manifold cited in the literature such as the work of G. Carmona et al. They determinate that the antimicrobial peptide Pin-2 in the isoform D antimicrobial has an activity in the same range as the parental L-Pin2 and has additionally an enhance serum stability [100].

Finally, to confirm the potent stabilizing activity of iCAL, further Ussing chamber experiments should be performed on human rectal biopsy samples of CF-patients. Besides comparing different CPP-iCAL conjugates also the Myr-iCAL compound should be tested – alone and in combination with VX-809 and VX-770. Furthermore, we should keep in mind that repeated application of peptide-based therapeutics could induce immunogenic reactions by means of anti-drug



antibodies interfering or neutralizing the drug effect. In this case, the addition of polyethylene glycol (PEG) molecules might decrease immunogenicity due to the interference with protein processing and presentation and by physically blocking antibody or HLA-epitope binding [40]. Additionally, PEGylated proteins show a decreased degradation by metabolic enzymes [40].

The gold goal would be to analyse iCAL peptide in a CF-animal model (mouse, ferret or pig) even if this animal models did not exactly reflect all pathology symptoms occurring in humans [70]. Each further successful step towards the development of new drugs such as the peptide iCAL will be a milestone for CF patients.

## 9 Danksagung

Zuallererst gilt meine Danksagung Herrn Dr. rer. nat. Rudolf Volkmer für die Betreuung und Begutachtung meiner Promotionsarbeit und allein für die Möglichkeit, diese in seiner Arbeitsgruppe geschrieben haben zu dürfen. Viele befruchtende und aufbauende Gespräche, Hinweise und Hilfen waren unschätzbare Bestandteil unserer gemeinsamen Arbeit an diesem Projekt.

Mein besonderer Dank gilt Dr. rer. nat. Prisca Boisguerin, die mir fachlich, menschlich und motivierend ein Vorbild ist. Sie stand mir stets kritisch und konstruktiv bei der Auswertung der Ergebnisse zur Seite und unterstützte mich hilfreich mit Rat und Tat in allen Phasen dieser Arbeit.

Professor Dr. Christian Freund danke ich für die Bereitschaft, sich der Begutachtung meiner Promotionsarbeit anzunehmen.

Ich danke Prof. Dr. Hans-Dieter Volk dafür, dass ich meine Arbeit in seinem Institut für Medizinische Immunologie durchführen durfte. Dort herrschte immer eine überaus angenehme Arbeitsatmosphäre und auch die wöchentlichen Institutsseminare haben mich in meinem Werdegang sehr positiv geprägt.

Dr. rer. nat. Thomas Korte danke ich für die ausgezeichnete Einführung und Betreuung über mehrere Jahre – die Methode der konfokalen Mikroskopie betreffend sowie für seine wertvolle fachliche Unterstützung bei allen auftauchenden Fragen und Problemen.

Dem Institut für Klinische Physiologie des Charité Campus Benjamin Franklin danke ich für die unkomplizierte und äußerst bereitwillige Aufnahme in Ihr Institut. Bei Prof. Dr. Dorothee Günzel möchte ich mich in diesem Rahmen besonders für die unendliche Zeit und die fachliche Kompetenz, die sie in meine Betreuung hinsichtlich der Ussing Kammer Messungen investiert hat, bedanken. In diesem Zusammenhang danke ich Britta Jebautzke und In-Fah M. Lee für die vorbereitenden Maßnahmen bezüglich der Zellkultur.

Ein herzlicher Dank gilt Dr. med. Nico Derichs, der die Ussing Kammer Messungen mit den Biopsien durchführte und mir diese auch für weiterführende Untersuchungen zur Verfügung stellte.

---

Ich danke aus tiefstem Herzen allen meinen Freunden, Vertrauten, Familienmitgliedern und einfach nur Liebsten, die mich immer unterstützten und immer für mich da waren. Besonders bedanke ich mich an dieser Stelle bei meiner Tochter Lotte Heiduk und ihrem Vater Jonas Werner, sowie meinem Freund Hans-Martin Sprenger, ohne deren Liebe, Rückhalt und Beistand die Arbeit so nicht möglich gewesen wäre.

## 10 References

- [1] Fanen, P., Wohlhuter-Haddad, A., Hinzpeter, A., *Int J Biochem Cell Biol.*, **2014** Jul;52:94-102.
- [2] Borowitz, D., Lubarsky, B., Wilschanski, M., Munck, A., Gelfond, D., Bodewes, F., Schwarzenberg, S.J., *Dig Dis Sci.*, **2015**; 61(1):198-207. doi: 10.1007/s10620-015-3834-2.
- [3] Goetzinger, K.R., Cahill, A.G., *Clin Lab Med.*, **2010** Sep;30(3):533-43.
- [4] De Boeck, K., Zolin, A., Cuppens, H., Olesen, H.V., Viviani, L., *J Cyst Fibros.*, **2014** Jul;13(4):403-9.
- [5] van Doorninck, J.H., French, P.J., Verbeek, E., Peters, R.H., Morreau, H., Bijman, J., Scholte, B.J., *EMBO J.*, **1995** Sep 15;14(18):4403-11.
- [6] Proesmans, M., Vermeulen, F., De Boeck, K., *Eur J Pediatr.*, **2008** Aug;167(8):839-49.
- [7] Keravec, M., Mounier, J., Prestat, E., Vallet, S., Jansson, J.K., Burgaud, G., Rosec, S., Gouriou, S., Rault G., Coton, E., Barbier, G., Héry-Arnaud, G., *Springerplus.*, **2015** Aug 9;4:405. doi: 10.1186/s40064-015-1207-0.
- [8] Li, C., Naren, A.P., *Integr Biol (Camb).*, **2010** Apr;2(4):161-77.
- [9] Farinha, C.M., Matos, P., Amaral, M.D., *FEBS J.*, **2013** Sep;280(18):4396-406.
- [10] Cant, N., Pollock, N., Ford, R.C., *Int J Biochem Cell Biol.*, **2014** Jul;52:15-25.
- [11] Riordan, J.R., *Annu Rev Biochem.*, **2008**;77:701-26.
- [12] Chmiel, J.F., Berger, M., Konstan, M.W., *Clin Rev Allergy Immunol.*, **2002** Aug;23(1):5-27.
- [13] Mall, M.A., Galietta, L.J., *J Cyst Fibros.*, **2015** Sep;14(5):561-70.
- [14] Quinton, P.M., *Physiology (Bethesda).*, **2007** Jun;22:212-25.
- [15] Becq, F., Mall, M.A., Sheppard, D.N., Conese, M., Zegarra-Moran, O., *J Cyst Fibros.*, **2011** Jun;10 Suppl 2:S129-45.
- [16] Rowe, S.M., Verkman, A.S., *Cold Spring Harb Perspect Med.*, 2013 Jul 1;3(7). pii: a009761.
- [17] Gosalia, N., Harris, A., *Genes (Basel).*, **2015** Jul 13;6(3):543-58.
- [18] Guggino, W.B., Stanton, B.A., *Nat Rev Mol Cell Biol.*, **2006** Jun;7(6):426-36.
- [19] Woods, D.F., Bryant, P.J., *Mech Dev.*, **1993** Dec;44(2-3):85-9.
- [20] Hung, A.Y., Sheng, M., *J Biol Chem.*, **2002** Feb 22;277(8):5699-702.

- [21] Tiwari, G., Mohanty, D., *J Chem Inf Model.*, **2014** Apr 28;54(4):1143-56.
- [22] Kundu, K., Backofen, R., *BMC Genomics.*, **2014**;15 Suppl 1:S5.
- [23] Raghuram, V., Mak, D.O., Foskett, J.K., *Proc Natl Acad Sci USA.*, **2001** Jan 30;98(3):1300-5.
- [24] Loureiro, C.A., Matos, A.M., Dias-Alves, Â., Pereira, J.F., Uliyakina, I., Barros, P., Amaral, M.D., Matos, P., *Sci Signal.*, **2015** May 19;8(377):ra48.
- [25] Rowe, S.M., Miller, S., Sorscher, E.J., *N Engl J Med.*, **2005** May 12;352(19):1992-2001.
- [26] Schwartz, M., Anvret, M., Claustres, M., Eiken, H.G., Eiklid, K., Schaedel, C., Stolpe, L., Tranebjaerg, L., *Hum Genet.*, **1994** Feb;93(2):157-61.
- [27] Osborne, L., Knight, R., Santis, G., Hodson, M., *Am J Hum Genet.*, **1991** Mar;48(3):608-12.
- [28] Illek, B., Zhang, L., Lewis, N.C., Moss, R.B., Dong, J.Y., Fischer, H., *Am J Physiol.*, **1999** Oct;277(4 Pt 1):C833-9.
- [29] Antiñolo, G., Borrego, S., Gili, M., Dapena, J., Alfageme, I., Reina, F., *J Med Genet.*, **1997** Feb;34(2):89-91.
- [30] Van Oene, M., Lukacs, G.L., Rommens, J.M., *J Biol Chem.*, **2000** Jun 30;275(26):19577-84.
- [31] Ramalho, A.S., Lewandowska, M.A., Farinha, C.M., Mendes, F., Gonçalves, J., Barreto, C., Harris, A., Amaral, M.D., *Cell Physiol Biochem.*, **2009**;24(5-6):335-46.
- [32] Ratjen, F.A., *Respir Care.*, **2009** May;54(5):595-605.
- [33] Bell, S.C., De Boeck, K., Amaral, M.D., *Pharmacol Ther.*, **2015** Jan;145:19-34.
- [34] Moskowitz, S.M., Gibson, R.L., Effmann, E.L., *Pediatr Radiol.*, **2005** Aug;35(8):739-57.
- [35] Chopra, R., Paul, L., Manickam, R., Aronow, W.S., Maguire, G.P., *Expert Opin Drug Saf.*, **2015** Mar;14(3):401-11.
- [36] Spahr, J.E., Love, R.B., Francois, M., Radford, K., Meyer, K.C., *J Cyst Fibros.*, **2007** Sep;6(5):334-50.
- [37] Pedemonte, N., Galiotta, L.J., *Front Pharmacol.*, **2012** Oct 5;3:175.
- [38] Griesenbach, U., Alton, E.W., *Hum Mol Genet.*, **2013** Oct 15;22(R1):R52-8.
- [39] Griesenbach, U., Alton, E.W., *F1000Prime Rep.*, **2015** May 27;7:64.
- [40] De Groot, A.S., Scott, D.W., *Trends Immunol.*, **2007** Nov;28(11):482-90.
- [41] Cushing, P.R., Vouilleme, L., Pellegrini, M., Boisguerin, P., Madden, D.R., *Angew Chem Int Ed Engl.*, **2010** Dec 17;49(51):9907-11.
- [42] Frank, R., *J Immunol Methods.*, **2002** Sep 1;267(1):13-26.

- [43] Boisguerin, P., Ay, B., Radziwill, G., Fritz, R.D., Moelling, K., Volkmer, R., *Chembiochem.*, **2007** Dec 17;8(18):2302-7.
- [44] Vouilleme, L., Cushing, P.R., Volkmer, R., Madden, D.R., Boisguerin, P., *Angew Chem Int Ed Engl.*, **2010** Dec 17;49(51):9912-6.
- [45] Vouillème, L., PhD Thesis: Engineering high specificity peptide inhibitors of a promiscuous protein-protein interaction domain with implications in Cystic Fibrosis., **2012**
- [46] Mohanty, S., Ovee, M., Banerjee, M., *Biology (Basel).*, **2015** Feb 5;4(1):88-103.
- [47] Ramsey, J.D., Flynn, N.H., *Pharmacol Ther.*, **2015** Oct;154:78-86.
- [48] Müller, J., Triebus, J., Kretzschmar, I., Volkmer, R., Boisguerin, P., *J Pept Sci.*, **2012** May;18(5):293-301.
- [49] Neumann, E., Schaefer-Ridder, M., Wang, Y., Hofschneider, P.H., *EMBO J.*, **1982**;1(7):841-5.
- [50] Guenther, C.M., Kuypers, B.E., Lam, M.T., Robinson, T.M., Zhao, J., Suh, J., *Wiley Interdiscip Rev Nanomed Nanobiotechnol.*, **2014** Nov-Dec;6(6):548-58.
- [51] Milletti, F., *Drug Discov Today.*, **2012** Aug;17(15-16):850-60.
- [52] Mäe, M., Langel, U., *Curr Opin Pharmacol.*, **2006** Oct;6(5):509-14.
- [53] Frankel, A.D., Pabo, C.O., *Cell.*, **1988** Dec 23;55(6):1189-93.
- [54] Green, M., Loewenstein, P.M., *Cell.*, **1988** Dec 23;55(6):1179-88.
- [55] Vivès, E., Brodin, P., Lebleu, B., *J Biol Chem.*, **1997** Jun 20;272(25):16010-7.
- [56] Derossi, D., Joliot, A.H., Chassaing, G., Prochiantz, A., *J Biol Chem.*, **1994** Apr 8;269(14):10444-50.
- [57] Wang, F., Wang, Y., Zhang, X., Zhang, W., Guo, S., Jin, F., *J Control Release.*, **2014** Jan 28;174:126-36.
- [58] Koren, E., Torchilin, V.P., *Trends Mol Med.*, **2012** Jul;18(7):385-93.
- [59] Bechara, C., Sagan, S., *FEBS Lett.*, **2013** Jun 19;587(12):1693-702.
- [60] Madani, F., Lindberg, S., Langel, U., Futaki, S., Gräslund, A., *J Biophys.*, **2011**;2011:414729.
- [61] Keller, A.A., Mussbach, F., Breitling, R., Hemmerich, P., Schaefer, B., Lorkowski, S., Reissmann, S., *Pharmaceuticals (Basel).*, **2013** Feb 6;6(2):184-203.
- [62] Morris, M.C., Depollier, J., Mery, J., Heitz, F., Divita, G., *Nat Biotechnol.*, **2001** Dec;19(12):1173-6.
- [63] Mayor, S., Pagano, R.E., *Nat Rev Mol Cell Biol.*, **2007** Aug;8(8):603-12.
- [64] Mao, Z., Zhou, X., Gao, C., *Biomater. Sci.*, **2013**,1, 896-911

- [65] Jiao, C.Y., Delaroché, D., Burlina, F., Alves, I.D., Chassaing, G., Sagan, S., *J Biol Chem.*, **2009** Dec 4;284(49):33957-65.
- [66] Vercauteren, D., Vandenbroucke, R.E., Jones, A.T., Rejman, J., Demeester, J., De Smedt, S.C., Sanders, N.N., Braeckmans, K., *Mol Ther.*, **2010** Mar;18(3):561-9.
- [67] Iversen, T.-G., Skotland, T., Sandvig, K., *Nano Today.*, **2011**, 176-185.
- [68] Wick, A.N., Drury, D.R., Nakada, H.I., Wolfe, J.B., *J Biol Chem.*, **1957** Feb;224(2):963-9.
- [69] Ishiguro, H., Yasuda, K., Ishii, N., Ihara, K., Ohkubo, T., Hiyoshi, M., Ono, K., Senoo-Matsuda, N., Shinohara, O., Yosshii, F., Murakami, M., Hartman, P.S., Tsuda, M., *IUBMB Life.*, **2001** Apr;51(4):263-8.
- [70] Fisher, J.T., Zhang, Y., Engelhardt, J.F., *Methods Mol Biol.*, **2011**;742:311-34.
- [71] Morris, M.C., Vidal, P., Chaloin, L., Heitz, F., Divita, G., *Nucleic Acids Res.* **1997** Jul 15;25(14):2730-6.
- [72] Simeoni, F., Morris, M.C., Heitz, F., Divita, G., *Nucleic Acids Res.*, **2003** Jun 1;31(11):2717-24.
- [73] Deshayes, S., Gerbal-Chaloin, S., Morris, M.C., Aldrian-Herrada, G., Charnet, P., Divita, G., Heitz, F., *Biochim Biophys Acta.*, **2004** Dec 15;1667(2):141-7.
- [74] Morris, M.C., Deshayes, S., Heitz, F., Divita, G., *Biol Cell.*, **2008** Apr;100(4):201-17.
- [75] Zorko, M., Langel, U., *Adv Drug Deliv Rev.*, **2005** Feb 28;57(4):529-45.
- [76] Dom, G., Shaw-Jackson, C., Matis, C., Bouffouix, O., Picard, J.J., Prochiantz, A., Mingeot-Leclercq, M.P., Brasseur, R., Rezsóhazy, R., *Nucleic Acids Res.*, **2003** Jan 15;31(2):556-61.
- [77] Alves, I.D., Jiao, C.Y., Aubry, S., Aussedat, B., Burlina, F., Chassaing, G., Sagan, S., *Biochim Biophys Acta.*, **2010** Dec;1798(12):2231-9.
- [78] Nelson, A.R., Borland, L., Allbritton, N.L., Sims, C.E., *Biochemistry.*, **2007** Dec 25;46(51):14771-81.
- [79] McLaughlin, S., Aderem, A., *Trends Biochem Sci.*, **1995** Jul;20(7):272-6.
- [80] Bastidas, A.C., Deal, M.S., Steichen, J.M., Keshwani, M.M., Guo, Y., Taylor, S.S., *J Mol Biol.*, **2012** Sep 14;422(2):215-29.
- [81] Farinha, C.M., Swiatecka-Urban, A., Brautigam, D.L., Jordan, P., *Front Chem.*, **2016** Jan 20;4:1.
- [82] Tien, X.Y., Brasitus, T.A., Kaetzel, M.A., Dedman, J.R., Nelson, D.J., *J Biol Chem.*, **1994** Jan 7;269(1):51-4.
- [83] Gosalia, N., Neems, D., Kerschner, J.L., Kosak, S.T., Harris, A., *Nucleic Acids Res.*, **2014** Sep;42(15):9612-22.
- [84] Hidalgo, I.J., Raub, T.J., Borchardt, R.T., *Gastroenterology.*, **1989** Mar;96(3):736-49.
- [85] Laohapitakworn, S., Thongbunchoo, J., Nakkrasae, L.I., Krishnamra, N., Charoenphandhu, N., *Am J Physiol Cell Physiol.*, **2011** Jul;301(1):C137-49.

- [87] Illek, B., Fischer, H., Machen, T.E., *Am J Physiol.*, **1996** Jan;270(1 Pt 1):C265-75.
- [88] De Boeck, K., Weren, M., Proesmans, M., Kerem, E., *Pediatrics.*, **2005** Apr;115(4):e463-9.
- [89] Pettit, R.S., Fellner, C., *P T.*, **2014** Jul;39(7):500-11.
- [90] Alton EW, Armstrong DK, Ashby D, Bayfield KJ, Bilton D, Bloomfield EV, Boyd AC, Brand J, Buchan R, Calcedo R, Carvelli P, Chan M, Cheng SH, Collie DD, Cunningham S, Davidson HE, Davies G, Davies JC, Davies LA, Dewar MH, Doherty A, Donovan J, Dwyer NS, Elgmati HI, Featherstone RF, Gavino J, Gea-Sorli S, Geddes DM, Gibson JS, Gill DR, Greening AP, Griesenbach U, Hansell DM, Harman K, Higgins TE, Hodges SL, Hyde SC, Hyndman L, Innes JA, Jacob J, Jones N, Keogh BF, Limberis MP, Lloyd-Evans P, Maclean AW, Manvell MC, McCormick D, McGovern M, McLachlan G, Meng C, Montero MA, Milligan H, Moyce LJ, Murray GD, Nicholson AG, Osadolor T, Parra-Leiton J, Porteous DJ, Pringle IA, Punch EK, Pytel KM, Quittner AL, Rivellini G, Saunders CJ, Scheule RK, Sheard S, Simmonds NJ, Smith K, Smith SN, Soussi N, Soussi S, Spearing EJ, Stevenson BJ, Sumner-Jones SG, Turkkila M, Ureta RP, Waller MD, Wasowicz MY, Wilson JM, Wolstenholme-Hogg P; UK Cystic Fibrosis Gene Therapy Consortium., *Lancet Respir Med.*, **2015** Sep;3(9):684-91.
- [91] Cheng, J., Wang, H., Guggino, W.B., *J Biol Chem.*, **2004** Jan 16;279(3):1892-8.
- [92] Cheng, J., Moyer B.D., Milewski, M., Loffing, J., Ikeda, M., Mickle, J.E., Cutting, G.R., Li, M., Stanton, B.A., Guggino, W.B., *J Biol Chem.* **2002** Feb 1;277(5):3520-9.
- [93] Wolde, M., Fellows, A., Cheng, J., Kivenson, A., Coutermarsh, B., Talebian, L., Karlson, K., Piserchio, A., Mierke, D.F., Stanton, B.A., Guggino, W.B., Madden, D.R., *J Biol Chem.*, **2007** Mar 16;282(11):8099-109.
- [94] Dietz, G.P., Bähr, M., *Mol Cell Neurosci.*, 2004 Oct;27(2):85-131.
- [95] Järver, P., Mäger, I., Langel, Ü., *Trends Pharmacol Sci.*, 2010 Nov;31(11):528-35.
- [96] Vergères, G., Manenti, S., Weber, T., Stürzinger, C., *J Biol Chem.*, **1995** Aug 25;270(34):19879-87.
- [97] Eisele, F., Kuhlmann, J., Waldmann, H., *Chemistry.*, **2002** Aug 2;8(15):3362-76.
- [98] Fischer-Parton, S., Parton, R.M., Hickey, P.C., Dijksterhuis, J., Atkinson, H.A., Read, N.D., *J Microsc.*, **2000** Jun;198(Pt 3):246-59.
- [99] Seidel, S.A., Dijkman, P.M., Lea, W.A., van den Bogaart, G., Jerabek-Willemsen, M., Lazic, A., Joseph, J.S., Srinivasan, P., Baaske, P., Simeonov, A., Katritch, I., Melo, F.A., Ladbury, J.E., Schreiber, G., Watts, A., Braun, D., Duhr, S., *Methods.*, **2013** Mar;59(3):301-15.
- [100] Carmona, G., Rodriguez, A., Juarez, D., Corzo, G., Villegas, E., *Protein J.*, **2013** Aug;32(6):456-66.



## **Eidesstattliche Erklärung**

Hiermit versichere ich, die vorliegende Dissertation selbstständig und ohne unerlaubte Hilfe angefertigt zu haben.

Bei der Verfassung der Dissertation wurden keine anderen als die im Text aufgeführten Hilfsmittel verwendet.

Ein Promotionsverfahren wurde zu keinem früheren Zeitpunkt an einer anderen Hochschule oder bei einem anderen Fachbereich beantragt.

Berlin,

Anja Heiduk

## Curriculum Vitae

### Work Experience

since 05/2012

#### PhD Thesis

AG Molekulare Bibliotheken

Institut für Medizinische Immunologie

Charité – Universitätsmedizin Berlin

- Vectorized peptidic inhibitors to rescue F508del-CFTR in Cystic Fibrosis.

06/2010 to 02/2011

#### Diploma Thesis

AG Molekulare Bibliotheken

Institut für Medizinische Immunologie

Charité – Universitätsmedizin Berlin

- Charakterisierung der Interaktion von PDZ Domänen aus bakteriellen und humane HtrA Proteasen mittels Peptidbibliotheken.